# Pt and Au as electrocatalysts for various electrochemical reactions

**MH Steyn**

**20109091**

Dissertation submitted in partial fulfilment of the requirements for the degree *Magister Scientiae* in Chemistry at the Potchefstroom Campus of the North-West University

Supervisor: Dr RJ Kriek

Co-supervisor: Prof V Ramani

May 2015

# Abstract

In this study the focus was on the electrochemical techniques and aspects behind the establishment of the better catalyst (platinum or gold) for the sulphur dioxide oxidation reaction (SDOR). One of the primary issues regarding the SDOR is the catalyst material, thus the comparative investigation of the performance of platinum and gold in the SDOR, as found in this study. Ultimately, the SDOR could lead to an effective way of producing hydrogen gas, which is an excellent energy carrier.

The electrochemical application of the oxygen reduction reaction (ORR) and ethanol oxidation reaction (EOR) is an integral part of the catalytic process of water electrolysis, and by using fuel cell technology, it becomes even more relevant to this study and can therefore be used as a control, guide and introduction to the techniques required for electrochemical investigation of catalyst effectiveness. Subsequently, the EOR as well as the ORR was used as introduction into the different electrochemical quantification and qualification techniques used in the electrochemical analyses of the SDOR.

Considering the ORR, gold showed no viable activity in acidic medium, contrarily in alkaline medium, it showed good competition to platinum. Gold also lacked activity towards the EOR in acidic medium compared to platinum, with platinum the best catalyst in both acidic and alkaline media. Ultimately, platinum was established to be the material with better activity for the ORR with gold a good competitor in alkaline medium, and platinum the better catalyst for the EOR in both acidic and alkaline media.

With the main focus of this study being the SDOR, gold proved to be the best catalyst in salt and gaseous forms of $SO_2$ administration compared to platinum when the onset potential, maximum current density, Tafel slope and number of electrons transferred are taken into consideration. The onset potential was determined as 0.52 V *vs.* NHE for both platinum and gold using $SO_2$ gas and 0.54 V and 0.5 V for gold and platinum respectively, using $Na_2SO_3$ salt. The maximum current density using gaseous $SO_2$ for platinum at 0 RPM was 400 $mA/cm^2$ with a Tafel slope of 891 mV/decade whereas gold had a maximum current density of 300 $mA/cm^2$ and a Tafel slope of 378 mV/decade. Using $Na_2SO_3$ salt, the maximum current density of gold was 25 $mA/cm^2$ with a Tafel slope of 59 mV/decade whereas platinum only achieved 18 $mA/cm^2$ with a Tafel slope of 172 mV/decade. Concerning the number of electrons transferred, gold achieves a transfer of 2 while platinum only 1 for both $SO_2$ gas and $Na_2SO_3$ salt. Taking all these summarised determinations into account, gold was established to be a very competitive catalyst material for the SDOR, compared to platinum.

**Keywords:** Polycrystalline, Gold, Platinum, Fuel Cell, Ethanol Oxidation Reaction, Sulphur Dioxide Oxidation Reaction, Oxygen Reduction Reaction, Tafel, Koutecký-Levich, Levich, Electrochemistry, Electrode, Sulphur Depolarised Electrolyser.

## Table of Contents

## List of Figures

## List of Tables

## List of Abbreviations

| | |
|---|---|
| ACE | Associated Chemical Enterprises |
| CA | Chronoamperometry |
| CO | Carbon Monoxide |
| CV | Cyclic Voltammetry/Voltammogram |
| EOR | Ethanol Oxidation Reaction |
| FTIR | Fourier Transform Infrared |
| HPLC | High Performance Liquid Chromatography |
| HTSOFC | High Temperature Solid Oxide Fuel Cells |
| HUPD or HUD | Hydrogen Under-potential Deposition |
| HyS | Hybrid Sulphur Cycle |
| LP | Linear Polarisation |
| NHE | Normal Hydrogen Electrode |
| OCP | Open Circuit Potential |
| ORR | Oxygen Reduction Reaction |
| OTEC | Ocean Thermal Energy Conversion |
| PEFC | Polymer Electrolyte Fuel Cell |
| PEMEC | Proton Exchange Membrane Electrolysis Cells |
| PEMFC | Proton Exchange Membrane Fuel Cells |
| PGM | Platinum Group Metals |
| PM | Particulate Matter |
| RDE | Rotating Disc Electrode |
| RPM | Revolutions per Minute |
| SDE | Sulphur Depolarised Electrolyser |
| SDOR | Sulphur Dioxide Oxidation Reaction |
| SERS | Surface Enhanced Raman Spectroscopy |
| SMR | Steam Methane Reforming |
| SPAIRS | Single Potential Alteration Infrared Reflectance Spectroscopy |
| XRD | X-Ray Diffraction |

# Chapter 1: Introduction

## 1.1. Fossil Fuels

The world's current industrial system relies greatly on the usage of fossil fuels as the primary source of energy [1, 2]. The estimated usage of fossil fuels as in the year 2013 in its different forms can be expressed in the following pie chart (Figure 1) [3]:

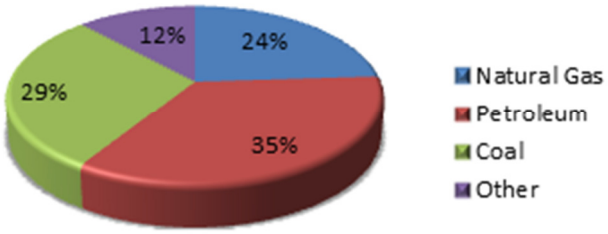


**Figure 1: The different forms of fossil fuels and their percentage applied usage**

Regardless of a growing demand for energy, i.e. fossil fuels based energy generation, and concerns about global fuel resources dwindling, many newly-found reserves have been discovered by horizontal drilling and hydraulic fracturing [3].

## 1.2. Energy Problem

The need for energy continues to increase as many countries grow economically [2, 4, 5]. The world has thus been confronted with a crisis regarding energy, due to the depletion of resources and an increase in environmental problems [6] as well as fossil fuel prices [4, 6, 7]. It is predicted that regardless of the large number of regulations and policies implemented globally, fossil fuel energy demand may continue to rise by up to 33% from the year 2010 until up to 2035 with the main fuel source, i.e. fossil fuels, still providing 75% of primary energy by 2035 [3]. Conte [2] speculates that within the next 50 years, the global energy demand may double with a probable reliance of about 80% on fossil fuels.

Over 80% of the world's energy is derived from fossil fuels [1, 3, 5, 7], which is the main contributor to atmospheric $CO_2$ radiative enforcers [1-3, 5-8] as well as carbon monoxide [6]. Many other emissions from different power generation methods, which do not include greenhouse gases, include substances such as $SO_2$, $NO_x$ and particulate matter (PM) [9]. These latter three basic types of emissions have a detrimental health and environmental effect. Consequently the world faces a great challenge in the promotion of energy driven economic growth as well as keeping $CO_2$ and other hazardous emissions to a minimum [3].

Fossil fuels in the form of oil, coal, gas, or petroleum, can be used as direct forms of energy generation, such as in automobile engines, as well as to produce electricity [3]. There are many different alternative energy sources that can be used to ultimately generate electricity, which include wind energy, as it is comparable to fossil fuels (coal for example) in terms of costs and effectiveness regarding electricity generation [4], hydro-generated electricity [10] that uses the flow of water to drive turbines [11], solar energy using solar panels containing titanium dioxide ($TiO_2$) [12] or silicon (Si) based alloys [13] to produce electricity, nuclear energy that uses high temperature uranium fuel rods [9] to generate steam that drives turbines [14], ocean thermal energy conversion (OTEC) [4] that involves the vaporisation of low boiling point ammonia gas that drives a turbine, and geothermal energy involving high temperature underground steam that travels to the earth's surface, eventually driving turbines [15]. The electricity generated by all these abovementioned techniques, can be used to electrolyse water to form hydrogen and oxygen gas [2, 5]. Hydrogen, an energy carrier, can also be regarded as a future alternative source of energy [5, 6], instead of using fossil fuels, as it can be used in fuel cells to power vehicles [16] and to generate electricity [17] for other applications, with pure water being the only emitted compound.

## 1.3. Hydrogen Economy

The most widely accepted view of the hydrogen economy is that the majority of fossil fuel based energy sources will be replaced with hydrogen gas, used either as the primary fuel or energy carrier [2, 6] in internal combustion engines utilised in almost any form of transportation [6] (land and even air); or by using fuel cell technology to achieve effective energy use. It is speculated by Balat [6] that if by the year 2040 about 150 million tons of hydrogen will be produced annually by using petroleum reforming technology, that would account for a net saving of about 11 million barrels of Brent crude oil per day. The appeal of the hydrogen economy is thus enormous as it can be a potential solution to fundamental energy scarcity issues by providing an abundant energy supply as well as having a minimum impact on the global atmospheric environment [5, 8].

The Hydrogen Economy can be based on the reaction of hydrogen with oxygen to produce water and electrical energy, as depicted in reaction (1) below [6].

$$H_2 + \tfrac{1}{2}O_2 \longrightarrow H_2O \qquad \Delta H = \text{-285.8 kJ/mol at 25 °C} \qquad \Delta G = \text{-237.2 kJ/mol at 25 °C} \qquad (1)$$

Acceleration of the development of energy systems employing hydrogen as energy carrier has been fuelled by concerns about the dependence on fossil fuels, poor air quality, greenhouse gas emissions and energy security in general, to name but a few reasons [18].

In the future, hydrogen will have a major role to play as energy carrier, ultimately being a source of energy supply, as is believed by many experts in literature [5, 6, 8]. As a source of energy, primary sources used in hydrogen production, will become readily available in the future, on a global scale [5, 6]. Since the isolation of hydrogen by Henry Cavendish in 1766, the main idea was to use it as a fuel [1]. Jules Verne predicted in the 1870s, that mankind will use water as the coal of the future, once earth's coal reserves have been depleted.

Hydrogen is important in energy generation and the refining of petroleum and also plays an important role in the generation of electricity through the use of proton exchange membrane fuel cells (*PEMFC*s), as hydrogen gas is an energy carrier [19]. In the form of combustion, hydrogen is able to release almost three times the amount of energy per gram of substance as gasoline ($H_2$ = 142 kJ/g; Gasoline = 48 kJ/g) [20].

As hydrogen is the most abundant element in the universe [1, 2, 6], the pure form thereof is not found on our planet [1, 5]. The most abundant form of hydrogen is found in water and fossil fuels in a combination with other elements that form hydrocarbon compounds [1, 2, 5].

Hydrogen is only a carrier of high-quality energy and not a primary energy source [2], therefore it needs to be produced just as electricity is produced [2, 5]. Different known techniques for hydrogen extraction include biological, electrochemical and thermal methods [18]. Water electrolysis is a well-known technique, which is used in the production of hydrogen with no unusable by-products when nuclear energy is involved in the process [2, 18]. Most production processes include photo-catalytic processes [6], electrochemical processes [2, 6], thermochemical processes, photochemical processes or even photo-electrochemical processes [6].

The pie chart in Figure 2 shows the share of the different sources of hydrogen in the production of hydrogen gas, with natural gas originating mostly from fossil fuels, the oils from heavy oils and naphtha, coal, then lastly from electrolysis as chlorine production's by-product [1]. Electrolysis of water can also be established by using technologies such as proton exchange membrane electrolysis cells (PEMEC) [21], alkaline electrolysis [22], high temperature solid oxide fuel cells (HTSOFC) [2], thermochemical processes [2, 6] and the hybrid sulphur cycle (HyS) [22-24]. The most economic and effective production of hydrogen is by means of steam methane reforming (SMR) [5, 6]. Processes based on fossil fuels thus account for 95% of the world's hydrogen production [7].

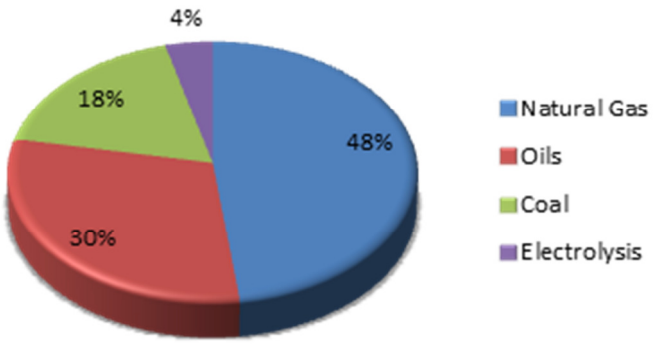


**Figure 2: Hydrogen production as in 2006 [1, 2, 6]**

The current uses of hydrogen include synthesis of nitrogenated fertilisers and ammonia, hazardous waste hydrogenation (*PCB*s and dioxins), methanol, ethanol and dimethyl-ether synthesis, gas to liquid synthesis technologies, fuel for rockets, internal combustion engine fuel, fuel for high temperature industrial furnaces, refining and desulphurisation processes, chemical plants and preparation of food and synthesis of alternative fuels by using the Fischer-Tropsch method [6].

The following pie chart (Figure 3), summarises the consumption or usage of hydrogen [6]:

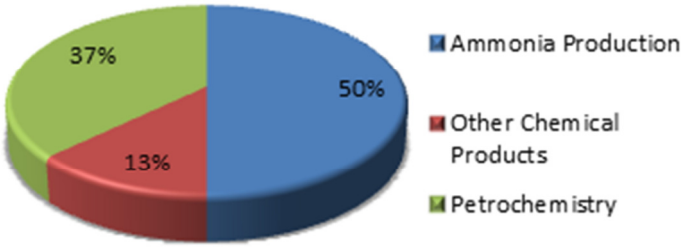


**Figure 3: Current worldwide hydrogen consumption by different uses**

Because of the extreme low density of hydrogen gas, the storage thereof is very difficult and requires cryogenic tanks for the storage of compressed $H_2$ [2, 6]. As a result of this low density, the range to which a hydrogen powered automobile will be able to travel will be much shorter, as much larger volumes of hydrogen gas are required to drive a vehicle the same distance compared to petroleum [6]. The major issue affecting the future of hydrogen usage is thus the storage thereof, making the on-demand production technologies extremely attractive as it is much safer and cheaper than to store in compressed cylinders or chambers [5, 6]. Regarding hydrogen as an energy carrier, the vision for the future is the implementation thereof as a primary energy carrier for the growth and development of economies and, at the same time, to resolve the concerns of negative environmental impact, storage issues and on demand production [6]. The hybrid sulphur cycle (HyS) process,

covered in the following section, is a technology, which among others, could contribute to solving the abovementioned implementation issues regarding hydrogen.

### 1.3.1. Hybrid Sulphur Cycle (HyS)

Research has been done to use the two step Westinghouse cycle [23] otherwise known as the sulphuric acid hybrid cycle, to produce hydrogen gas [18, 23, 25, 26]. HyS is a promising process which might enable implementation of the hydrogen economy as this thermochemical water-splitting cycle enables the mass production of hydrogen gas [23, 27].

The main challenge encountered with the HyS process development, is the development of a cost-effective electrochemical reactor [24] using the sulphur depolarised electrolyser (SDE). The most important inherent component of HyS is the SDE, which uses sulphur oxide based intermediates to split water with high efficiencies where energy input can be obtained by solar or nuclear energy [23, 24, 27]. Thermal energy is used to split sulphuric acid, and electrical energy to electrolyse the gas. The obstacle to overcome is the electrolysis step, which exhibits reduced kinetics [23]. The electrolyser part also accounts for more than 50% of the total cost of the manufacturing of the process plant.

In the hybrid sulphur cycle the first step involves the decomposition of sulphuric acid at 700 - 1000 ℃ (reaction (2)) with the $SO_2$ and $H_2O$ being recycled for the oxidation of $SO_2$ [18, 23, 25-27] followed by the production of sulphuric acid and hydrogen by the electrochemical oxidation of $SO_2$ (reaction (3)).

$$H_2SO_4 \xrightarrow{\Delta\ 700 - 1000\ ℃} SO_2 + H_2O + ½O_2 \quad (2)$$

$$SO_2 + 2H_2O \longrightarrow H_2SO_4 + H_2 \quad (3)$$

The reactions take place as follows (reactions (4) - (5)) [18, 23, 25, 26]:

Anode: $SO_{2(aq)} + 2H_2O_{(l)} \longrightarrow H_2SO_{4(aq)} + 2H^+_{(aq)} + 2e^-$ $E^0 = 0.17$ V [25] or 0.157 V [26] (4)

Cathode: $2H^+ + 2e^- \longrightarrow H_{2(g)}$ (5)

The main attribute of the SDE is that the electrolysis of water occurs at ca. -0.158 V and not at the normal higher theoretical voltage of -1.23 V [18, 24]. Compared to conventional water

electrolysis, the SDE has the potential to use one eighth of the power needed to produce the same amount of hydrogen.

The advantage of the SDE using PEM technology, is that it has a high efficiency electrochemically, which leaves a small environmental footprint, thus enabling a prominent possibility to be commercially viable [24].

Challenges for the SDE include the high working temperature in strong sulphuric acid under heightened pressure as to enable the ensuing reaction of water with $SO_2$ [24] and also the electrolyser component, as described earlier, which is the most expensive and sluggish part. The main focus of electrode materials for the $SO_2$ electro-oxidation thus far was limited to noble metals and transitional metal alloys [26] and to obtain the most stable and cost effective catalyst [23]. Because of the complex nature of the reaction and the sensitivity towards the surface state of the electrode, understanding of the reaction mechanism might be helpful in assisting the search for the best catalyst [26].

The search for inexpensive electrode material is on-going and currently not too successful with many different catalyst materials being investigated ranging from metals to carbon based electrodes [25].

### 1.3.2. Approach to the Hydrogen Economy

A fuel cell uses a catalyst material such as platinum and hydrogen to power different devices, thus fuel cells can be regarded as the hydrogen engine [5]. In a fuel cell, as depicted in Figure 4 below, hydrogen oxidation occurs at the anode and oxygen reduction at the cathode giving a final product of water [5, 21, 28, 29]. A fuel cell can also be used as a water electrolysis cell by the electrolytic reduction of water at the cathode, forming hydrogen gas whilst water is oxidised at the anode, forming oxygen, as depicted in Figure 5 [21].

Consider the following diagrams (Figure 4 & Figure 5) to demonstrate the basic structure or components of a fuel cell and electrolytic fuel cell [5, 21]. In both Figure 4 and Figure 5, ‘A’ represents the anode or anodic catalyst, ‘B’ the proton exchange membrane, ‘C’ the cathode or cathodic catalyst and ‘L’ the load, either in the form of current drawn from the fuel cell (galvanic) or current being forced into the fuel cell (electrolysis).

In Figure 5 (electrolysis cell), the water is oxidised at the anode to form oxygen whilst protons coming from the water oxidation are reduced at the cathode, forming hydrogen gas [21]. This electrolytic process can thus produce hydrogen gas to be used in a PEMFC to produce electricity.

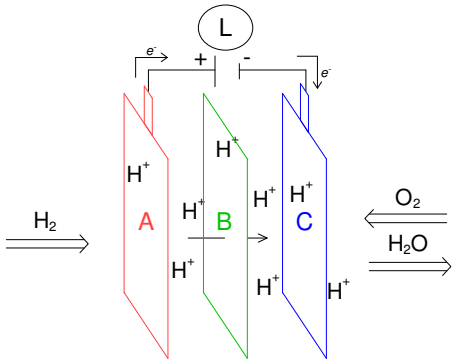


**Figure 4: The fuel cell being used as a power generator (galvanic cell) using $H_2$ and $O_2$ to form water [5, 21]**

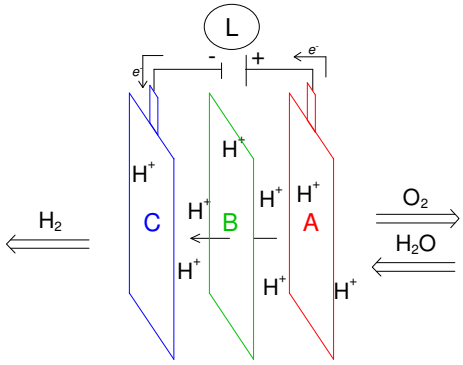


**Figure 5: Using the fuel cell as an electrolysis cell to split water into $H_2$ and $O_2$ [21]**

The commercialisation of fuel cell technology is hampered by the sluggishness of the catalyst, which includes the high overpotential required for reduction of oxygen to take place [5, 28-30], as well as the high cost of the catalyst and the short lifetime thereof [28, 29]. Because of this reaction sluggishness, the output potential of fuel cells is easily reduced to 0.8 V and even less, from the ideal voltage value of 1.23 V [5]. Investigation into catalyst material, which is more effective and less costly than platinum for the electro-reduction of oxygen, is thus crucial in the successful commercial implementation of fuel cell technology [28, 31]. With alcohol fuel cells the poisoning of the electrode with carbon monoxide (CO) inhibits the reactivity of the electrode and also shortens the lifetime thereof [32].

## 1.4. Motivation for this study

As will be evident from Chapter 2 the main focus of this study is on the sulphur dioxide electro-oxidation reaction (SDOR) and to that regard platinum and gold were investigated as electrocatalysts employing different electrochemical techniques.

# Chapter 2: Literature Study

Platinum and gold were the two catalyst materials investigated in this study, subsequently their respective catalytic properties was evaluated.

## 2.1. Catalytic Properties

Regarding the metal interaction with molecular species in solution the following is of main concern with regards to electrode effectiveness and selectivity. The adsorption and desorption of oxide on noble metal electrode surfaces under dynamic potential cycling has been extensively investigated in literature [23]. Both ad- and de-sorption can be clearly seen on cyclic voltammograms as both have respective anodic and cathodic currents. Electrode preconditioning can give reproducibility of the different peaks in a voltammogram but not the same surface roughness of the electrode [33].

Platinum and gold have been used in literature for various electrochemical applications and have therefore been chosen as the two main electrode materials for the investigation into their catalytic activity towards the different model reactions in this study i.e. ORR, EOR and SDOR. Platinum was used in this study, as the literature on its performance is readily available, and could thus be used as a reference point to compare gold's electrocatalytic performance. Gold is readily available and if proven to be an effective electro-catalyst, could be used for a diversity of electrochemical applications.

The double layer region on a metal catalyst's CV is the region of potential where no change in current density occurs as to indicate a reaction taking place [23, 34-39]. For polycrystalline platinum it occurs in the potential range between oxide adsorption/desorption and hydrogen adsorption/desorption potential regions in alkaline and acidic media.

### 2.1.1. Platinum

The cleanliness of Pt particles can be established from the hydrogen adsorption/desorption region of the characteristic voltammogram, which can indicate whether or not the electrode is in an uncontaminated state [40]. The hydrogen sorption region can be used as a fingerprint in the characterisation of the electrode (refer to Figure 6 below).

The well-known hysteresis observed in the voltammograms of noble metal surfaces (Figure 6 below) is due to the change in the dipoles of the adsorbed hydroxide on the metal surfaces as depicted in the reaction mechanism in equations (6) - (8) [23, 26], as can be derived from

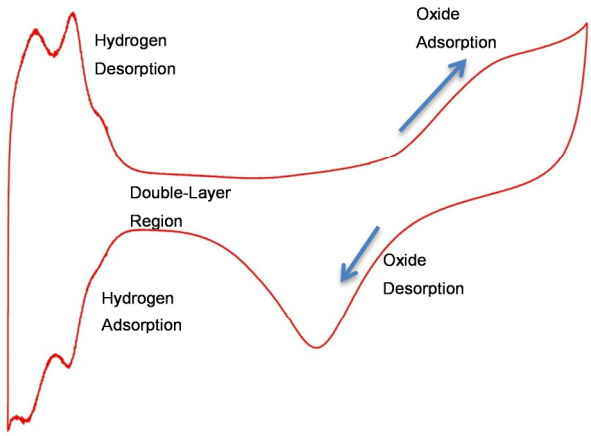


**Figure 6: Typical hysteresis of platinum in acidic medium depicting hydrogen and oxygen adsorption and desorption (adapted from [23])**

the mechanism for gold oxidation described in section 2.1.2 and demonstrated in equations (9) - (11) [41],

$$Pt\text{-}(H_2O)_{ads} \longrightarrow Pt\text{-}\dot{O}H + H^+ + e^- \quad (6)$$

$$Pt\text{-}\dot{O}H \longrightarrow Pt{=}O + H^+ + e^- \quad (7)$$

$$Pt{=}O + H_2O \longrightarrow Pt{=}O\text{-}(H_2O)_{ads} \quad (8)$$

which have repulsive interactions and in turn cause the surface lattice to reconstruct from the parallel dipole orientation to the anti-parallel orientation [42]. In the voltammograms, as demonstrated in Figure 6, the shape and onset of oxide adsorption and desorption depends on the solution pH and surface structure [23]. Activation of platinum is believed to occur when the oxide species have been desorbed by either chemical or electrochemical stripping. It has also been found that activation of the electrode does not necessarily entail the removal of the oxide layer where, in some instances, certain reaction species have been found to activate the catalytic effectiveness of the electrode.

### 2.1.2. Gold

For a long time gold was believed to be a relatively inert material and not preferable as an electrocatalyst [31, 43, 44]. Gold has been shown to have a much higher electrocatalytic activity towards the oxidation of organic compounds in alkaline than in acidic medium [40, 45-47]. It was shown to have the lowest reactivity towards gases and liquids at its interface

[47]. It has been suggested that gold has great potential as a catalyst for use in fuel cells and hydrogen fuel processing related to that technology by taking into account the relative scarcity and high cost of platinum [45, 48, 49] although the recent trends in gold prices tend towards the contrary.

Gold is a very electronegative metal that can draw electrons from the surrounding metal atoms especially when not of the same origin [50]. Activated electrode surfaces have been shown to be less effective because of over-oxidation of the surface, causing competition with the electrocatalytic process [45]. Ill-defined surfaces are mostly produced by pre-treatment of the electrode by electrochemical, chemical or thermal techniques. It is thus important to have a standardised method of pre-treatment, to attempt to maximise the surface reproducibility.

Consider Figure 7 below. Active gold pre-monolayer oxidation is more facile in alkaline than in acidic medium because of the stability of the hydrous oxide product, which inadvertently affects electrocatalytic activity [45, 46], even though gold is known to bind hydroxyl anions more weakly than platinum [31]. The anodic process, better known as the oxidation process, in an alkaline solution, begins with the hydroxyl ion adsorbing on the surface of the electrode, which then further oxidises to form the oxide layer and continues to grow until the whole electrode surface has been covered by an oxide film; this process takes place just below the oxygen evolution potential [33]. The composition of the initial surface film and the mechanism of formation remains an unresolved question [41]. In an acidic solution a possible mechanistic approach includes a one-electron transfer oxidation reaction of adsorbed water on the gold electrode surface, forming an adsorbed hydroxyl radical - reaction (9). The oxide film forming process in alkaline medium follows almost the same path as the acidic by skipping the first water adsorption step by following the same route as reaction (10):

$$Au\text{-}(H_2O)_{ads} \longrightarrow Au\text{-}\dot{O}H + H^+ + e^- \quad (9)$$

The subsequent reaction is also a one-electron transfer reaction to form the oxide (10):

$$Au\text{-}\dot{O}H \longrightarrow Au{=}O + H^+ + e^- \quad (10)$$

$$Au{=}O + H_2O \longrightarrow Au{=}O\text{-}(H_2O)_{ads} \quad (11)$$

The net effect of these three reactions above is to introduce the oxygen atom to the surface gold lattice below the electrode/electrolyte interface [41].

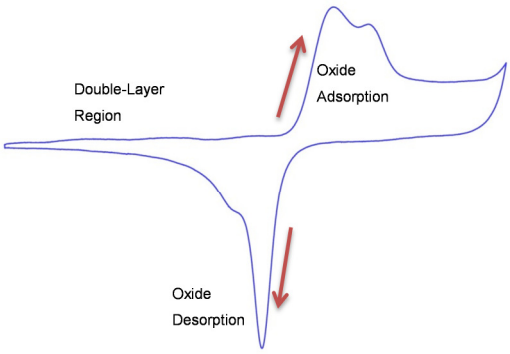


**Figure 7: A typical CV of gold in acidic medium depicting the oxide ad- and de-sorption (adapted from [23])**

The reverse path is followed when the oxide layer is being reduced. Hence, the typical electrochemical hysteresis as depicted in Figure 7 above.

## 2.2. Electrode Characteristics

Reaction kinetics can be more easily evaluated on rotating disc electrodes (*RDE*s) than stationary electrodes [51]. Because of higher convective diffusion rates, adsorption processes can be easily hidden and consequently, more difficult to identify. It is therefore recommended to study complex reactions on both stationary and rotating electrodes, as many reactions have adsorption and diffusion character combined. Using rotating electrodes, the effect of diffusion limitation can be excluded from the mechanistic studies [52]. Thus the source of reaction limitation can be determined as either diffusion or kinetic by monitoring the limiting current, should it not change with the rotation rate of the electrode [26].

Three main advantages of *RDE*s include: i.) The fixation of the rotational velocity $\omega$ of the electrode, which enables the exact control of the rate of mass transport of reactants to the electrode surface [53]; ii.) Steady state values $\delta I/\delta t = 0$ of electrode currents $I$ are quickly achieved after the applied electrode potential $E_{app}$ has been established with a moderate to high rate of rotation velocity ($\omega$ > ca.10 rad/s). iii.) Response of current is not affected by incidental vibrations coming from the electrochemical apparatus.

## 2.3. Electrochemical Qualification Techniques

Electrochemical techniques used in this study will include cyclic voltammetry (CV) that enables quick interpretation of qualitative data without requiring mathematical analysis [54]

and linear polarisation (LP) that is the same as *CV*s without the return/backwards voltage scan [54], which can be used to further analyse a reaction by means of mathematical processes described in this section's following subsections. A chrono-amperometry run (CA) is used to investigate the diffusion characteristics of species in solution to and from the electrode surface [55] and can be used to clean the electrode from contaminating species or to polarise it.

In Figure 8 below, a generic LP is given with the different control regions indicated. It includes kinetic control, mixed control and diffusion control. The Koutecký-Levich analysis technique (section 2.3.3) is applied on the mixed control region and Levich (section 2.3.2) on the diffusion control region.

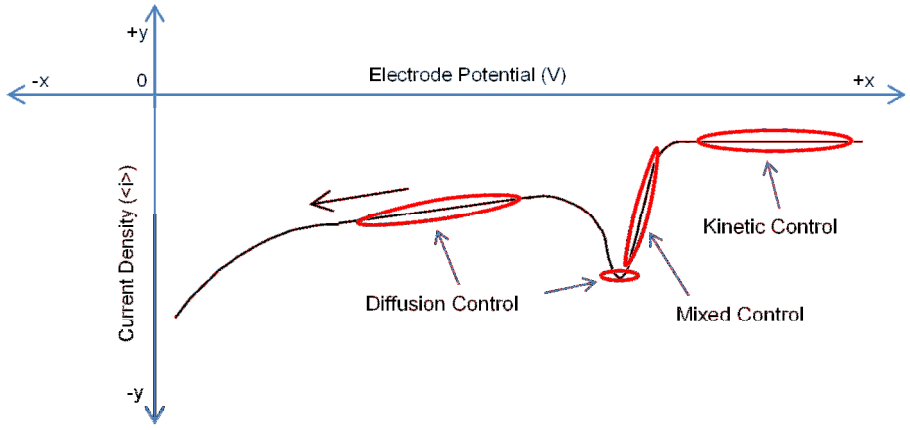


**Figure 8: An LP to demonstrate the different control regions (adapted from [23])**

## 2.3.1. Tafel Slope

Qualification techniques such as the Tafel slope have been developed as a measure of the reaction kinetics, with a large Tafel slope indicating a sluggish reaction and a small Tafel slope indicating a reaction with favourable kinetics [23] in different experimental conditions.

The Tafel equation can be mathematically expressed as follows [56]:

$$j = j_a = j_0 \exp\frac{\alpha_a nF\eta}{RT} \qquad (12)$$

$j$ is the experimental current density, $j_a$ the anodic current density, $j_0$ the exchange current density, $\alpha$ the transfer coefficient, n the number of electrons involved in the electrode reaction, F the Faraday constant, $\eta$ the overpotential, $R$ the universal gas constant and $T$ the temperature. The subscripts 'a' and 'c' for $\alpha$ indicate the anodic or cathodic forms of current.

Equation (12) can be rewritten as equation (13) for anodic reactions

$$\log j = \log j_0 + \frac{\alpha_a nF}{2.3RT}\eta \quad (13)$$

and as equation (14) for cathodic reactions:

$$\log(-j) = \log j_0 - \frac{\alpha_c nF}{2.3RT}\eta \quad (14)$$

Equations (13) and (14) are in a linear form with the slope facilitating the determination of the transfer coefficient $\alpha$.

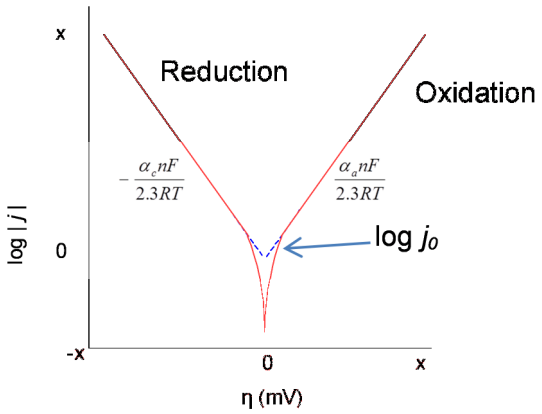


**Figure 9: A representation of Tafel plots used in the analysis of current versus overpotential data as to obtain kinetic parameters (adapted from [56])**

Tafel behaviour is the area of overpotential, where the current density changes by a factor of more than 1 for every increase in overpotential of 120 mV [56] and is used to determine the Tafel slope. In this study the Tafel slope was used to compare the sluggishness of each reaction on gold and platinum, by plotting overpotential $\eta$ *vs.* log(j), towards the reaction i.e. oxygen reduction reaction (ORR), ethanol oxidation reaction (EOR) and sulphur dioxide oxidation reaction (SDOR).

### 2.3.2. Levich Analysis

The Levich equation can be used to determine the number of electrons transferred in an electrochemical reaction by plotting the limiting current against the square root of the rotation rate by using the current in the diffusion controlled regions of the *LP*s (Figure 8) [23].

The Levich equation is given below in equation (15) [23, 53, 57]:

$$I_{\lim,c} = 0.62\frac{nF\pi r^2 D_A^{2/3}\omega^{1/2}C_A^b}{\nu^{1/6}} \quad (15)$$

In equation (15), $n$ is the number of electrons, $F$ the Faraday constant, $\pi r^2$ the electrode surface area, $D$ the diffusion coefficient, $c$ the concentration of the active species, with $\nu$ the kinematic viscosity and lastly $\omega$ the electrode rotation rate [23].

Linearity of Levich plots ($I$ *vs.* $\omega^{1/2}$), over a wide range of rotation rates such as 50-10 000 revolutions per minute (RPM), indicates a response mechanism that can be approximated as single-step resulting in the rapid transfer of electrons, characterised by a large heterogeneous rate constant $k_h$ [53]. The slope of the plots can be used to reliably estimate the value of $n$ by using literature values of $\nu$ and $D$. An estimation of those values can be used for most aqueous media and small reactant species in aqueous media as follows: $\nu = 1.0\times10^{-2}$ cm$^2$/s and $D = 1.0\times10^{-5}$ cm$^2$/s. Negative plots of $I$ *vs.* $\omega^{1/2}$ can be an indication of a kinetically slow charge transfer.

### 2.3.3. Koutecký-Levich Analysis

The following equation is the Koutecký-Levich equation, from which the number of electrons (n) that partake in a certain electrochemical reaction can be determined [53, 58, 59]. The data used for the plot is obtained from the mixed control region as indicated in Figure 8.

$$I_c = \frac{nF\pi r^2 D_A C_A^b}{\delta + D_A/k_h} \tag{16}$$

$\delta$ represents the thickness of the diffusion layer at the electrode surface and is defined as:

$$\delta = [0.620]^{-1} D_A^{1/3} \nu^{1/6} \omega^{-1/2} \tag{17}$$

Equations (16) and (17) can be combined and rearranged to be used in a linear regression line-fitting for determination of the number of electrons, as well as $k_h$, which is the heterogeneous rate constant of electron transfer [53]. The rearranged form of equations (16) and (17) (equation (18)) is given below [23, 53]:

$$\frac{1}{I_c} = \frac{1}{0.62nF\pi r^2 D_A^{2/3} \nu^{-1/6} \omega^{1/2} C_A^b} + \frac{1}{nF\pi r^2 k_h C_A^b} \tag{18}$$

The symbols used in equation (18) are defined as follows: $I_c$ - cathodic electrode current; $n$ – the number of electrons; $F$ - is the Faraday Constant; $r$ - is radius of the electrode surface; $D_A$ is known as the diffusivity constant for species A; $\nu$ - is used for the kinematic viscosity; $\omega$ - depicts the rotation rate of the electrode; $C_A^b$ - is used for the concentration of species A in the bulk solution; and lastly $k_h$ - is the heterogeneous rate constant of electron transfer [53]. If the inverse of current density is plotted against the inverted square root of the

electrode rotation rate the number of electrons $n$ transferred can be calculated from the slope and the rate constant $k_h$ from the y-intercept [53, 58, 59].

In the context of the Koutecký-Levich analysis, the diffusion coefficient for gases can be easily obtained in the literature; however, values for the diffusion coefficient vary greatly [60]. Refer to a list of diffusion coefficients in Table 20 in Appendix 1 – Data on page 130.

Also used in the Koutecký-Levich analysis is the kinematic viscosity, which is defined as the ratio of viscosity to density [60]: $\nu = \mu/\rho$ with units of $m^2/s$. In Appendix 1 – Data on page 130 Table 21 the viscosity of different compounds is listed. The next important variable is the concentration of a compound in solution. For gases the saturated concentration can be easily calculated with the use of the mole fraction solubility equation (63), which was determined at a partial pressure of 1 atm [60]. The solubility of gases such as oxygen and sulphur dioxide is given in Table 22, Appendix 1 – Data, on page 130. Results from literature for the variables used in the Koutecký-Levich equation are given below in Appendix 1 – Data in Table 23.

### 2.3.4. Arrhenius

For experiments at different temperatures, the Arrhenius equation (19) is a very useful expression to determine the activation energy required to drive the reaction, as it is dependent on the collision frequency and energy of the reacting molecules, which directly translates to temperature dependence and whether or not the inter-molecular collisions have the correct geometry [61, 62]. The higher the activation energy of the reaction, the higher the temperature dependence [61].

$$k = Ae^{-E_a/RT} \tag{19}$$

$$\ln k = \ln A - \frac{E_a}{RT} \tag{20}$$

From equations (19) and (20), $k$ is the rate constant, $A$ the Arrhenius parameter or collision frequency, $E_a$ the activation energy, $R$ the universal gas constant $R$ = 8.314 J/K.mol$^{-1}$ and $T$ the temperature in Kelvin; with equation (20) the linear form of equation (19).

From a plot of ln $k$ against $T^{-1}$ the activation energy $E_a$ can be established from the slope of the plot and the collision frequency $A$ a.k.a. the Arrhenius parameter from the y-intercept.

### 2.3.5. Reaction Diagnoses

To diagnose or establish the reaction effectiveness (otherwise known as activity) the above-mentioned sections (2.3.1 up to 2.3.4) play an integral role in determining the more effective catalyst towards the ORR, EOR and SDOR.

The primary objective is to establish the number of electrons *n* transferred in a hydrodynamic electrode system, which corresponds to the charge component of the response mechanism [53]. The secondary objective is to identify the simplest mechanism consistent with the variations observed with regard to the response of the electrode as a function of the rate change, linked to convective-diffusional mass transport [53]. The third, equally important objective, is the establishment or evaluation of the rate constant of the rate limiting step of the electrochemical reaction [53].

If the value of *n* calculated by the Levich plot (equation (15)), for low values of $\omega$, is larger than the Koutecký-Levich plot for large values of $\omega$, the interpretation may lead in the direction of consecutive charge transfer mechanisms of two or more steps, where the second step of charge transfer has a much smaller $k_h$ value than the first step [53]. For cases such as these the best would be to determine an overall *n* value from coulometric data from exhaustive electrolysis. Another worthy note of the characteristics of the Koutecký-Levich graphs is that, should the plots be in a straight line formation, the reaction order is 1 [63].

The methods used to evaluate the reactions in this study, are powerful tools to evaluate the reaction mechanism of each reaction, although it was not part of this investigation's scope.

## 2.4. Goal of this study

The main goal of this study was to investigate the electro-oxidation of $SO_2$ in aqueous medium on polycrystalline smooth platinum and gold surfaces.

As discussed in section 1.2, there is a significant global demand for more and clean energy so as to develop countries' economies. A potential solution to that problem is the considered hydrogen economy as described in section 1.3. To implement hydrogen as a viable energy carrier, extensive research needs to be done so as to improve the generation efficiency thereof, as there are various issues with, among other areas, storage and production.

As $SO_2$ is one of the main pollutant gases emitted at coal driven power stations and as strict regulations are being implemented globally to decrease emissions, it is in the best interest of companies and governments to investigate innovative technologies to reduce pollutant emissions. This provides opportunities to investigate gas cleaning methods by which power

station exhaust emissions of $SO_2$ can be reduced by use of electrochemistry. By integrating the SDE into the emission cleaning process, hydrogen can be generated with the HyS process by using the SDE, while providing a simultaneous renewable energy source. As this technology needs a lot of work to be perfected, several issues have come to light.

One of the primary issues regarding the SDOR is the catalyst that needs to outperform the most popular catalyst, i.e. platinum, which leads to the investigation of different metals' performance with regard to the SDOR. As platinum research can be easily found in the literature, it is used as a benchmark for comparison of gold's performance and to indirectly guide the investigation process regarding gold. In the SDOR, platinum is the main catalyst material used in the SDE. Gold might be a worthy alternative and was thus chosen to partake in the investigation. Ultimately, the comparison might introduce gold as an alternative catalyst material to platinum for use in the SDE. Commercial implementation of the SDE might then become more viable should gold be a better catalyst.

The electrochemical application of ORR and EOR forms an integral part of electrochemical catalytic processes, and can therefore be used as a control, guide and introduction to the techniques required for electrochemical investigation of catalyst effectiveness.

The activity and selectivity of both gold and platinum is to be established by using electrochemical analysis techniques. To enable the useful application of these techniques, consequent experiments include cyclic voltammetry (CV), chrono-amperometry (CA) and linear polarimetry (LP). *CV*s were used to activate or precondition the electrode surface for use in the electro-analytical process, while *CA*s were used for electrode polarisation and *LP*s to establish the reaction route. The processing of the results was done by using the Tafel plot, Levich plot and Koutecký-Levich method of analysis. The Tafel slope was also used to determine the reaction sluggishness whereas the Levich and Koutecký-Levich were used to determine and check the number of electrons transferred during the respective reaction (section 2.3).

The Arrhenius equation was applied to determine the activation energy of reactions where experiments were conducted at different temperatures.

# Chapter 3: Oxygen Reduction Reaction (ORR)

## 3.1. Literature

The electrochemical reduction of oxygen has experienced great levels of interest and extensive investigation in the past, both theoretically and experimentally [31, 59, 64-68]. The oxygen reduction reaction is an integral part of the cathodic reaction in fuel cell technology [31, 59, 65, 66, 68-73] as well as metal-air battery technology [59, 70, 71]. If the reaction rate is sufficient, it could be used in many industrial processes as well as for the direct conversion of chemical energy into electrical energy as is the case in fuel cell technology [44, 64, 69, 71].

The direct formation of water from $O_2$ is more desirable as $H_2O_2$ is corrosive and damaging to fuel cells and as more power can be withdrawn from a four electron reduction pathway [73]. For the goal of understanding the catalytic activity of a metal towards the ORR, the fundamentals of the structure and nature of the electrode surface need to be considered [74]. It was also proposed that the catalytic activity of a metal is associated with its effectiveness in breaking the O-O bond so as to form the O-H bond [28, 31, 69].

$$O_2 + 4e^- + 4H^+ \longrightarrow 2H_2O \quad [58] \tag{21}$$

A very interesting phenomenon was found in which the hardness of the metal was directly related to the reactivity of the electro-reduction of oxygen – the lower the physical metal hardness, the higher the reactivity, such as in gold for example, which is characteristically soft [28].

In the literature it is found that the best performance of an electrode is acquired when the electrode surface is conditioned in de-aerated ($N_2$ or Ar saturated) electrolyte, i.e. acidic or alkaline media, by cyclic voltammetry until the voltammograms stabilise [31, 59].

### 3.1.1. Catalyst & Oxygen Reduction Issues

The electro-reduction reaction of oxygen is very complex and might include several different reaction pathways that involve several electrons [28, 67]. Development of effective electrocatalysts to improve the kinetics of the electroreduction of oxygen has not been

achieved as of yet, even though a great deal of effort has been invested in the investigation of the reaction mechanism and catalyst [28, 67]. For a catalyst to be classified as an effective or good catalyst, the O-O bond breaking rate and OH hydrogenation rate should be high [31]. The current status of oxygen electroreduction could be improved by achieving a lower overpotential for the electro-reduction of oxygen [71]. An effective catalyst can also be regarded as one which requires low activation energy for $O_2$ reduction and a reversible potential of each intermediate reaction the same as the potential of the overall four electron reduction process [73].

It has been speculated that because of the high cost of platinum [58] and low availability thereof [49], the noble metals, which include silver, gold, palladium, platinum, rhodium, ruthenium, osmium and iridium, with the latter six metals being known as the platinum group metals (PGM) [75], should be improved scientifically by a factor of four [58] to be able to replace platinum as the most popular noble metal for the ORR [58, 59]. Platinum-free catalysts are thus intensively investigated and present a great challenge [49].

### 3.1.2. Reaction Pathways & Kinetics

There are two main reaction pathways; one pathway consisting of two two-electron transfer steps and one pathway with a four electron transfer step [67, 69, 71]. The two electron reaction leads to peroxide [65, 67, 68, 71], which could be further reduced or decomposed [67, 71] whilst the four electron reduction reaction is only found on few distinct metals used as electrode material forming water [67, 71], as in a sulphuric acid solution for example [65].

The dissociation energy for the O-O bond is 494 kJ/mol whereas the peroxide's dissociation energy is 146 kJ/mol, which accounts for the scarcity of literature coverage regarding the four electron route [67].

In literature there are different possible mechanistic pathways for the electro-reduction of oxygen [28, 74, 76, 77]:

i. A four-electron reduction directly into water ($H_2O$) in acidic media and to hydroxyl anions ($OH^-$) in alkaline media.
ii. A two-electron pathway reducing oxygen to hydrogen peroxide.
iii. A pathway involving a series of two- and four-electron reduction.
iv. A series of reactions i-iii in parallel.
v. A pathway in which the diffusion of species interactively involve a series path into a direct path.

In the literature the mechanism of reaction is still unclear for all the different metals, including platinum [28, 69, 74]. Valdes and Cheh [77] state that the mechanism can be considered as a network of elementary reaction steps that interconnect a set of various chemical species.

### 3.1.3. Aqueous Media Effects

The solution pH plays just as important a role in the ORR as the electrode material [44, 70, 77]. Literature indicates that the cathodic oxygen reduction reaction has a faster and more effective reaction mechanism and electro-kinetics in alkaline media compared to acidic media [48].

On platinum it is well known that sulphate ions in sulphuric acid attach to the molecular adsorption sites of oxygen on the metal surface, which negatively affects the electronic behaviour of the reaction kinetics of the ORR, thus inhibiting the reaction and in turn producing increased amounts of peroxide, unlike perchloric acid which does not adsorb too strongly [31, 49].

Depicted below in reaction scheme (22) is the typical 2 electron reduction reaction of oxygen as can be found in literature for acidic medium [64]:

$$\begin{aligned} &O_2 + e^- \longrightarrow \dot{O}_2^- \\ &\dot{O}_2^- + H^+ \longrightarrow H\dot{O}_2 \\ &H\dot{O}_2 + e^- \longrightarrow HO_2^- \\ &HO_2^- + H^+ \longrightarrow H_2O_2 \end{aligned} \qquad (22)$$

The reduction reaction of oxygen is faster in alkaline medium [30]. Because of this increased rate, a wide variety of cheaper-than-platinum electrode materials can be considered for the ORR.

The most widely accepted reaction mechanism for the electroreduction of oxygen in alkaline media is stipulated in reaction scheme (23) below [63, 78]:

$$\begin{aligned} &O_2 + e^- \longrightarrow \dot{O}_2^- \\ &\dot{O}_2^- + H_2O + e^- \longrightarrow HO_2^- + OH^- \\ &2\dot{O}_2^- + H_2O \longrightarrow O_2 + HO_2^- + OH^- \end{aligned} \qquad (23)$$

The first step where the first electron is transferred is the rate determining step [30].

From the literature, it can be concluded that the electroreduction of oxygen is sluggish if the two electron pathway is followed, as found in acidic and alkaline media, while the four electron direct reduction route is the more effective route [29].

Many authors have investigated the different electrolyte media and have each determined the number of electrons involved in the ORR. The following table lists results acquired by some authors in the literature using Koutecký-Levich or Levich analysis to determine the number of electrons using different electrode materials:

**Table 1: Results from literature for the oxygen electroreduction reaction**

| Source | Electrode Material | Electrolyte Medium | Results |
|---|---|---|---|
| Kullapere *et al.* [78] | GC | 0.1 M KOH | 2 $e^-$ |
| Jeon *et al.* [58] | Platinum-yttrium alloys | 0.5 M $H_2SO_4$ | 4 $e^-$ |
| Maciá *et al.* [79] | Platinum Pt(111) | 0.5 M $H_2SO_4$ & 0.1 M $HClO_4$ | 2 $e^-$ |
| Van Brussel *et al.* [67] | Platinum modified gold | 0.1 M $HClO_4$ | 4$e^-$ |
| Vilambi *et al.* [80] | Platinum (oxidised) | 1.0 M KOH | 2$e^-$ |
| Palitiero *et al.* [81] | Gold (100) with $Pb_{ads}$ | 1 M NaOH | 4$e^-$ |
| Wang *et al.* [69] | $Au_{nano}$ - DNA film on GC | Acetate Buffer pH = 5.2 | 2$e^-$ |
| Andoralov *et al.* [82] | Gold | 0.5 M $H_2SO_4$ | 2 – 4$e^-$ * |
| Erikson *et al.* [59] | Bulk Gold | 0.1 M KOH | 4$e^-$ |
| Zhang *et al.* [73] | Platinum | 0.1 – 1 M acid | 3$e^-$ |

*dependent on the lowest potential the scan was taken to.

As can be seen from Table 1, the different values obtained for the number of electrons transferred in the ORR are very precarious, with many studies done on single crystal surfaces and different catalyst supports. The differences might be attributable to the different preconditioning methods employed and the different nature of each of the alkaline and acidic media [49].

Most of the authors listed in Table 1 have determined Tafel slopes for the ORR in acid and alkaline media on different forms of platinum and gold crystalline structures. On a platinum (111) stepped lattice in acidic medium, Macia *et al.* [79] determined a mass-transport-corrected Tafel slope of 120 mV whereas Van Brussel *et al.* [67] stated a range of -60 - -120 mV for smooth platinum in acidic medium. Rizo *et al.* determined a Tafel slope for Pt(111) in alkaline medium as 70 mV with the value reaching as high as 200 mV for surfaces vicinal to (100) crystal terraces [76]. On a gold electrode, Andoralov *et al.* [82] referenced Tafel slope values in acidic medium from 120 – 180 mV with 120 the more desired value whereas their own determination of the slope was 118 mV. Tafel slopes in literature found for gold in alkaline media was -60 mV for a Au(100) single crystal lattice [81] and -107 mV for bulk gold on a glassy carbon support [59]. Although single crystal lattices were not part of the scope in this study, it could be deduced that the Tafel slope is surface-structure sensitive, especially

in alkaline medium. With the varied Tafel slope values, it should be noted that a large Tafel slope indicates an inhibition effect [76] or sluggish process [23]. Platinum and gold was subsequently investigated in more detail, in the following sections.

### 3.1.4. Platinum

Platinum is currently known in literature as the most electro-active metal for use as an electrocatalyst [65-67, 79] in the ORR, even though it still exhibits a high overpotential for the reaction [65, 66]. Bulk platinum binds oxygen very strongly, which inhibits the ORR because of the build-up of oxygen adsorbed on the electrode's surface, taking up all the available binding positions for new incoming oxygen molecules [31, 74], hence the high overpotential. Platinum has been shown to be the best catalyst with the highest activity towards this $4e^-$ pathway (reaction(21)) of all the pure metals studied in the past [40, 79]. Adsorbed hydrogen can inhibit the adsorption of $O_2$ on the surface [83] and prevent O-O bond scission [79], leading to a two electron reaction mechanism instead of a four electron reaction.

The ORR is very structure-sensitive on platinum [74, 76, 79, 83]. This structure sensitivity affects the reaction sensitivity towards adsorbed anions such as $OH^-$, $ClO_4^-$ and $HSO_4^-$, respectively obtained from the electrolyte media NaOH, $HClO_4$ and $H_2SO_4$ [83].

#### 3.1.4.1. Mechanism and Kinetics

Platinum is one of the few metals in literature found to follow the predominant mechanism involved in the direct four electron electroreduction of oxygen [67, 84].

The mechanistic pathway of platinum in acidic medium was found to take place via a series of either two two-electron transfer reactions [84] or the direct four electron pathway [67, 84]. Electrochemical cycling of a platinum electrode in acidic medium may deactivate the electrode surface for the oxygen reduction reaction [67].

Until now, there have not been many studies of the ORR in alkaline medium [76, 85]. Vilambi *et al.* [80] stated that the authors that had studied the ORR in alkaline medium had found different results for the number of electrons transferred, being either two or four [77, 80], regardless of the oxidised state of the electrode surface. Consequently, there is a large degree of uncertainty with regard to peroxide formation [80] and mechanistic pathways [77].

The kinetics of the ORR on platinum is also affected by the formation of a platinum hydroxyl bond (Pt-OH) [67]. Adsorbed hydroxide (OH) on the surface of the platinum electrode has been shown to inhibit the electroreduction reaction of oxygen by blocking binding sites [31, 76, 86] as well as through electronic effects [31]. The active sites on platinum are the sites not occupied by adsorbed OH as to allow $O_2$ to bind for reaction, with the interaction of OH

with $O_2$ repulsive in nature on a platinum surface [76]. Rizo *et al.* [76] have found that the OH involvement in the reaction mechanism should not be disregarded, regardless of many findings and theories that OH acts as an ORR inhibiter. For alkaline medium, electrochemical scans were found to have a much lower potential difference between the forward and backward direction for hysteresis to form [67] as described in section 2.1.1., thus proving the influence of OH on the electrode effectiveness.

According to literature, the improved activity of Platinum for the ORR in alkaline medium is due to less steric hindrance of the $O_2$ adsorption process by $OH^-$ while the size of the complex oxy-anions in acidic media ($ClO_4^-$ and $HSO_4^-$), hampers the adsorption process, with the difference in the reaction mechanism also playing a role in the enhanced activity [83].

The performance of platinum towards the ORR in alkaline and acidic media is expected to be similar although literature has found many differences significantly affecting the reactivity, especially regarding the different crystal lattices [76].

### 3.1.5. Gold

According to literature, the ORR pathway on gold is dependent on the reaction pH, and electrode potential as well as the surface structure [72]. The bond strength of oxygen on the surface of gold strongly affects the reaction kinetics of the ORR, which implies that the ideal bond strength should not be so strong that oxygen cannot escape after reaction or so weak that oxygen escapes before effective reduction [49].

#### 3.1.5.1. Mechanism and Kinetics

Gold was found to be electrochemically inactive for the electro-reduction of oxygen in acidic media [31, 49] or to have a modest activity at the very least [59] even though studies were done on gold in acidic media with relative success in literature, showing that gold is active as an electro-catalyst in both alkaline and acidic media [81]. The mechanism of oxygen reduction enjoyed intense interest in acidic medium as many authors produced results that differ greatly from one another [82]. The deviations of the results might be due to the different electrode preparation techniques employed.

The following reaction scheme (24) demonstrates the ORR when a transfer of either two or four electrons takes place in acidic medium [82]:

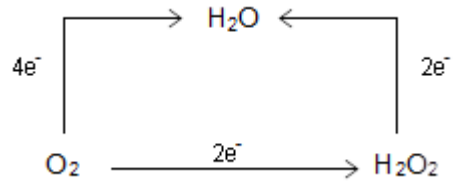


(24)

The ratio of crystal planes on a polycrystalline gold electrode, has an effect on the reaction kinetics and consequent mechanism [82]. Because of this structure sensitivity, it is insufficient to consider the ORR as a simple reaction that involves two electrons [82].

In alkaline medium, the oxygen electro-reduction reaction is highly dependent on the oxidised state of the gold electrode surface [87]. If the electrode surface has been reduced, the electro-reduction reaction of oxygen reaches a diffusion-limited current density plateau in the potential scan whereas the oxidised state of the gold electrode produces a well-defined maximum peak before decreasing in current density and reaching a diffusion-controlled plateau in the reduction area of the polarisation curve [87]. The well-defined maximum could be a result of species dissociating from the gold surface, which in turn facilitate the further reduction of species such as $HO_2^-$ at that maximum. As $HO_2^-$ is produced from the reduction reaction of oxygen, it can once again be oxidised in a reverse potential sweep to produce oxygen if all the dissolved oxygen has not been reduced to OH.

In general the number of electrons transferred for a polycrystalline gold electrode in alkaline medium is 2, which results in $HO_2^-$ (reaction (25)) being the final product [40, 63, 70].

$$O_2 + H_2O + 2e^- \longrightarrow HO_2^- + OH^- \quad (25)$$

As $OH^-$ concentration increases so too does the peak current, which shows the importance of the $OH^-$ in the catalytic reduction of oxygen [63].

The electrochemical reduction of oxygen has attracted a lot of attention because of the application in fuel cell technology especially on a gold surface, which was shown to be very structure sensitive in a basic/alkaline medium [40, 49, 59]. The structure sensitivity was first reported for single crystal electrode surfaces, which indicated how immensely sensitive the reaction was towards the surface morphology [40, 49, 59, 65, 88]. The Au(100) crystal surface was shown to deliver an amount of 4 electrons [40, 63, 65] to the reduction reaction with the main yield of product in alkaline medium being $OH^-$ (reaction (26)) [40, 72].

$$O_2 + 2H_2O + 4e^- \longrightarrow 4OH^- \quad (26)$$

## 3.2. Experimental Procedure

### 3.2.1. Instrumentation and Kits

All experiments were conducted at room temperature (25 °C) and controlled by a Julabo F12 ED-refrigerated waterbath. The counter electrode consisted of a 15 cm L-coiled platinum wire from Pine Research Instrumentation. The working electrodes consisted of a smooth gold disc electrode from Pine Research Instrumentation and a smooth platinum disc electrode also from Pine Research Instrumentation with a surface area of 0.196 $cm^2$ for each electrode. The reference electrode was a saturated calomel electrode from Radiometer Analytical with a relative potential of 0.241 V *vs.* NHE.

The polishing kit used for polishing of the electrodes consisted of either Alpha Micropolish Alumina 5 µm & 0.05 µm from Buehler or 5µm Aluminium Oxide Polishing Solution & 0.05 µm Alumina Suspension from Allied High Tech Products Inc.

The electrodes were screwed onto a rotating shaft positioned on a rotating motor from Pine Research Instrumentation, and linked to a digital Motor Rotating Electrode Speed Control from Pine Research Instrumentation. The electrode rotating motor and all the electrodes were connected to a VSP potentiostat from Biologic Science Instruments, which was in turn connected to a desktop with EC-Lab V10.21 software and newer.

The ultrasonic bath used to dissolve reagents or clean the electrodes after polishing was a Digital Ultrasonic Cleaner PS-10A from Jeken. The weighing balance used for weighing reagents and chemicals was a Mettler Toledo NewClassic MS 205 DU.

All solutions were made up using 18.2 MΩ.cm Milli-Q water produced by a Millipore Milli-Q PLUS Ultra-pure Water System.

### 3.2.2. Reagents

The following reagents were used for the experiments: absolute ethanol (UnivAR from Merck) to be used for the EOR, medical grade oxygen gas (from Afrox) for the ORR and High Purity $SO_2$ gas (from Afrox) for the SDOR as well as anhydrous sodium sulphite (Platinum Line AR grade from Associated Chemical Enterprises – (ACE)) dissolved in diluted solutions of 95-99% Sulphuric Acid (UnivAR from Merck). The electrolytes for ORR and EOR were made from diluted solutions of 70% perchloric acid (Platinum Line AR grade from Associated Chemical Enterprises – (ACE)) for the acidic media, and potassium hydroxide pellets (UnivAR from Merck) for the alkaline media. The nitrogen gas was high purity grade (from Afrox), which was used to de-aerate all the electrolytes before experimentation.

### 3.2.3. Experimental Setup

The following diagram depicts the typical electrochemical experimental setup used for all experiments in this project (Figure 10):

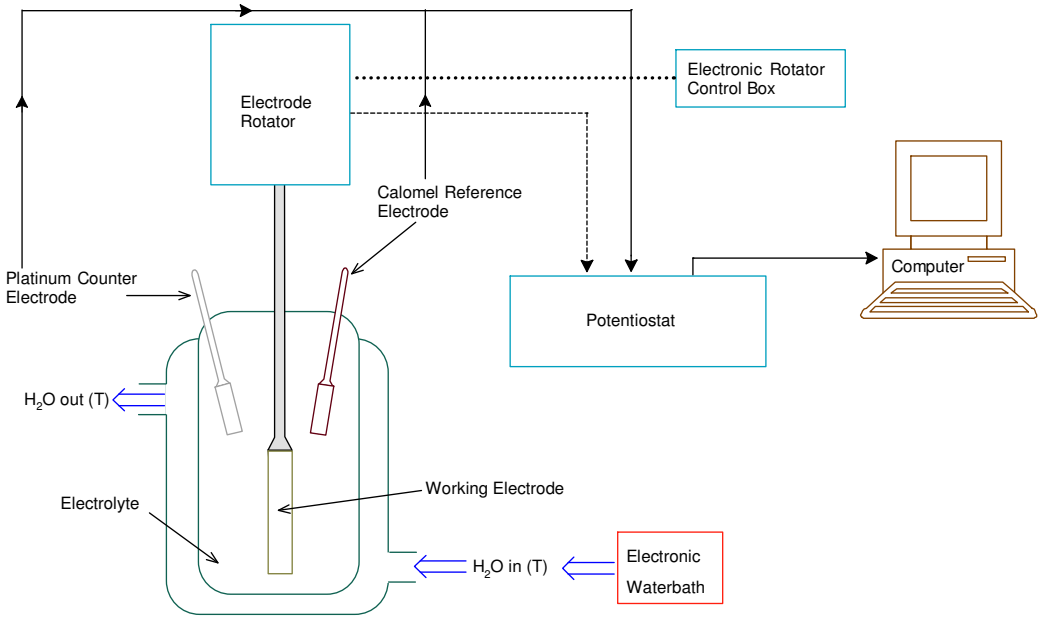


Figure 10: Experimental Setup

### 3.2.4. Experimental Procedure

Before electrochemical experiments were done, the electrodes were polished and cleaned as described in the following section.

#### 3.2.4.1. Polishing Procedure

Using the polishing kit described in section 3.2.1, the electrode being tested was polished in the following manner: The working electrode was rinsed with Milli-Q water with the excess water shaken off. It was then polished on a wet nylon mat by rubbing the electrode's metal surface in contact with the mat in a figure eight movement for 40 repeats, after which it was dried. The same figure eight movement was used to polish the electrode on a fibre mat with a big drop of 5µ alumina gel and then wiped clean. The final polishing step was done on a fibre mat with a big drop of 0.05µ alumina gel and rinsed with Milli-Q water after polishing. To ensure cleanliness, the electrode was sonicated for 5 minutes in the Jeken ultrasonic bath. For the subsequent electrochemical experiments, the electrode needed to be preconditioned as described in the following section.

### 3.2.4.2. Preconditioning Procedure

After polishing, preconditioning of the electrode was done in the inert electrolyte which the investigated reaction showed activity in, according to the best-suited preconditioning method. After preconditioning, the electrode was rinsed and placed into the acid or alkaline electrolyte of investigation filled with the reagent being investigated. All gaseous reagents were bubbled through the electrolyte until the solution reached saturation of the gas. A cyclic voltammogram was conducted in the pure, inert electrolyte and another then in the electrolyte containing the reagent, to see whether the electrode showed any prominent activity towards the reagent contained in solution. The different reactions were investigated at different rotation rates to eliminate the mass transfer reaction inhibition effects during the LP runs. All the following experiments were conducted at room temperature of 25 ℃.

Gaseous reagents, such as oxygen, was set to flow over the surface of the electrolyte solution in which it was dissolved, so as to maintain the saturated concentration [68]. Bubbling of oxygen gas through the electrolyte solution was thus carried out for 10 minutes to ensure the solution was saturated with oxygen. In this chapter, the reduction of oxygen was studied in acid and alkaline media for both platinum and gold.

### 3.2.4.3. Platinum

For the ORR investigation in acidic medium on platinum, the experimental procedure was executed as follows: The electrode was polished and then preconditioned in an inert 0.1 M $HClO_4$ solution at 50 mV/s scan rate until the voltammogram stabilised and produced repeatable *CV*s within the fingerprint area of the voltammogram for platinum, which included the potential range of 1.159 V – -0.241 V *vs.* SCE. After preconditioning, control *CV*s with and without $O_2$ in solution was run in the same voltage range as the preconditioning voltage range with the difference being the scan rate of 10 mV/s. The scan was started at 1.159 V *vs.* SCE and ran in a reducing direction up until -0.241 V *vs.* SCE. The *LP*s were run at 25 ℃ for rotations of 0, 100, 400, 900 and 2500 *RPM*s at a scan rate of 10 mV/s starting from 0.959 V *vs.* SCE down to -0.241 V *vs.* SCE in 0.1 M $HClO_4$ saturated with $O_2$ gas.

In alkaline medium the ORR experiments were done by starting with the preconditioning as described in section 3.2.4.2 after electrode polishing (section 3.2.4.1) in 0.1 M KOH within the fingerprint area of the CV with a scan rate of 50 mV/s until the voltammogram stabilised or became repeatable in the potential range of -1.018 V – 0.231 V *vs.* SCE. The *CV*s used to check the reaction with and without saturated $O_2$ in solution were run in the same potential range as the preconditioning *CV*s for 5 cycles at a scan rate of 10 mV/s. Subsequent *LP*s were then respectively run in fresh 0.1 M KOH solution saturated with $O_2$ gas for every

repeat and rotation rate, scanning at a rate of 10 mV/s starting from 0.155 V down to -0.895 V *vs.* SCE for every rotation rate of 0, 100, 400, 900 and 2500 RPM. After all the platinum experiments were run, gold was the next electrode material to be investigated.

#### 3.2.4.4. Gold

Acidic medium was investigated first. As with platinum, polishing of the gold electrode (section 3.2.4.1) was done after which preconditioning was executed in a 0.1 M $HClO_4$ solution at 50 mV/s starting from the open circuit potential up to 1.6 V and down to 0.1 V *vs.* SCE, which then ended at 0.1 V for 10 cycles. A subsequent CA was performed at -0.45 V *vs.* SCE for 2 minutes. In a fresh 0.1 M $HClO_4$ solution without oxygen, a CV was done after electrode preconditioning to show the electrode behaviour without reagent. The CV was set to start at the open circuit potential up to 1.6 V and down to -0.55 V *vs.* SCE at 10 mV/s for 5 repeats. All the steps above were repeated with a fresh $HClO_4$ solution saturated with oxygen gas to show the behaviour of the electrode in oxygen-containing solution. To study the subsequent electrode activity, fresh $HClO_4$ solutions were used, and after preconditioning, the reaction was studied with *LP*s starting at 0.3 V down -0.55 V *vs.* SCE at 10 mV/s repeated until repeatable results were produced. The electrode rotations investigated consisted of 0, 100, 400, 900 and 2500 RPM. After these experiments, gold was investigated in alkaline medium.

As with acidic medium, after polishing and cleaning of the electrode (section 3.2.4.1) it was preconditioned in an inert 0.1 M KOH solution at a scan rate of 50 mV/s for 10 cycles, starting from 0.0 V *vs.* OCP (ca. -0.1 V *vs.* SCE) up to 0.6 V *vs.* SCE down to -1.021 and up to 0.6 V *vs.* SCE. A CA was then run for two minutes at -1.2 V *vs.* SCE in the same preconditioning solution to ensure a reduced electrode surface. Subsequently a fresh inert 0.1 M KOH solution was used for a CV to show how the electrode would behave in a solution without $O_2$ by scanning at 10 mV/s for 5 cycles starting from 0.0 V up to 0.6 V then down to -1.5 V and ending at 0.6 V *vs.* SCE. These cycles were repeated at 10 mV/s, for $O_2$ gas that was bubbled in a fresh 0.1 M KOH solution until the solution was saturated, then followed by 5 CV cycles in the potential range of 0.6 V down to -1.5 V, which ended at 0.6 V *vs.* SCE so as to show the electrode behaviour with reagent dissolved in solution. After the electrode behaviour was analysed, preconditioning was done once again for each and every rotation rate and repeat thereof, followed by a CA after which *LP*s were done at 10 mV/s starting the scan from 0.0 V down to -1.5 V *vs.* SCE in a fresh 0.1 M KOH solution for every LP with saturated $O_2$ gas in solution. The *LP*s were investigated at 0, 100, 400, 900, 1600 and 2500 RPM.

As smooth, polycrystalline platinum and gold were used in this study, the crystalline structure needed to be confirmed by using XRD testing.

### 3.2.5. Third Party XRD Testing

The platinum and gold electrodes were sent to the North-West University Geology department (Geo XRD & XRF LAB) for XRD analysis of the electrode surface crystal structure. The department used a zero-background silica disc for the analysis of the sample on an X'Pert Pro XRD instrument with a copper (Cu) tube. Their software package to identify the different phases was the X'Pert Highscore plus software with the ICDD database being used as reference.

## 3.3. Results and Discussion

Polishing of the electrode is important so as to remove any impurities from the electrode surface that cannot be removed by electrochemical oxidation or reduction alone. After polishing, electrochemical preconditioning ensures starting with a repeatable surface so as to produce more repeatable electrochemical results. Electrode preconditioning can give reproducibility of the different peaks in the voltammogram but not of the same surface roughness of the electrode [33].

### 3.3.1. XRD Results

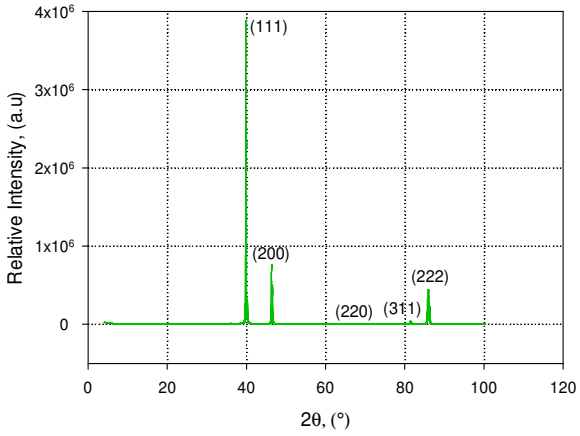


Figure 11: XRD for polycrystalline platinum, indicating the different crystal planes

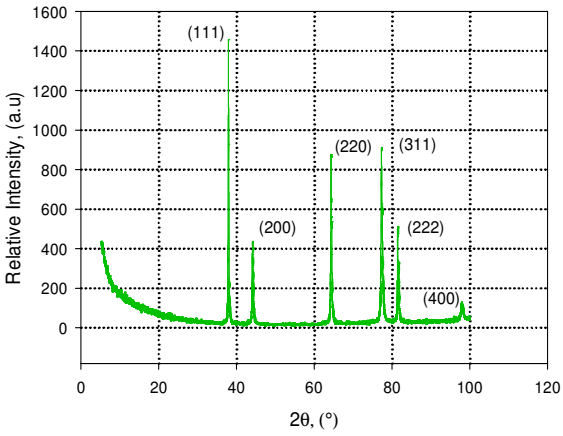


Figure 12: XRD for polycrystalline gold with the different crystal planes indicated

Depicted in Figure 11 and Figure 12 are the XRD patterns for polycrystalline platinum and gold respectively. The (111) crystal lattice is the most dominant in the surface lattice for both platinum and gold, hence the high relative diffraction peak intensity. The XRD pattern visible

in Figure 11 for platinum corresponds very well with literature [89] as does the pattern of gold in Figure 12 [90, 91]. It can thus be confirmed that both electrodes are polycrystalline.

### 3.3.2. Preconditioning

The following subsections contain the preconditioning graphs for every electrode in acidic and alkaline media. Any deviation from it will be pointed out and showed under each reagent reaction's section. Also, any reference made to onset potential and determination thereof, will directly imply graphical determination.

For all preconditioning steps for both electrodes the CV cycles were repeated at least 10 times or until the voltammograms became reproducible. The preconditioning was executed after the electrode was polished and sonicated as described in section 3.2.4.2.

#### 3.3.2.1. Acidic

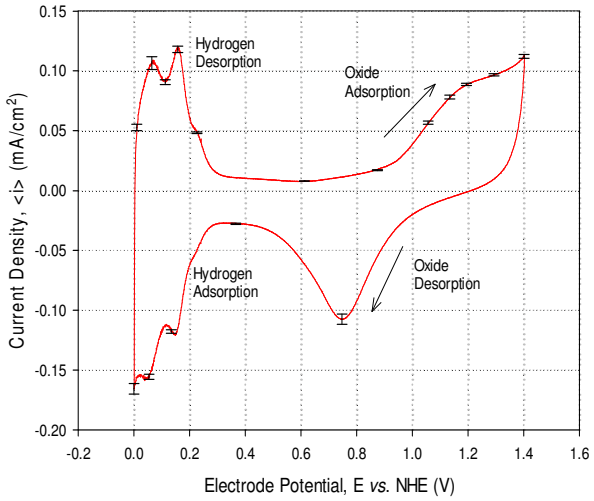


**Figure 13: A typical preconditioning CV representation for Pt in 0.1 M HClO4 averaged over the 10th, 15th and 19th cycles at a scan rate of 50 mV/s initially starting the scan at the OCP of 0.875 V**

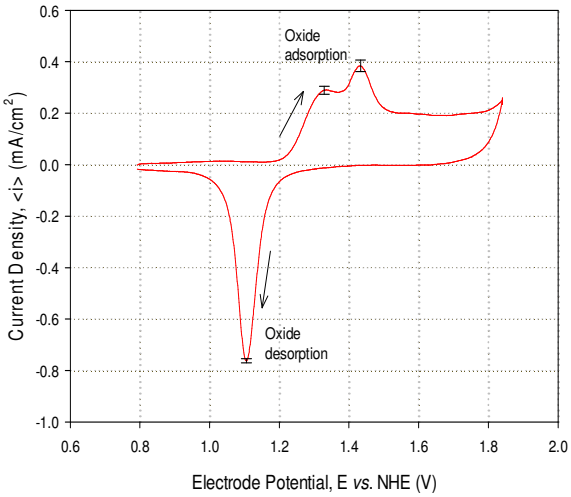


**Figure 14: A typical preconditioning CV representation for Au in 0.1 M $HClO_4$ averaged over the 10th, 15th and 21st cycles at a scan rate of 50 mV/s initially starting the scan at the OCP of 1.1 V**

Refer to section 2.1 for a detailed discussion on the chemical reactions involved in the hysteresis of the voltammograms for both platinum and gold as depicted in Figure 13 and Figure 14 respectively. The preconditioning *CV*s in Figure 13 and Figure 14 show the respective behaviour of Pt and Au in acid medium. The oxide formation and hydrogen adsorption areas are clearly visible in each voltammogram. For Pt, the oxide adsorption starts in the potential range of ca. 0.8 V and 1.0 V, reaching a maximum peak at about 1.2 V *vs.* NHE, whereas the gold oxide adsorption peak starts at ca. 1.2 V *vs.* NHE with the

desorption of oxide starting to occur at about 1.1 V for platinum. A maximum peak is reached at about 0.75 V *vs.* NHE in the reverse scan for Pt and from ca. 1.1 V *vs.* NHE for gold.

On the platinum electrode, the hydrogen adsorption and desorption potential range is between 0.3 V down to 0.0 V *vs.* NHE. Hydrogen adsorption starts from about 0.3 V, reaching several shouldered peak maxima approaching 0.0 V *vs.* NHE with desorption of hydrogen occurring immediately with the forward scan in the oxidative current direction with two distinct oxidation maxima occurring right before the big decline in current density at ca. 0.3 V *vs.* NHE.

According to literature, as described in section 2.1, and equations (6) - (8) for platinum and equations (9) – (11) for gold, the hysteresis is because of oxide film formation on the surface of the gold [33, 41, 45, 46] and platinum [23, 26] electrode surfaces. The oxide formation in acidic medium does not take place as readily as in alkaline media as there is a lack of hydroxide ions in solution to promote the oxide formation because in acidic media, water needs to adsorb and then be changed into hydroxide before the process described in equations (6) – (11) can take place. The reverse of equations (6) – (11) takes place in the reverse scan as the oxide layer is being reduced to produce a reduced electrode surface crystal lattice. On gold, the double peak in the forward scan can be attributed to the different crystal surfaces.

Once the voltammogram of each electrode stabilised, it was ready to be used for the subsequent analytical experiments.

#### 3.3.2.2. Alkaline

Refer to section 2.1 for background into the hysteresis and the chemical reactions involved with equations (6) - (8) (for platinum) and equations (9) – (11) (for gold) demonstrating the chemical reactions behind the hysteresis.

The potentials used for the preconditioning CV of platinum in Figure 16 were set to start at the OCP (ca. 0.0 V) up to 0.472 V and back down to -0.779 V *vs.* NHE at 50 mV/s while the vertex potentials for gold in Figure 17 were set to the maximum of 0.841 V *vs.* NHE and the minimum vertex as -0.78 V *vs.* NHE with cycling started at -0.78 V *vs.* NHE at a scan rate of 50 mV/s. The cycles for both electrodes were repeated for at least 10 cycles or until the voltammograms became reproducible. In Figure 16 the oxide adsorption and desorption as well as the hydrogen adsorption and desorption areas can be clearly seen as described in section 2.1.1. The voltage range for oxide adsorption and desorption is from ca. -0.2 V up to 0.472 V and the hydrogen adsorption and desorption is from about -0.3 V down to -0.779 V *vs.* NHE. The fingerprint character of platinum can be clearly recognised in the CV. In Figure

17 the oxide adsorption peak on gold starts at about 0.4 V *vs.* NHE reaching a high of ca. 0.135 mA/cm$^2$ at 0.5 V *vs.* NHE. In the reverse scan the oxide desorption peak commences at about 0.6 V *vs.* NHE reaching a peak current density of ca. -0.2 mA/cm$^2$ at about 0.35 V *vs.* NHE.

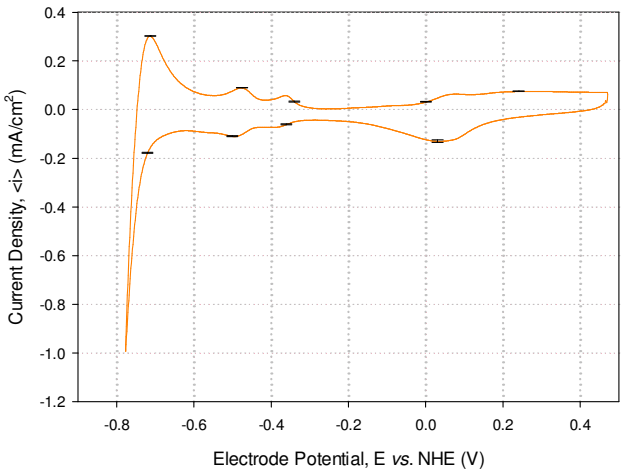


**Figure 15: The typical resemblance of a CV for preconditioning of platinum in 0.1 M KOH**

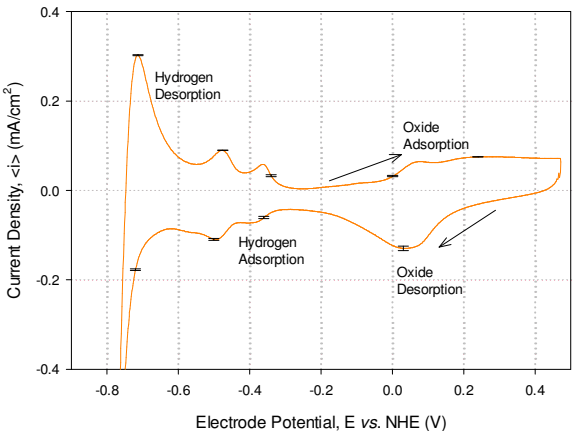


**Figure 16: The preconditioning CV of platinum in 0.1 M KOH averaged over cycles 10, 15 and 19 with the initial scan starting at the OCP of 0.0 V at a scan rate of 50 mV/s with the y-axis ranged reduced from the voltammogram depicted in Figure 15**

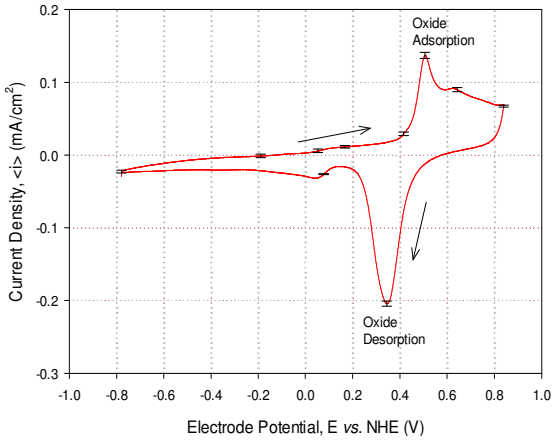


**Figure 17: The preconditioning CV of gold in 0.1 M KOH averaged over cycles 10, 16 and 21 with the initial scan starting at -0.78 V at a scan rate of 50 mV/s**

The oxide adsorption and desorption is more facile in alkaline than acidic medium, as can be seen by the potential at which the oxidation current starts to appear on the voltammograms. Acidic media require a much higher potential for the adsorption process to start compared to alkaline media, which is clearly in support of literature findings [45, 46] for both platinum and gold. The difference in current density between acidic and alkaline oxide formation on gold can be attributed to the fact, as stated in literature [31], that gold binds hydroxyl anions

weakly, thus the lower current density for oxide formation on gold in alkaline medium compared to acidic medium regardless of the lower overpotential required to drive the oxide formation in alkaline medium.

After preconditioning, both the electrodes were investigated using *CV*s with and without oxygen in order to ascertain whether or not the electrodes showed activity towards the ORR in acid and alkaline media.

### 3.3.3. Acidic

The ORR in acidic media is discussed here for platinum and gold in comparison.

#### 3.3.3.1. Effect of Reagent in Solution

The *CV*s displayed in Figure 18 and Figure 19 for platinum and gold includes a CV with saturated $O_2$ in solution and a CV without saturated $O_2$ in solution. Note that for eligibility purposes, the scale of the y-axes is not the same.

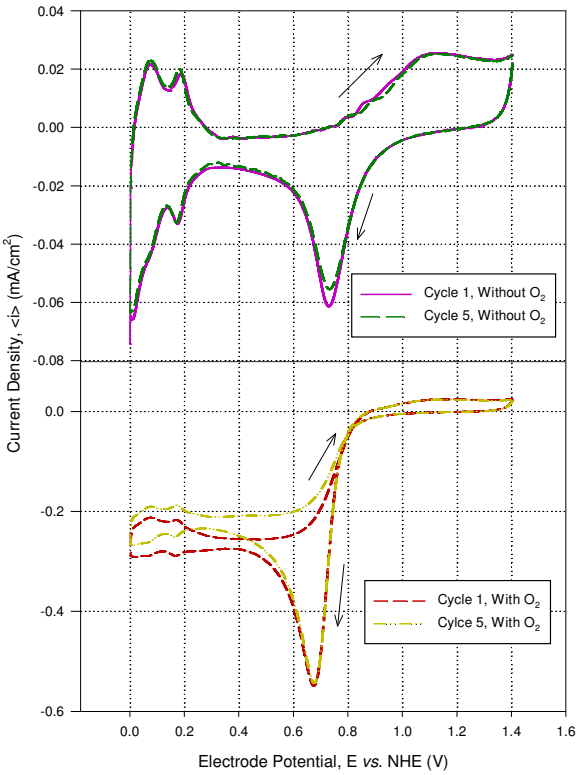


**Figure 18: Control *CV*s for the reduction of oxygen on Pt in 0.1 M $HClO_4$ with and without $O_2$ at 0 RPM and 10 mV/s scan rate at 25 °C**

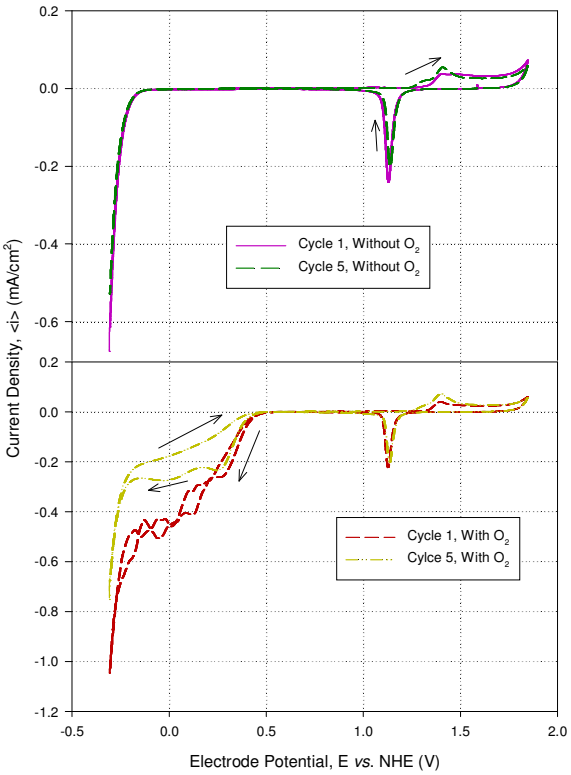


**Figure 19: Control *CV*s for the reduction of oxygen on Pt in 0.1 M $HClO_4$ with and without $O_2$ at 0 RPM and 10 mV/s scan rate at 25 °C**

The scans for platinum were initiated at 1.4 V and ran in a reducing direction up until 0 V *vs.* NHE with the scans of gold initiated at 0.58 V. The reduction of oxygen on platinum starts

together with the potential of the oxide reduction or desorption potential of ca. 1.1 V *vs.* NHE and reaches a maximum peak at ca. 0.67 V *vs*. NHE, reaching a current density of ca. -0.55 mA/cm$^2$ with a large decrease in current density reaching a steady diffusion-limited current density plateau down to 0.0 V *vs.* NHE with a current density maximum approaching -0.3 mA/cm$^2$. On the gold electrode, the current density starts to increase in a reductive or cathodic direction at ca. 0.45 V *vs.* NHE reaching a shoulder at about 0.27 V *vs.* NHE for the first cycle and a shoulder at ca. 0.26 V *vs.* NHE for the fifth cycle. The reaction reaches an increase in current density where water reduction occurs at about -0.309 V *vs.* NHE. For both electrodes, when the *CV*s with saturated $O_2$ are compared to the *CV*s without $O_2$ in acidic media, it is clear that each electrode is active towards the electro-reduction of oxygen.

The scan on platinum from 1.4 V down to 0.0 V *vs.* NHE shows clearly that the current density for the oxygen reduction increases together with the current that would flow for the reduction of the electrode surface, otherwise known as the oxide desorption. This corresponds to literature's indication that the surface needs to be in a reduced state to be effective for the ORR [31, 74] as oxygen binds strongly on the electrode surface, consequently inhibiting the ORR by decreasing the available adsorption sites for subsequent oxygen reduction. Gold, on the other hand, shows the reduction of oxygen taking place on a reduced gold electrode surface as the surface oxide had been reduced at ca. 1.1 V *vs.* NHE (section 2.1.2 and equations (9) to (11)) [33, 41, 45, 46]. When Figure 18 and Figure 19 are compared, it is clear that the reduction of dissolved oxygen occurs together with the adsorbed oxide reduction on platinum, whereas the gold's adsorbed oxide reduction takes place at a much higher potential than the reduction of dissolved oxygen with a difference of slightly more than 0.5 V.

In the forward scan for platinum, the reductive current turns to oxidative current right before the oxide adsorption potential (from ca. 1.0 V *vs.* NHE). Even with the saturated oxygen solution the current density of the oxide adsorption did not show any apparent increase. Gold however, showed a slightly higher current density for the $O_2$-containing solution at the oxide formation region in the forward scan from ca. 1.25 V *vs.* NHE, indicating that the presence of oxygen in the solution catalyses the oxide layer formation on the surface of the gold electrode, as stated in literature [42, 45, 46].

It is therefore clear that the ORR on platinum prefers a reduced electrode surface without any adsorbed oxide on the electrode surface as is the case in literature [67] as well as gold. An interesting observation is that the hydrogen adsorption and desorption peaks corresponding to the electrochemical crystal lattice behaviour of the platinum surface within the hydrogen adsorption and desorption fingerprint voltage areas (demonstrated in Figure 6

of section 2.1.1) are very clear in the oxygen containing voltammogram of Figure 18, from ca. 0.2 – 0.0 V *vs.* NHE.

According to literature, platinum is the best catalyst for the ORR to form water [65-67, 79]. Therefore it can be concluded that the well-defined maximum peak at ca. 0.67 V *vs.* NHE is the reduction of oxygen. As for gold, the first shoulder in the current density at ca. 0.26 V *vs.* NHE might be due to the reduction of $O_2$ to $H_2O_2$ [82] and the small peak at 0.0 V the further reduction of $H_2O_2$ to $H_2O$ as depicted in reaction scheme (24) in section 3.1.5.1. As the potential is taken fairly low, the latter might be possible as a very low overpotential drives the peroxide reduction.

### 3.3.3.2. Effect of Rotation Rate

After electrode cleaning (section 3.2.4.1) and preconditioning (Figure 13 and Figure 14, in section 3.3.2.1) between every experiment, the following *LP*s were produced for platinum and gold, plotted in Figure 20 and Figure 21 respectively:

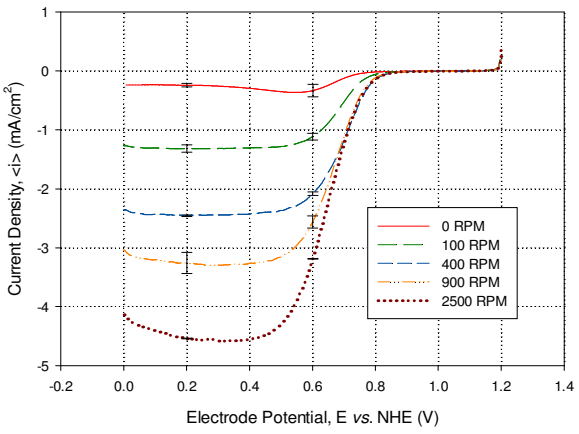


**Figure 20: Comparison of Pt *LP*s at different rotation rates in 0.1 M perchloric acid with saturated oxygen at a scan rate of 10 mV/s**

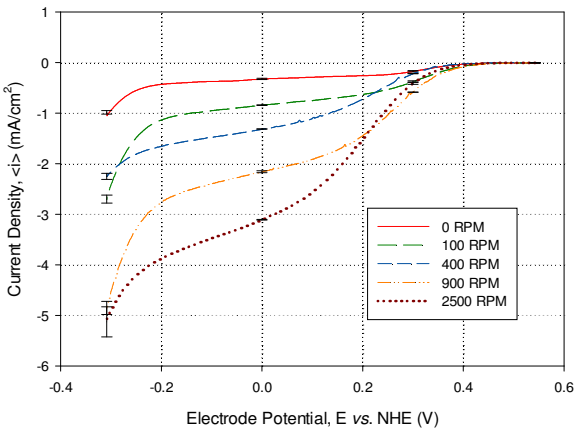


**Figure 21: Comparison of Au *LP*s at different rotation rates in 0.1 M perchloric acid with saturated oxygen at a scan rate of 10 mV/s**

The *LP*s of platinum and gold in 0.1 M perchloric acid solution saturated with oxygen at different rotation rates are depicted in Figure 20 and Figure 21 respectively, with each metal showing a clear increase in current density as the rotation rate of the electrode increases. The platinum *LP*s reaches a limiting current density plateau, as was found in literature [31], with gold exhibiting almost the same behaviour with a slight continuous increase in current density as the potential reaches the end of the scan, which is indicative of a mixed control reaction as there is no limiting diffusion controlled current, which was the case as found in literature [82].

The current density starts to increase from ca. 0.8 V *vs.* NHE for all rotation rates, reaching a high at ca. 0.4 V *vs.* NHE for 2500 RPM for platinum with the reduction of dissolved oxygen, on a reduced gold electrode surface, beginning from ca. 0.4 V *vs.* NHE with no apparent maximum peak reached as there is no limiting diffusion controlled current. Many authors in literature have found contradicting results for gold in acid medium, to which Andoralov *et al.* [82] attributed the different electrode preparation techniques employed by different authors.

In Figure 20, when rotation rates are implemented with a platinum electrode, the current density experiences a decrease from ca. 0.2 V to 0.0 V *vs.* NHE with the 100 and 400 RPMs only experiencing the decline much closer to 0.0 V. According to literature this is hydrogen adsorption inhibiting the ORR, which might account for the decline in reductive current density [79, 83]. From Figure 20 it is clear that the effect of hydrogen inhibition is much more apparent at higher rotation rates. The ORR depicted in Figure 21 on gold, might consist of the simultaneous reduction of $O_2$ to $H_2O_2$ and $H_2O_2$ to $H_2O$ as found in literature and depicted in reaction scheme (24) in section 3.1.5.1 as there is no limiting diffusion controlled current.

As the *LP*s in Figure 20 and Figure 21 show a linear increase in current density with increasing rotation rate the Koutecký-Levich and Levich equations could be applied, as the reaction is clearly diffusion or mass transfer limited. Gold does not show a steady linear increase in current density in the mixed control region of the *LP*s in Figure 21 with LP crossover in the mixed control region, which might restrict the application of the Koutecký-Levich and Levich equation.

#### 3.3.3.3. Tafel Plots

The Tafel Slopes for the ORR on platinum and gold in 0.1 M $HClO_4$ as depicted in Figure 22 and Figure 23 respectively, was calculated as -205 mV/decade for platinum and for gold as -129 mV/decade. The potential regions of the *LP*s from Figure 20 and Figure 21 for the Tafel plots were chosen by the region of Tafel behaviour as described in section 2.3.1. The literature value for the mass transport corrected Tafel slope is ca. 120 mV for nano-crystalline Pt(111) [79]. The platinum in this study was polycrystalline in nature, which might account for the difference noted between the calculated and literature values. In this study, on the platinum electrode, the Tafel slope decreased as the electrode rotation rate increased (plots not shown), which act as support of the mass transfer limitation, ultimately implying the ORR is less sluggish with less mass transport inhibition. This decrease might also indicate more than one reaction pathway being followed [82] by platinum with regards to the ORR. Literature values for the Tafel slope on polycrystalline gold varies greatly with Andoralov *et*

*al.* [82], establishing a value of 118 mV, which is close to the calculated value for gold in this study.

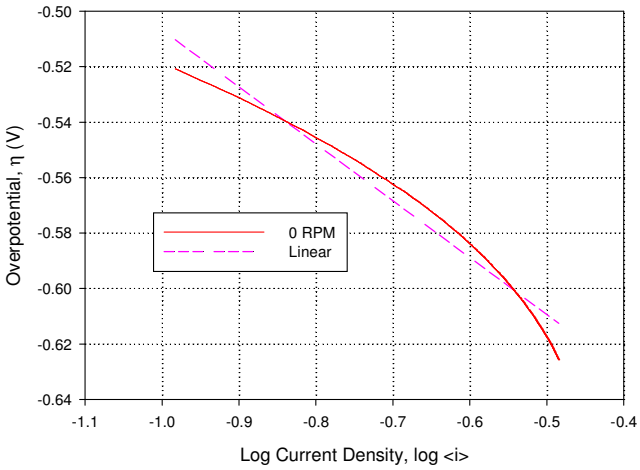


**Figure 22: Tafel plot of ORR for Pt in 0.1 M $HClO_4$ at 0 RPM taken from the potential range of 0.709 – 0.604 V *vs.* NHE with an $R^2$ of 0.966**

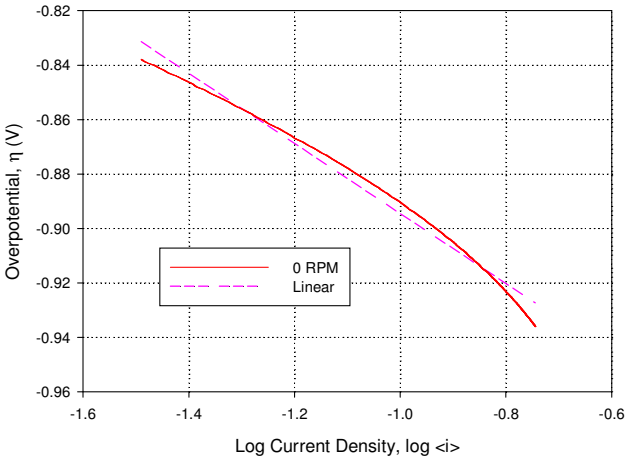


**Figure 23: Tafel plot of ORR for Au in 0.1 M $HClO_4$ at 0 RPM taken from the potential range of 0.392 – 0.294 V *vs.* NHE with an $R^2$ of 0.984**

### 3.3.3.4. Koutecký-Levich Plots

In Figure 24 below the Koutecký-Levich plots are given for platinum. For gold it can be concluded from Figure 21 that the application of the Koutecký-Levich plots would not be viable as the different rotation rates showed an overlap in the mixed control regions of the *LP*s.

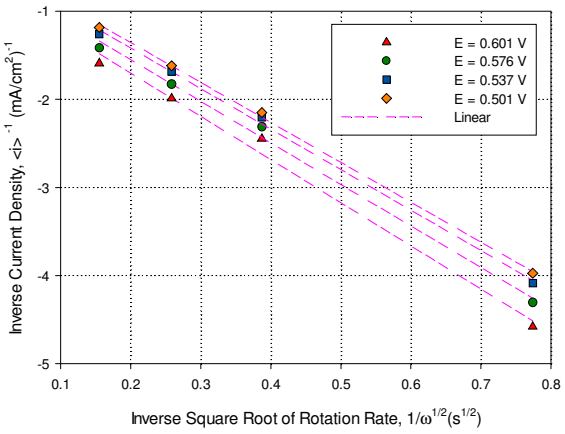


**Figure 24: Koutecký-Levich plots for Pt in 0.1 M $HClO_4$ and saturated $O_2$ gas, based on the results from Figure 20**

Even with extensive repeats on gold, results with less overlapping could not be produced. The parallelism of slopes in Figure 24 is indicative of a single mechanism being followed in the mixed control region of the ORR [53, 81, 85]. The lack of linearity of plots in Koutecký-

Levich plots is also indicative of a change in the mechanism with increasing potentials or rotation rates. In Figure 24 it can be seen that the plots for E = 0.601 V do not show linearity as those of the E = 0.501 V plots do. It might be possible that the mechanism does not follow a single mechanism in the mixed control region of the *LP*s. The mechanism was not part of the scope of this study, therefore, no further in-depth investigation was done in that regard.

The calculated number of electrons for the ORR on platinum is given in Table 2.

**Table 2: Summarised results of the Koutecký-Levich plots in Figure 24**

| **Potential used (E *vs.* NHE)** | **Corresponding Slope (1/mA.s$^{-1/2}$)** | **Number of electrons** |
|---|---|---|
| 0.601 | -4.900 | -2.9 |
| 0.576 | -4.716 | -3.1 |
| 0.537 | -4.595 | -3.1 |
| 0.501 | -4.531 | -3.2 |
| | Average Electrons: | -3.1 |

The values for the variables used in the Koutecký-Levich equation (18) can be found in Table 20 to Table 23 (Appendix 1 – Data). The relevant values are summarised below in Table 3.

**Table 3: Values for variables used in the Koutecký-Levich calculations**

| | |
|---|---|
| **Kinematic Viscosity (cm$^2$/s)** | $8.93\times10^{-03}$ [60] |
| **Diffusivity (cm$^2$/s)** | $2.42\times10^{-05}$ [60] |
| **Radius (cm)** | $2.50\times10^{-01}$ |
| **Faraday Constant (mA.s/mol)** | $9.65\times10^{7}$ |
| **Concentration Sat. $O_2$ (mol/cm$^3$)** | $1.269\times10^{-06}$ [60] |

The number of electrons calculated for the oxygen reduction reaction is ca. 3, which does not correspond to literature although Zhang *et al.* [73] mentioned a three electron transfer with peroxide dissociating from the electrode surface after two electrons were transferred and the third electron used in the reduction of adsorbed O and OH to form two water molecules, as the radical formed in reaction (27) is not stable and might react with adsorbed hydroxyl and oxygen to form two water molecules [73].

The reaction could thus be illustrated as:

$$2O_2 + 3e^- + 3H^+ \longrightarrow H_2O_2 + H\dot{O}_2 \qquad (27)$$

As the Koutecký-Levich plot is done in the mixed control region of the *LP*s (Figure 8 above), it can be deduced that the reaction depicted in reaction (27) might be part of the mechanism where peroxide is formed before being completely reduced to water [84]. It should be noted that, for platinum, the mechanism of reaction is still unclear, regardless of the extensive studies performed on it in the literature [28, 69, 74]. In literature it is speculated that the mechanism can follow the two electron transfer mechanism or the four electron transfer mechanism [67, 84], which supports the conclusion that the mechanism might differ in the mixed control region and the diffusion-controlled region.

### 3.3.3.5. Levich Plots

As a means of confirmation of the calculated number of electrons using Koutecký-Levich, the Levich plot was used to calculate the number of electrons using equation (15).

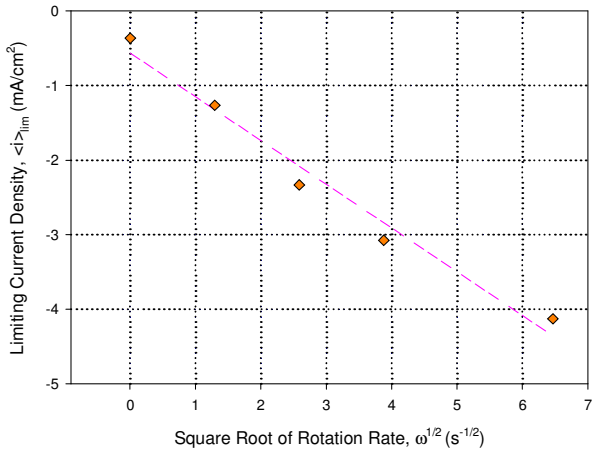


**Figure 25: Levich plot for platinum, based on *LP*s from Figure 20 using current densities at 0.526 V *vs.* NHE plotted from all the different rotation rates**

Using the slope of the plot in Figure 25 and equation (15), the number of electrons transferred on platinum for the ORR in acidic medium in the diffusion controlled region of the *LP*s is 4, implying a direct reduction of oxygen to water (reaction (28)).

$$O_2 + 4e^- + 4H^+ \longrightarrow 2H_2O \qquad (28)$$

As the ORR on gold does not show diffusion-controlled behaviour (Figure 21), the Levich equation could not be applied. The variables used for the Levich equation are listed in Table 3 above.

On platinum, the number of electrons calculated using the Koutecký-Levich equation, differs from that calculated by using the Levich equation, by one electron (Koutecký-Levich = 3 and

Levich = 4), which suggests that the mechanism being followed in the mixed control region is different from the mechanism in the diffusion-controlled region. As the plots in Figure 25 show linearity, it indicates a rapid single step transfer of electrons [53]. Ultimately, the difference between the results of the Koutecký-Levich and Levich analyses implies a mechanism involving more than one step. As the mechanism was not in the scope of this study, further investigation was not done.

#### 3.3.3.6. Conclusion

An electrode is described as effective when it completely reduces oxygen to water [31]. As the ORR is a complex reaction [28, 67], it is possible to have intermediate species formed in the reaction as depicted in reaction (27).

Platinum binds OH very strongly [67], which might account for the formation of peroxide and the protonated oxygen radical in the mixed control region of the *LP*s, as the O-O bond requires much more energy to be broken (494 kJ/mol) than the energy required to form $H_2O_2$ (146 kJ/mol) [67]. As the diffusion-controlled region showed a number of four electrons being transferred contrary to the mixed control region of three electrons, it implies the mechanism takes place in more than one step. Gold's behaviour, as depicted in Figure 21, might be due to the ratio of crystal planes on the polycrystalline electrode, as according to literature, the ratio may have an effect on the reaction kinetics and consequent mechanism [82].

The Tafel slope for platinum in literature had been mass transport corrected (at 600 RPM [79]) whereas this study only considered 0 RPM rotation rates without mass transport corrections of the Tafel slope. The values were used to compare the reaction in different media as well as different metal surfaces. There was consequently no un-corrected Tafel slope value to compare the calculated value to. As the calculated Tafel slope is relatively large, it indicates the reaction as being sluggish.

The Tafel slope for platinum was determined as -205 and for gold as -129 mV/decade indicating gold as being less sluggish than platinum towards the ORR. The number of electrons transferred on platinum was calculated as 3 in the mixed control region of *LP*s and 4 in the diffusion controlled region. The literature covering a three electron reduction process is not abundant; regardless, the three electron transfer reaction corresponds to literature [73] as well as the four electron transfer reaction [53]. The final reaction is thus speculative, based on the results obtained in this study. The final ORR on platinum in acidic medium is thus:

$$O_2 + 4e^- + 4H^+ \longrightarrow 2H_2O \quad (29)$$

Platinum can therefore be considered to be an effective catalyst for the ORR in acidic medium compared to gold in this study, as it was established in literature that it is the best metal to use for the ORR regardless of its high overpotential [40, 79]. Gold was determined to be electrochemically inactive for the ORR in acidic media in literature [31, 49] or to have at least a modest activity [59]. Thus the ORR on gold in acidic medium also corresponds with literature as platinum does.

### 3.3.4. Alkaline

The ORR was investigated in alkaline medium on both platinum and gold so as to compare their activity towards the ORR.

#### 3.3.4.1. Effect of Reagent in Solution

The activity of ORR on platinum and gold in alkaline medium is demonstrated in the *CV*s of Figure 26 and Figure 27 respectively.

As could be expected, the behaviour of platinum in alkaline medium is similar to the acidic behaviour, as literature had also indicated [76] although differences have been found in the reactivity of different crystal lattices in the different media. For gold it can be deduced from Figure 27 that the oxygen electro-reduction reaction is very active in alkaline medium, with the reductive current density markedly higher than the CV without oxygen in solution.

The oxygen reduction on platinum initiates at ca. 0.22 V *vs.* NHE together with the oxide desorption process that occurs at ca. 0.1 V *vs.* NHE, which then forms a well-defined peak at ca. 0.09 V *vs.* NHE due to peroxide formation [76, 80], that then decreases in current density (passivation) to reach a mass transfer inhibited current density plateau from ca. -0.1 V to ca. -0.7 V *vs.* NHE. In the voltammogram with $O_2$ on gold, the peak at ca. 0.1 V *vs.* NHE is the reduction of oxygen [72]. After the peak a sharp decrease in current density takes place (passivation) with an increase to a diffusion-controlled current density plateau at ca. 0.7 V *vs.* NHE. Both platinum and gold experience passivation right after the oxygen reduction peak appears. In the forward scan for platinum, the reductive current density starts to decrease and change to an oxidative current from about 0.1 V, following the path of oxide adsorption in the voltage area above 0.2 V *vs.* NHE with gold following the same behaviour as platinum on the forward scan, with the current density direction change occurring at ca. 0.25 V *vs.* NHE.

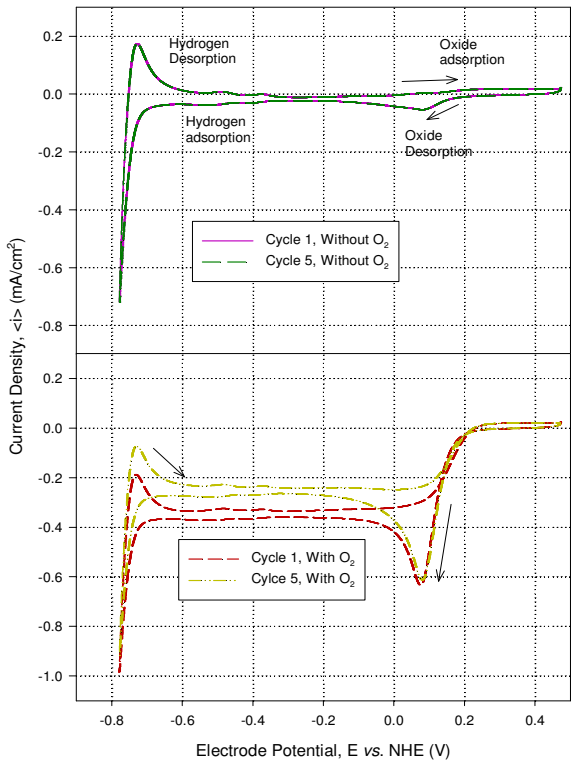


**Figure 26: ORR control *CV*s for platinum in 0.1 M KOH with and without saturated $O_2$ in solution at a scan rate of 10 mV/s and 0 RPM rotation rate**

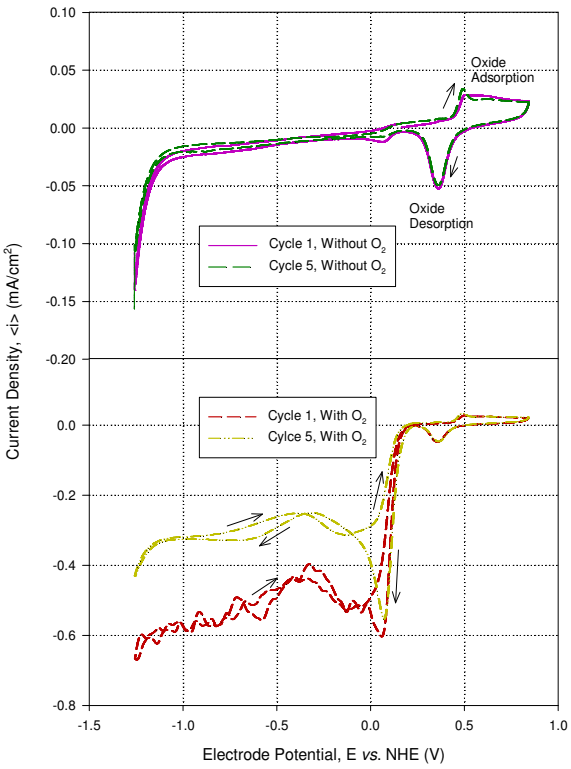


**Figure 27: ORR control *CV*s for gold in 0.1 M KOH with and without saturated $O_2$ in solution at a scan rate of 10 mV/s and 0 RPM rotation rate**

The typical oxide adsorption and desorption voltage areas as depicted in Figure 7 of section 2.1.2 can be seen at respectively ca. 0.5 V and 0.36 V *vs.* NHE for gold and 0.2 and 0.1 V *vs.* NHE for platinum with the hydrogen adsorption and desorption fingerprint area of platinum (Figure 6 in section 2.1.1) also visible to the end of the potential scan in the potential region of ca. -0.35 V to ca. -0.779 V *vs.* NHE. On gold in Figure 27 the oxide adsorption peak (reactions (10) and (11)) with the saturated oxygen solution showed no increase in current density compared to the oxide adsorption current density without $O_2$ in solution, thus supporting the literature conclusion that OH is the species partaking in the oxide formation on the electrode surface and not $O_2$ [41]. Dissolved oxygen had been shown to enhance the surface oxidation, ultimately leading to undefined surface structure [74]. The fifth cycle for platinum shows a much lower mass transfer-inhibited current density, most probably due to inhibition effects of formed $H_2O_2$ as a product of oxygen reduction or by the strong adsorption of $O_2$ and OH [31, 76] with gold following the same decrease in current density in the fifth cycle as platinum.

### 3.3.4.2. Effect of Rotation Rate

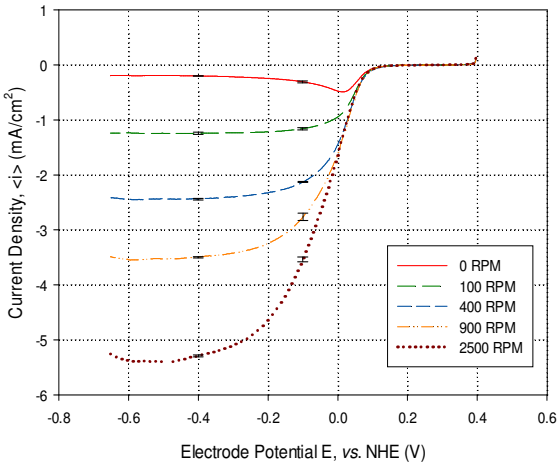


**Figure 28: *LP*s for Pt at different rotation rates in 0.1 M KOH and saturated oxygen gas at a scan rate of 10 mV/s**

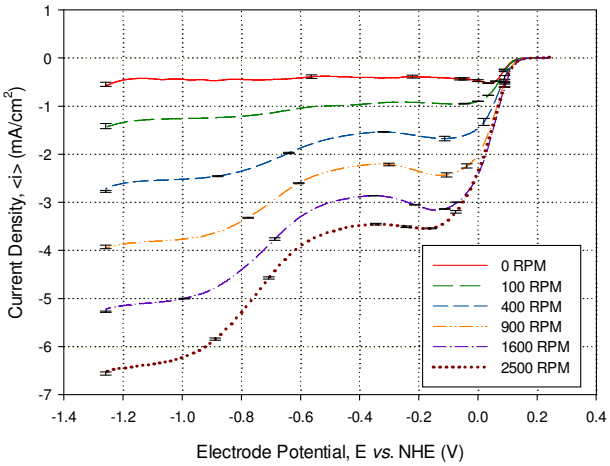


**Figure 29: *LP*s for Au at different rotation rates in 0.1 M KOH and saturated oxygen gas at a scan rate of 10 mV/s**

The linear sweeps for platinum and gold at different rotation rates in oxygen saturated 0.1 M KOH are given above in Figure 28 and Figure 29 respectively. Platinum and gold both exhibit a steady increase of current density with each rotation rate, indicating a mass transfer limited reaction, thus enabling the use of Koutecký-Levich (equation (18)) and Levich (equation (15)) so as to calculate the number of electrons involved in the ORR. The LP scans were scanned in a reductive direction from high to low potentials for both platinum and gold. The current density on platinum starts to increase from ca. 0.14 V *vs.* NHE, reaching a limiting current density at about -0.2 V *vs.* NHE for 0 RPM with a negative increase in the potential of the diffusion-limited current density plateau as the rotation rate increases. This behaviour is in accordance with literature [67, 80]. The current decrease for increased rotation rates from ca. -0.6 V *vs.* NHE is most probably due to the formation of peroxide anions reducing the reductive effectiveness of the electrode [76] with gold's current starting to increase from ca. 0.1 V *vs.* NHE, where an apparent limiting current starts at ca. -0.2 V *vs.* NHE, with an increase as the electrode rotation rate increases. The forming mass transport limited plateau and the lack of a well-defined reduction peak also suggest that the electrode is in a reduced state as an oxidised electrode would have a well-defined peak [87].

On gold, there are two potential range regions with a reduction reaction taking place, the first region from ca. 0.1 V - -0.4 V *vs.* NHE and the second region from ca. -0.4 V - -1.2 V *vs.* NHE, which corresponds to literature findings, even though the electrode used in literature was gold deposited on a carbon support [59]. The first region is the reduction of $O_2$ to form peroxide and the second region, the further reduction of peroxide to form water [59, 72]. As

the O-O bond requires higher energy to break than the formation of peroxide (494 kJ/mol *vs.* 146 kJ/mol respectively [67]) it can be concluded that the first region is the formation of peroxide and the second region, the formation of water. Shao *et al.* [72] had also spectroscopically determined that the reduction of oxygen to water takes place in a serial process by first producing peroxide at low potentials then water at even lower potentials (higher reduction overpotential). As this study was interested in the reduction of oxygen and not peroxide, the first region will be investigated and processed by means of Levich and Koutecký-Levich.

### 3.3.4.3. Tafel Plots

To compare the sluggishness or effectiveness of the ORR on platinum and gold, the Tafel slope can be used as a guideline.

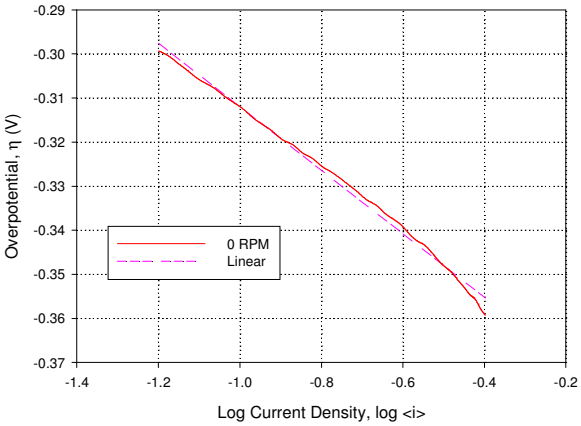


**Figure 30: Tafel Plot of ORR on Pt in 0.1 M KOH at 0 RPM plotted from the potential range 0.101 – 0.041 V *vs.* NHE with the linear plot $R^2$ = 0.994**

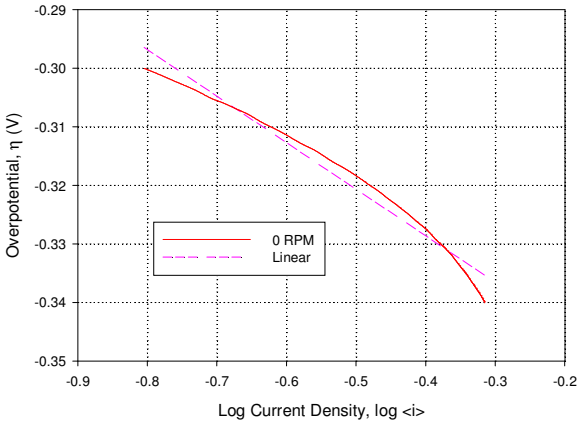


**Figure 31: Tafel Plot of ORR on Au in 0.1 M KOH at 0 RPM plotted from the potential range 0.1 – 0.06 V *vs.* NHE with the linear plot $R^2$ = 0.971**

The slope of the Tafel plot for the ORR on platinum is -72 mV/decade, which is a relatively small Tafel slope, ultimately indicating an increased activity towards the ORR, with a high slope indicating sluggishness [76]. Literature values for the Tafel slope range from -60 - -120 mV [67] thus the determined value in this study corresponds well with literature values for the ORR on platinum in alkaline medium. Based on Figure 29 for gold, the plot of Figure 31 was used to calculate the Tafel slope of -80 mV/decade, which lies between the literature values of -60 mV (for Au(110) lattice) [81] and -107 mV [59] for bulk gold. Considering the magnitudes of the Tafel slopes and the ranges found in literature for both electrodes [59, 67, 81], irrespective of whether or not platinum was found to be less sluggish than gold in literature [23], the difference in slope magnitudes are not significant, with a difference of 8 units. Taking into account experimental error, Tafel region used for extrapolation (region of

Tafel behaviour - section 2.3.1), and uncontrolled variables such as surface lattices and area, platinum and gold's activity could be regarded as similar.

### 3.3.4.4. Koutecký-Levich Plots

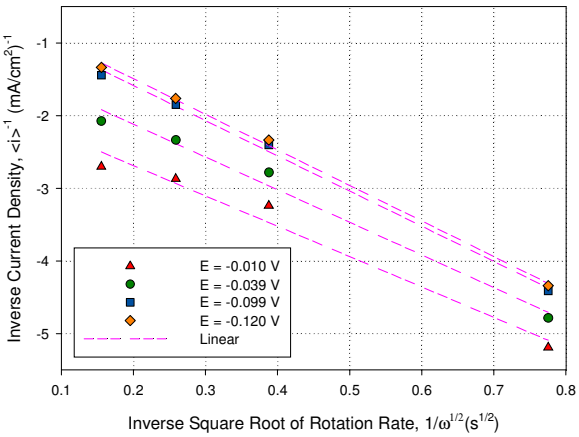


**Figure 32: Koutecký-Levich plot of Pt in 0.1 M KOH for the ORR based on the results from Figure 28**

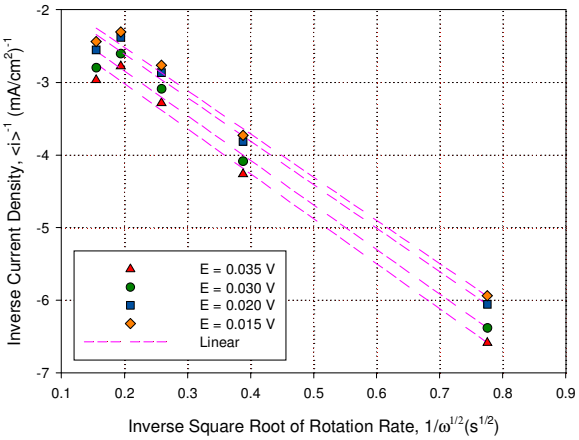


**Figure 33: Koutecký-Levich plot of Au in 0.1 M KOH for the ORR based on the results from Figure 29, plotted for the first reductive current potential area of 0.1 V - -0.4 V *vs.* NHE**

The Koutecký-Levich plot for platinum is given in Figure 32, and gold in Figure 33 with the results summarised in Table 4 below. The Koutecký-Levich plot for gold is based on the first reductive potential region (as was described in section 3.3.4.2 ) from ca. 0.1 V - -0.4 V *vs.* NHE. The values used for the Koutecký-Levich calculations, using equation (18), are summarised in Table 5 below. The kinematic viscosity in Table 5 has been calculated from values in Table 21 (Appendix 1 – Data).

**Table 4: Summarised results for the Koutecký-Levich plots in Figure 32 and Figure 33**

| Catalyst | Potential used (E vs. NHE) | Corresponding Slope (1/mA.s$^{-1/2}$) | Number of electrons |
|---|---|---|---|
| Pt | -0.010 | -4.186 | -2.4 |
| | -0.039 | -4.504 | -2.2 |
| | -0.099 | -4.848 | -2.1 |
| | -0.120 | -4.905 | -2.0 |
| | Average Electrons: | | -2.2 |
| | | | |
| Au | 0.0350 | -6.204 | -1.4 |
| | 0.0299 | -6.152 | -1.5 |
| | 0.0200 | -6.001 | -1.5 |
| | 0.0149 | -5.963 | -1.5 |
| | Average Electrons: | | -1.5 |

In Figure 32 and Figure 33, the parallelism in the slopes indicates a single mechanism being followed [53, 81, 85] in the mixed control region of the ORR for both platinum and gold. The lack of strict linearity of plots in the plots for both platinum and gold can also indicate a change in the mechanism [63] as the potentials increase or rotation rates increase.

The number of electrons was determined to be 2 for both platinum [63, 78] and gold [40, 63, 70] in the mixed control potential region.

**Table 5: Values for variables used in the Koutecký-Levich analysis**

| | |
|---|---|
| **Kinematic Viscosity ($cm^2/s$)** | $1.004\times10^{-03}$ [60] |
| **Diffusivity ($cm^2/s$)** | $2.420\times10^{-05}$ [60] |
| **Radius (cm)** | $2.5\times10^{-01}$ |
| **Faraday Constant(mA.s/mol)** | $9.65\times10^{07}$ |
| **Concentration Sat. $O_2$ ($mol/cm^3$)** | $1.269\times10^{-06}$ [60] |

The typical reaction for a 2 electron transfer reaction is depicted in reaction (30), based on reaction scheme (23).

$$O_2 + H_2O + 2e^- \longrightarrow HO_2^- + OH^- \quad (30)$$

As literature has indicated that the mechanism involves either a 2 or a 4 electron mechanism [76, 77, 80, 86] with many authors differing in opinion about the exact mechanism being followed by the ORR, as the oxygen reduction reaction is said to be a very complex reaction [28, 67], the results correspond with literature findings.

### 3.3.4.5. Levich Plots

In conjunction with Koutecký-Levich, the Levich plot was compiled to confirm the number of electrons transferred during the ORR, using equation (15).

Using the slopes of the plots in Figure 34 and Figure 35 and equation (15), the number of electrons transferred in the diffusion controlled region of the *LP*s in acidic medium on platinum for the ORR was calculated as 4 and for gold as 2, implying a direct reduction of oxygen to water on platinum (reaction (31)) and a reduction of $O_2$ to $H_2O_2$ on gold as in reaction (32).

$$O_2 + 4e^- + 4H^+ \longrightarrow 2H_2O \quad (31)$$

$$O_2 + H_2O + 2e^- \longrightarrow HO_2^- + OH^- \quad (32)$$

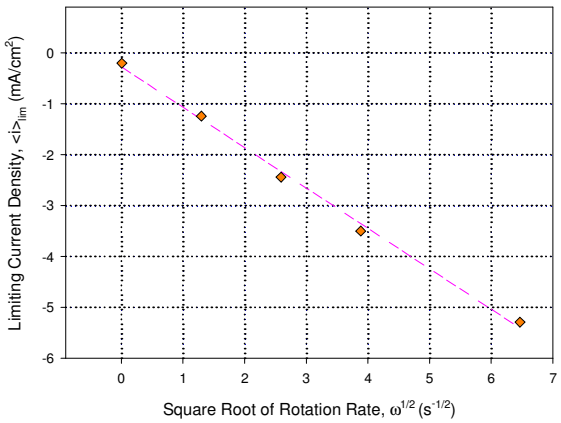


**Figure 34: Levich plot of the ORR for platinum in 0.1 M KOH, based on *LP*s from Figure 28 using current densities from all the different rotation rates at -0.400 V *vs.* NHE**

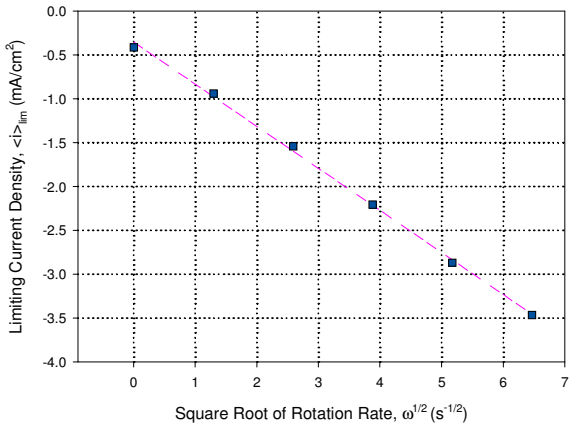


**Figure 35: Levich plot of the ORR for gold in 0.1 M KOH, based on *LP*s from Figure 29 using current densities from all the different rotation rates at -0.340 V *vs.* NHE**

The variables used for the Levich equation are listed in Table 5 above.

On platinum, the number of electrons calculated using the Koutecký-Levich equation differs from the Levich approach by two electrons (Koutecký-Levich = 2 and Levich = 4), which suggests that the mechanism being followed in the mixed control region is different from the mechanism in the diffusion-controlled region, involving more than one step, as was also found with platinum in acidic medium, while gold had given the same number of electrons in both the mixed control and diffusion controlled regions, therefore implying the same mechanism being followed on gold in the mixed- and diffusion-controlled regions [53]. The Levich plots for both platinum and gold respectively, depicted in Figure 34 and Figure 35, show linearity, which indicates a rapid single step transfer of electrons [53]. Once again, as the mechanism of the ORR was not part of the scope of this study, further investigation into the reaction mechanism was not attempted.

### 3.3.4.6. Conclusion

The literature indicates that the platinum electrode follows a predominant 4 electron reduction reaction pathway [40, 67], with a 2 electron pathway also possible as there are two pathways that can be followed for the ORR [28, 74, 76, 77].

The two electron reaction pathway on platinum in the mixed control region, as determined in this study, might be due to the strong adsorption of oxygen on bulk platinum and consequent build-up thereof taking up available binding positions that causes reduced activity due to

resulting alteration by geometric and electronic effects [31]. The 2-electron pathway might be the result of an intermediate reaction step only, as peroxide can be further reduced or decomposed [67, 71] as was confirmed by using Levich analysis that gave 4 electrons in the diffusion controlled region of the *LP*s. The net reaction can thus be depicted as reaction (33) [40, 63, 72, 87].

$$O_2 + 4e^- + 2H_2O \longrightarrow 4OH^- \quad (33)$$

The results produced for platinum correspond well with literature findings, with literature containing great uncertainty regarding the reaction pathway and mechanism followed on platinum in alkaline medium [77, 80]. Many authors found a two electron transfer reaction while many other authors found contrary mechanistic pathways consisting of four electrons being transferred. Literature has thus proposed either a two or four electron transfer pathway [28, 74, 76, 77]. Notwithstanding, the ORR in alkaline medium on platinum needs a great amount of further extensive investigation as to ultimately solve the mystery behind the ORR in alkaline medium due to the current lack of literature coverage [76, 85].

The ORR on gold in alkaline medium has been established to consist of two consecutive reduction processes (section 3.3.4.2), the first most likely being the reduction of $O_2$ to $H_2O_2$ [40, 63, 70] and the second, the further reduction of $H_2O_2$ to $H_2O$ or, in the case of alkaline medium, $OH^-$ [59, 72, 87]. Some authors claim that the ORR in alkaline medium on gold involves only two electrons with some cases and reaction conditions leading to a four electron transfer [40, 63, 70].

By means of the Levich and Koutecký-Levich analyses, the number of electrons transferred in the first reduction region of *LP*s on gold was calculated as 2, thus producing $H_2O_2$ as in reaction (34):

$$O_2 + H_2O + 2e^- \longrightarrow HO_2^- + OH^- \quad (34)$$

As the ORR is pH sensitive [72], faster in alkaline medium [30], with a more effective reaction mechanism and electro-kinetics compared to acidic media [48], it is an acceptable conclusion that the ORR is more effective on platinum than on gold in alkaline medium. The results generated correspond well with literature findings [59, 72, 87], although many studies

that found the 4 electron route were studies on nano-crystalline surfaces or gold deposited electrode supports [59, 63, 81, 87].

The Tafel slope for platinum in alkaline medium was determined as -72 mV/decade and for gold -80 mV/decade, showing that the ORR is less sluggish on platinum than on gold. As discussed in section 3.3.4.3, platinum and gold's activity could be regarded as similar irrespective of whether or not platinum was found to be less sluggish than gold in literature [23]. This is due to the small difference in slope magnitudes of only 8 units, as well as taking into account experimental error, Tafel region used for extrapolation (region of Tafel behaviour - section 2.3.1), and uncontrolled variables such as surface lattices and area.

Using Koutecký-Levich (equation (18)) the number of electrons transferred on platinum was determined as being 2 in the mixed control region of the *LP*s, with the diffusion controlled region giving a number of 4. The final ORR in alkaline medium on platinum is thus depicted in reaction (35) and the 2 electron reduction of $O_2$ on gold in reaction (36):

$$O_2 + 4e^- + 2H_2O \longrightarrow 4OH^- \quad (35)$$

$$O_2 + H_2O + 2e^- \longrightarrow HO_2^- + OH^- \quad (36)$$

Platinum and gold can thus be considered as equally best catalysts for the ORR as the reaction is relatively active, with a small and almost equal Tafel slope for both catalysts, which might be due to the reduction of oxygen in alkaline medium being generally faster [30].

## 3.4. Conclusion of the Oxygen Reduction Reaction

The ORR overpotential plays an important role in the determination of the best catalyst material. As literature has indicated, the overpotential of oxygen reduction on platinum is high [31, 74], it is thus important to determine a catalyst material with a lower ORR onset potential; therefore, in this case, gold showed a lower onset potential (0.4 V *vs.* NHE) *vs.* platinum (0.8 V *vs.* NHE), which directs the conclusion that gold might be the better catalyst for the ORR in acidic medium, regardless of the lack of results, to enable more in-depth processing of possible mechanistic indications of the reaction effectiveness in acidic medium. The characteristic physical softness of gold as a metal might also be a factor in the improved reactivity of it towards the ORR, compared to the harder platinum electrode [28].

The very slightly smaller Tafel slope of Platinum over gold for the ORR in alkaline medium is most probably due to the less steric hindrance of $OH^-$ to the $O_2$ adsorption process [83], regardless of speculation or claims by literature that adsorbed hydroxide (OH) on the surface of the platinum electrode could inhibit the ORR by blocking binding sites for $O_2$ [31, 76]. As the main abundance of crystal lattice on the electrode in this study was Pt(111) (Figure 11) with an apparent improved interaction towards OH in alkaline medium [76], it might thus account for the slightly smaller Tafel slope of platinum to gold.

Regardless of the small difference in Tafel slope for the two catalysts, the onset potential is lower for the ORR on gold in alkaline medium, compared to platinum. As the effectiveness of a metal could be determined by its ability to transfer an increased number of electrons [28, 31, 69], regardless of whether or not the potential region of the gold electrode in the range of ca. -0.4 V - -1.2 V *vs.* NHE might have produced another increase in number of electrons transferred, the effectiveness of the ORR on platinum can thus be concluded to be the same as gold in alkaline medium. Gold was determined to be electrochemically inactive for the ORR in acidic media in literature [31, 49] or with a modest activity [59] as was determined in this study with the produced results not viable for extensive analysis.

### 3.4.1. Results Comparison

The results for both electrodes in alkaline and acid media is summarised below.

**Table 6: Results summary for ORR in alkaline and acid medium for Au and Pt**

| | Onset Potential E *vs.* NHE | | Tafel Slope (mV/decade) | | $e^-$ Number | |
|---|---|---|---|---|---|---|
| **Medium** | **Au** | **Pt** | **Au** | **Pt** | **Au** | **Pt** |
| **Acid** | 0.4 | 0.8 | -129 | -205 | - | 4 |
| **Alkaline** | 0.1 | 0.14 | -80 | -72 | 2 | 4 |

The number of electrons transferred is greater on platinum in both media. In acid medium, the Tafel slope for the ORR on gold is lower than that of platinum, although the results in this study was not viable to do further investigations using Koutecký-Levich and Levich analyses on gold, thus leading to the conclusion that platinum is the better catalyst in acid medium. In this study, both platinum and gold was concluded to be equally effective catalysts towards the ORR in alkaline media. Regardless of the lower onset potential exhibited on gold in both media, literature conclusions that platinum is the best catalyst, was supported in this study in acidic medium, with the highest activity towards this ideally $4e^-$ ORR mechanistic pathway [40, 79]. Should the price of gold per fine ounce decrease to levels lower than platinum, gold might be a very worthy alternative to platinum for use in the ORR in alkaline media.

The ORR was thus a good attempt to become familiar with the techniques used in this study for the investigation into the SDOR. The following chapter covers the EOR in an on-going attempt to become familiar with the electrochemical concepts used in the analysis of the SDOR.

# Chapter 4: Ethanol Oxidation Reaction (EOR)

## 4.1. Literature

Ethanol, easily produced from agricultural crops or biomass [32, 48, 92-104], is more environmentally friendly for use in fuel cell technology compared to methanol, which is readily available, highly toxic and environmentally unfriendly [105, 106]. Ethanol is also very high in energy compared to fossil fuels and even hydrogen [92, 93, 95, 96, 99, 101-103, 105, 106].

As a point of reference, let's consider the typical oxidation reaction pathway of ethanol. The following reaction scheme (37) illustrates the ethanol oxidation reaction (EOR) on a metal substrate [32]:

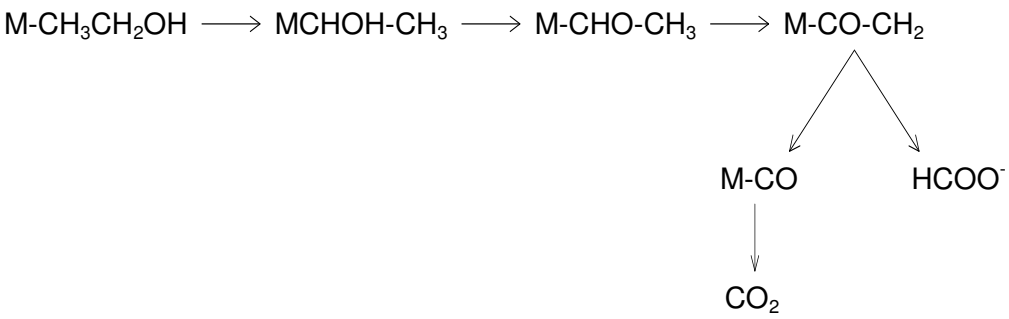


(37)

From reaction scheme (37) it can be derived that the oxidation of ethanol produces different products as is described in literature with reaction (38) showing the reaction producing $CO_2$, reaction (39) the production of bicarbonate and reaction (40) carbonate [101]:

$$CH_3CH_2OH + 3H_2O \longrightarrow 2CO_2 + 12H^+ + 12e^- \qquad E^0 = 0.10\ V\ vs.\ NHE \qquad (38)$$

$$CH_3CH_2OH + 5H_2O \longrightarrow 2HCO_3^- + 14H^+ + 12e^- \qquad E^0 = 0.18\ V\ vs.\ NHE \qquad (39)$$

$$CH_3CH_2OH + 5H_2O \longrightarrow 2CO_3^{2-} + 16H^+ + 12e^- \qquad E^0 = 0.19\ V\ vs.\ NHE \qquad (40)$$

From literature [103], a dual pathway mechanism for the EOR can be considered as shown in reaction scheme (41) below producing acetic acid or carbon dioxide:

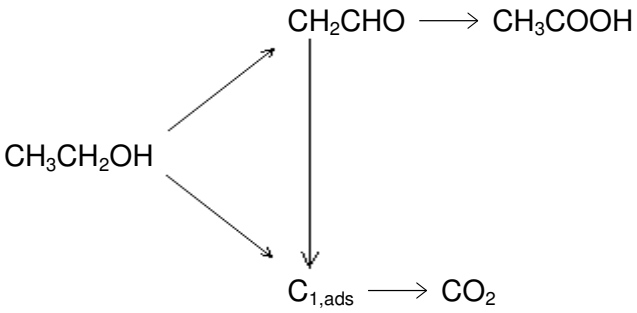


(41)

In reaction scheme (41), the $C_{1,ads}$ is indicative of an intermediate species with only one carbon atom to be oxidised to $CO_2$. Ethanol can be oxidised to acetaldehyde then subsequently to acetic acid with a loss of 4 electrons, with acetic acid a bit more difficult to oxidise to $CO_2$ as it requires a much higher overpotential to be achieved [103]. The moment the C-C bond is broken, the adsorbed species include $CH_x$ and CO, which can be easily oxidised to $CO_2$ totalling a loss of 12 electrons.

The kinetics associated with ethanol electrocatalysis comprises the process of breaking the carbon-carbon bond [94, 97, 98, 100, 103]. The breakage of the C-C bond in ethanol occurs at relatively low potentials, producing CH and CO, which adsorb on the electrode surface [101, 103]. As the potential increases the adsorbed CH are converted into CO, which in turn oxidises to $CO_2$. Literature has proven that both the carbon atoms in the ethanol molecule are oxidised to $CO_2$, by using $^{13}C$ labelled ethanol [107].

The incomplete oxidation of ethanol has a great industrial interest as such oxidation products could lead to the production of compounds such as acetaldehyde and acetic acid, depending on the reaction conditions [94, 97, 98, 100, 101, 103, 107-110], rather than carbon dioxide. At low concentrations of ethanol the main intermediate species or products consist of acetic acid and carbon dioxide while high concentrations of ethanol produce mainly acetaldehyde as intermediate species [109].

Conclusively, ethanol electro-oxidation can produce the following products: (i) $CO_2$, (ii) acetaldehyde, (iii) acetic acid and (iv) ethyl acetate by means of homogeneous chemical reaction of ethanol with acetic acid [107].

### 4.1.1. Electrolyte Concentration Effects

In the extensive investigation of Lai *et al.* [101] into the effects of electrolytes on the EOR, they found that the pH and concentration of ethanol plays such an important role in its electro-oxidation that it might influence the intermediate species during the reaction and imply that less noble metals might be considered for the electro-oxidation of ethanol. The

stability of intermediate species, and even the reaction mechanism, together with the distribution of product can be influenced by the pH [101, 110].

In alkaline medium, the oxidation of organic fuels is much more electro-catalytically active compared to acidic medium, as the hydroxyl ions play an important role in the complete oxidation to $CO_2$ of the organic fuel or alcohol, and the oxidation of the metal surface that contributes to the oxidation of the alcohol [103].

Regardless of the surface structure, literature indicates that, in acidic medium, adsorbed aliphatic carbon intermediates ($CH_{x,ads}$) can be found [101]. On the other hand, polycrystalline metal surfaces in alkaline medium showed adsorbed CO as intermediate species while single crystal surfaces with long terraces showed the presence of intermediate aliphatic carbon species.

### 4.1.2. Reaction Diagnosis

As the reaction is not diffusion limited, most authors in literature used supplementary analytical techniques such as Fourier Transform Infrared (FTIR), High Performance Liquid Chromatography (HPLC), and Surface Enhanced Raman Spectroscopy (SERS) to diagnose the reaction mechanism and confirm the intermediate species [101].

The reaction is hardly affected by mass transport [93, 111], which implies kinetic control playing the predominant role in the reaction rate. Thus the application of Levich and Koutecký-Levich is limited or even not applicable at all. Application of the Arrhenius equation will be appropriate for evaluating the activation energy for the EOR at different temperatures, as the reaction is mainly kinetically controlled [110]. Refer to section 2.3.4 for the Arrhenius equation as well as background information.

### 4.1.3. Platinum

Platinum [32, 93, 112, 113] is one of the most investigated electrode materials in literature for alcohol fuel cells and was found to be poisoned by intermediate carbonaceous species, including CO [93, 94, 105, 112]. In the literature, infrared spectroscopy applied in situ with an electrochemical cell had shown how CO is a main, poisoning, intermediate product in the electro-oxidation of ethanol on a platinum electrode [109, 114]. From literature it can be concluded that the poisoning of the platinum electrode originates from the incomplete oxidation of carbon to CO [94, 97].

Lai *et al.* [101] found that the current density showed little or no increase at all when electrode rotation was introduced using an RDE, as compared to a stationary electrode in

both alkaline and acidic conditions. They concluded that the oxidation of ethanol in both alkaline and acid media was not mass transfer limited but rather kinetically controlled.

The following reaction (42) is a typical representation of the reaction of ethanol or other higher alcohols on platinum [115]:

$$RCH_2OH \longrightarrow CO_{ads} + R\text{-}H + 2H^+ + 2e^- \quad (42)$$

Voltammetric studies of EOR showed three peaks in acidic medium, two in the forward scan and one peak in the backward scan [37, 94, 100-102, 106, 107, 110, 111, 116-120]. The *first peak* in the forward scan can be attributed to ethanol being oxidised to acetaldehyde [111], the *second peak* the consequent oxidation of acetaldehyde to acetic acid as the metal surface can donate the oxygen atom to the adsorbed intermediate as this peak occurs just after the metal oxide formation potential. The backward scan's peak occurs after the electrode surface has been reduced [110]. It is speculated, in literature, that it is the oxidation of adsorbed ethanol to form acetaldehyde [101, 110] as the ethanol has adequate time to adsorb from the start of the backward scan to where the oxidation peak occurs after electrode surface reduction [110].

It is speculated in literature that the higher concentrations of ethanol reduce the effectiveness of hydroxyl adsorption due to adsorption competition and thus fail to provide an extra oxygen atom for the complete oxidation of ethanol to $CO_2$ or acetic acid [107]. Higher poisoning effects could thus be expected with higher ethanol concentrations. The main product at low ethanol concentrations (< 0.1 M) is acetic acid whilst at high concentrations (> 0.1 M) acetaldehyde is the main reaction product [111].

#### 4.1.3.1. Effect of Increased Temperature

There aren't many studies in literature done at different temperatures for polycrystalline platinum. For that matter, studies in perchloric acid and potassium hydroxide have not been done thus far. A group of authors, Camargo *et al.* [102], studied the EOR at different temperatures in phosphoric acid ($H_3PO_4$) on polycrystalline platinum. Their study implemented elevated pressure (up to 20 atm) to ensure no evaporation of the ethanol occurs during the study of the reaction. It could thus be used as a guideline in the approach of this study to investigate the temperature effect on the EOR.

Regardless of the 12 electrons needed per molecule of ethanol for complete oxidation to $CO_2$, lower temperatures at which oxidation occurs, can influence the outcome of the

reaction products [102]. As the temperature decreases, the kinetics becomes slow, to such an extent that acetaldehyde and acetic acid, or even carbon monoxide formation, is favoured.

Camargo *et al.* [102] found that the EOR onset potential changed significantly (up to 330 mV) for a temperature range of 55 °C from 25 °C, attributable to a decrease of intermediate species and poisoning reaction products that dissociates with more ease from the electrode surface. As speculated by Camargo *et al.* [102], desorption of anions, intermediate species and/or poisons occurs simultaneously with the adsorption of un-oxidised ethanol, which could be linked to the decrease in onset potential in higher concentrations of electrolyte as the temperature increases.

With ethanol in solution, surface oxide species are consumed at a greater rate due to the ethanol oxidation [102]. That might be the basis of the increase reaction rate of ethanol oxidation at higher temperatures.

Arrhenius plots were used by Camargo *et al.* [102] to obtain apparent activation energies ($E_{app}$) for ethanol oxidation on platinum in 14.6 M $H_3PO_4$ of 71.3 kJ/mol for temperatures from 160 – 180 °C, 9.2 kJ/mol for 50 – 160 °C and 90.6 kJ/mol for temperatures ranging from 25 – 50 °C. A diluted acid concentration (5M $H_3PO_4$) was determined to be 23.7 kJ/mol from 25 – 125 °C [102].

The effect of temperature can be concluded as follows: i.) water plays an important role in the oxidation rate of ethanol at low potentials [102], ii.) the temperature being elevated helps the surface active sites become available for adsorption and reaction, iii.) adsorbed poisons and reaction intermediates are easily dissociated from the electrode surface and iv.) changes in temperature might change the reaction mechanism as can be seen by the change in activation energies.

#### 4.1.3.2. Acidic Medium

Lai *et al.* [101] and Snell *et al.* [110] found that there were two oxidation peaks present in forward CV scans (before 1.5 V *vs.* NHE) with both peaks disappearing in the reverse scan. A single oxidation peak appears in the reverse scan right after the metal surface had been reduced [101]. Ethanol ultimately oxidises to acetic acid, acetaldehyde and carbon monoxide with acetaldehyde being further oxidised to large adsorbed residual CO amounts, and small amounts of acetaldehyde residues [106]. CO can also be further oxidised to $CO_2$.

It was established that perchlorate anions interfere the least with the electro-oxidation reaction of ethanol as it adsorbs less strongly on the platinum surface [110]. Thus $HClO_4$

would be the best electrolyte to study the EOR. The overall rate of reaction is controlled by adsorption as mass transfer contribution is minimal [111].

At low ethanol concentrations (< 0.1 M) the electron number was determined to be 4, which supports the formation of acetic acid (reaction (43)) [111].

$$CH_3—CH_2OH + H_2O \longrightarrow CH_3—COOH + 4H^+ + 4e^- \quad (43)$$

High ethanol concentrations (> 0.1 M) that produce mainly acetaldehyde involve the transfer of two electrons as depicted in reaction (44) [111]:

$$CH_3—CH_2OH \longrightarrow CH_3—CHO + 2H^+ + 2e^- \quad (44)$$

Hitmi *et al.* [111] obtained the Tafel slope for ethanol oxidation on platinum in acidic medium as $\alpha n = 0.44$ from *CV*s.

#### 4.1.3.3. Alkaline Medium

The electrocatalytic activity of platinum towards ethanol oxidation is greatly increased in alkaline medium, compared to acidic medium [103].

CV scans of ethanol oxidation in alkaline medium showed one oxidation peak in the forward scans with no second oxidation peak, as is the case with acidic medium [101, 103]. On the backward scan only one peak was found, right after the electrode surface had been reduced. In the hydrogen under-potential deposition (HUD) region (hydrogen adsorption/desorption), decomposition products block the surface from interacting with dissolved ethanol [103]. Thus, in the forward or anodic scan, the adsorbed species in the HUD are oxidised so as to open up the electrode surface's active sites for the oxidation of ethanol. As the oxide formation potential is reached, the reactivity of the electrode decreases as active sites are blocked once again for the successful adsorption of ethanol for oxidation. On the subsequent backward or cathodic scan, the electrode surface is reduced and the active sites become available once again for ethanol to adsorb and the oxidative currents appear accordingly, with the electrode activity decreasing once again as the HUD region is reached. This indicates that an oxidised electrode surface becomes inactive towards ethanol oxidation.

Regardless of the improved electro-catalytic activity, the mechanism of the electro-oxidation of ethanol is still not well understood [103].

The breaking of the C-C bond in alkaline solution takes place at relatively low potentials, forming adsorbed CO species, thus indicating that $CH_x$ is unstable in alkaline medium on a polycrystalline platinum surface [101, 103]. The poisoning of platinum in alkaline medium can thus be regarded as a consequence of un-oxidised $CH_x$ species.

#### 4.1.3.4. Acidic *vs.* Alkaline Medium

According to literature there are a few differences between acidic and alkaline media [103]. The activity of alkaline medium is greatly enhanced compared to acidic medium. There is a decrease in the starting potential of the EOR in alkaline medium, compared to acidic medium, due to the greater affinity of the hydroxyl anion adsorption to the electrode surface. The hysteresis between the positive and negative scans of alkaline medium differs in comparison to acidic medium with the alkaline medium presenting much lower current density in the backwards scan, compared to acidic medium, which can act as an indication of the inhibitive effect of intermediate species in alkaline medium.

### 4.1.4. Gold

Smooth polycrystalline gold surfaces showed very little, to almost no activity towards the electro-oxidation of ethanol [92, 93, 112]. Un-activated gold electrode surface, which have a layer of oxide in its activated form as described in section 2.1.2, proved to be better catalysts for the oxidation of ethanol [47]. Alcohols might only be partially oxidised to aldehydes on gold surfaces.

#### 4.1.4.1. Effect of Increased Temperature

Contrary to platinum (section 4.1.3.1), there was no literature found in any searches regarding the ethanol oxidation on gold in either acidic or alkaline media at different temperatures. This lack of literature coverage could be a very valuable subject for further investigation in the future.

#### 4.1.4.2. Acidic Medium

In literature [101, 114, 121], gold is considered a very poor catalyst for any form of alcohol oxidation in acidic medium because [46, 114] of weak interactions and, consequently, adsorption properties with alcohols. It has been speculated in literature that the possible inhibition of gold activity towards ethanol electro-oxidation in acidic medium might be because of oxygen species from the electrolyte solution that adsorb onto the surface of the electrode [114]. In perchloric acid it was found that the main reaction product was acetaldehyde that could be further oxidised to acetic acid, depending on the applied

electrode potential [101, 108]. Because of the lack of hydroxides in acidic medium, dehydrogenation of ethanol that leads to the formation of acetaldehyde is low, with a consequent formation of acetic acid also low, demonstrating the need for hydroxides to form acetic acid [114]. Thus the final product of ethanol oxidation on gold in acidic medium is acetaldehyde [114].

It was found that there were no oxidation peaks for ethanol with concentrations below 1 M with lower concentrations' oxidation peaks being superimposed on the peaks of the electrode surface oxidation wave [114]. Oxidation peaks for ethanol oxidation were found in the potential range of 1.0 and 1.4 V *vs.* NHE with 1 M ethanol, with the maximum oxidation occurring in the exact range of gold oxide formation potentials. It was also found that potentials above 1.5 V *vs.* NHE were due to the activity of oxidised gold towards ethanol oxidation. In acidic medium, as the main product formed was determined to be acetaldehyde, the number of electrons transferred as determined by literature, was 2 [114].

#### 4.1.4.3. Alkaline Medium

In alkaline medium, gold has been found to have better electro-catalytic dehydrogenation properties of organic compounds, compared to platinum [46]. The reactivity of ethanol on gold in alkaline media is mainly due to the fact that no poisoning intermediates such as CO adsorb onto the electrode surface. It is thought in literature, that the adsorbed hydroxide ion plays a very important role in the electro-activity of gold towards the electro-oxidation of ethanol [93, 114].

The number of electrons in the EOR was determined by Tremiliosi-Filho [114] using HPLC and Single Potential Alteration Infrared Reflectance Spectroscopy (SPAIRS) as supplementary analysis techniques to monitor the change in ethanol concentration and intermediate species formation rates. The reaction was concluded as follows (reaction (45)) with a loss of 4 electrons [114]:

$$H_3C—CH_2OH + 4OH^- \longrightarrow H_3C—COOH + 3H_2O + 4e^- \quad (45)$$

In the literature it was found that gold exhibited a lower activity compared to platinum towards the electro-oxidation of ethanol in alkaline medium [114].

#### 4.1.4.4. Acidic *vs.* Alkaline Medium

Literature has shown that in alkaline solution, the main product of the electro-oxidation of ethanol was acetic acid [34, 108, 114] while the main product in acidic medium was shown to produce mainly acetaldehyde, which could in turn be further oxidised to acetic acid at high enough overpotential [108]. Gold was found to be ideal for the studying of the $C_2$-pathway of ethanol oxidation, which leads to the production of acetaldehyde and acetic acid (or acetate in alkaline medium) without the C-C bond being broken in the process [101].

## 4.2. Experimental Procedure

Refer to sections 3.2.1 – 3.2.3 for the instrumentation, reagents and experimental setup. For the polishing procedure refer to section 3.2.4.1.

Experiments involving ethanol were conducted in acidic and alkaline medium with an ethanol concentration of 1 molar.

### 4.2.1. Platinum

Platinum was investigated in acid and alkaline medium. The procedures are thus described for each electrolyte medium.

#### 4.2.1.1. Acidic

Polishing of the electrode was always done before preconditioning. After polishing, preconditioning was done using *CV*s starting at the OCP up to 1.2 V and down to 0.1 V *vs.* SCE at 50 mV/s for 10 repeats. Activity control was determined in (i) fresh 0.1 M perchloric acid solution and (ii) a fresh acid solution containing 1 M ethanol by using *CV*s at 10 mV/s for 5 cycles starting at the open circuit potential up to 1.5 V and back down to -0.241 V *vs.* SCE. Platinum was studied at only 0 and 100 RPM rotation rates with the reason being discussed in section 4.3.

##### 4.2.1.1.1. Effect of Different Temperatures

For the investigation into the effect of a change in temperature on the EOR, for both gold and platinum (at 0 RPM), preconditioning was done the same as for the normal LP experiments. The temperatures studied, besides 25 ℃, were 10 and 40 ℃, to provide a range of temperatures to which the electrode performance could be compared to and to calculate the activation energy.

#### 4.2.1.2. Alkaline

The electrode was polished and cleaned as described in section 3.2.4.1 before every experimental run. In a 0.1 M KOH solution the preconditioning settings were set for *CV*s at 50 mV/s to run within the platinum fingerprint CV area until it became stable and repeatable, indicating electrode cleanliness. The potential range was set to -1.018 V – 0.231 V *vs.* SCE. *LP*s were run at 0, 100, 900 and 1600 RPM starting from -1.0 V *vs.* SCE up to 0.23 V *vs.* SCE at 25 ℃ in 1 M KOH containing 1 M ethanol.

##### 4.2.1.2.1. Different Temperatures

The LP experimental runs were repeated with the same settings as the investigation into the different rotation rates with the cell and experimental temperatures ranging from 10 ℃ up to 40 ℃ with 10 ℃ intervals producing four different temperature investigations.

### 4.2.2. Gold

#### 4.2.2.1. Acidic

After electrode polishing, as described in section 3.2.4.1, preconditioning of the electrode was done using *CV*s in a fresh 0.1 M $HClO_4$ solution at 50 mV/s starting from the OCP and cycling up to 1.6 V and back down to 0.1 V *vs.* SCE with the run ending at 0.1 V, for a total of 10 cycles. No subsequent *CA*s were performed. This procedure was executed before each and every electrochemical experiment. Reaction activity was studied with a CV performed in (i) fresh 0.1 M perchloric acid and (ii) in fresh 0.1 M perchloric acid containing 1 M ethanol. The parameters for both solutions, with and without ethanol, were set to 10 mV/s for 5 cycles, starting from the OCP down to 0.0 V and up to 1.65 V *vs.* SCE. *LP*s were conducted at rotation rates of 0, 100, 900 and 2500 RPM starting at 0 V and ending at 1.65 V *vs.* SCE.

##### 4.2.2.1.1. Different Temperatures

Refer to section 4.2.1.1.1.

#### 4.2.2.2. Alkaline

The electrode was polished and cleaned as described in section 3.2.4.1.

The effect of the electrolyte concentration on preconditioning was investigated by doing electrode preconditioning in 0.1 M KOH and then running an LP at 0 RPM in 1 M KOH with 1 M ethanol in solution. The second preconditioning electrolyte concentration investigated was 1 M KOH after which the LP at 0 RPM was done in 1 M KOH, containing 1 M ethanol.

The results indicated that the most suitable method was to do preconditioning in 0.1 M KOH and to do the final experimentation in 1 M KOH with 1 M ethanol in solution. Thus, after polishing, electrode preconditioning for both gold and platinum was done in 0.1 M KOH where after 1 M ethanol was studied in 1 M KOH.

Preconditioning settings were set to -1.021 V up to 0.6 V *vs.* SCE at 50 mV/s for 20 cycles in 0.1 M KOH. The experimental settings of the reaction control *CV*s for ethanol oxidation was started at -1.021 up to 0.6 V *vs.* SCE at 10 mV/s for 5 runs in 1 M KOH. The CV experiment with 1 M ethanol in 1 M KOH was set to run at 10 mV/s scan rate for 5 cycles, starting at -1.021 up to 0.6 V *vs.* SCE. The experimental LP runs were done in 1 M KOH containing 1 M ethanol with a scan rate of 10 mV/s, starting from -1.021 V and ending at 0.5 V *vs.* SCE, repeated at rotations of 0, 100, 900 and 1600 RPM.

#### 4.2.2.2.1. Different Temperatures

The same procedure for polishing and preconditioning was used in the experiments at different temperatures as for the experiments at the different rotation rates at 25 ℃. The KOH concentration of the preconditioning solution was 0.1 M and for the experiments 1 M with 1 M ethanol in solution. The rotation rate for each experiment was 0 RPM with the different temperatures set to 10, 20, 30 and 40 ℃.

## 4.3. Results and Discussion

According to literature, the electro-oxidative activity of gold towards ethanol oxidation is very weak compared to platinum, especially in acidic medium. The results obtained (shown below) support these literature findings.

### 4.3.1. Acidic

The electrode preparation was followed as described in the experimental section (3.2.4.1.). The preconditioning of the Pt electrode for the ethanol oxidation reaction was followed just as depicted in Figure 13 in section 3.3.2.1 above.

#### 4.3.1.1. Effect of Reagent in Solution

According to Casella [112] a smooth or polycrystalline gold electrode has almost no electrochemical activity for the electro-oxidation of ethanol. However, Tremiliosi-Filho *et al.* [114] indicated that the main product in the electro-oxidation of ethanol in acidic media was acetaldehyde, which might be further oxidised to acetic acid if the oxidative overpotential was kept high enough for adequate time.

The *CV*s shown in Figure 36 shows the activity and behaviour of platinum in 0.1 M perchloric acid with and without ethanol (1 M) and Figure 37 the behaviour of gold. Note the difference in the y-axis scale between the *CV*s with and without ethanol. The first and fifth cycles with ethanol, as well as the first and fifth cycles of the perchloric acid solution without ethanol, are depicted for both platinum and gold. In Figure 36 for platinum, it is clear that there are no foreign peaks in the voltammogram without ethanol, with the oxide adsorption and desorption peaks noticeable and starting at ca. 0.8 V *vs.* NHE for adsorption and ca. 1.0 V for desorption. Gold, on the other hand, showed behaviour as described in literature [46, 48, 121] with a weak interaction with any form of alcohol, especially in acidic medium. In Figure 37 the CV of gold, with ethanol in solution, showed a rapid decrease of current density for each sequential cycle with regards to the oxidation peak at ca. 1.256 V *vs.* NHE, which is the potential at which the ethanol oxidation reaction takes place, corresponding to literature's finding of the oxidation wave between 1.0 and 1.4 V [114].

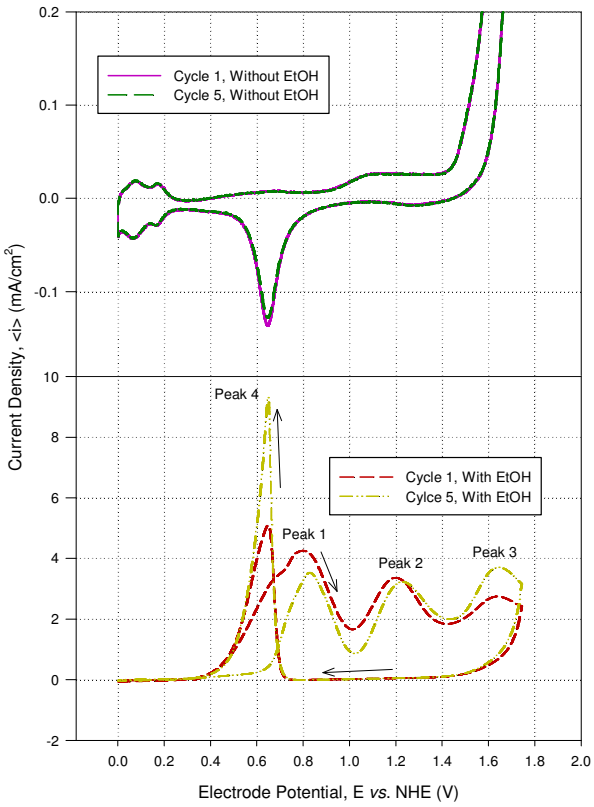


**Figure 36: Control *CV*s of Pt in 0.1 M $HClO_4$ with and without 1 M ethanol at 25 °C and 10 mV/s scan rate**

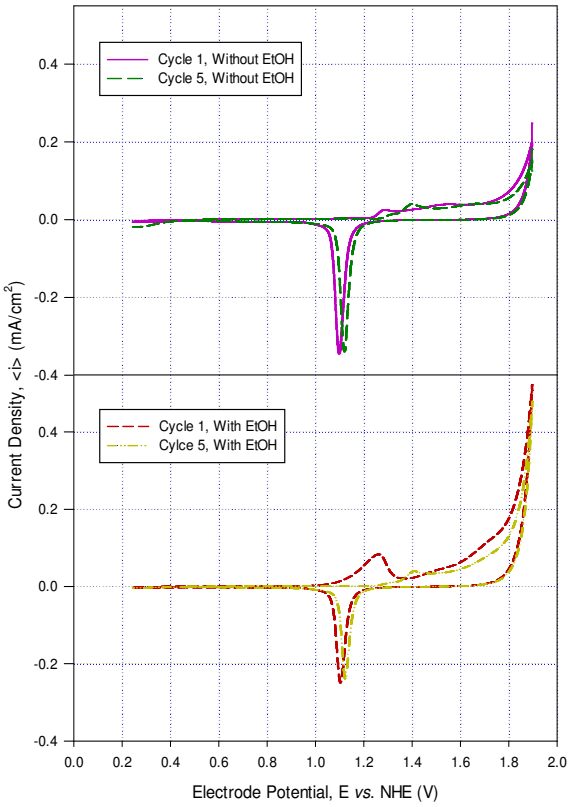


**Figure 37: Control *CV*s of Au in 0.1 M $HClO_4$ with and without 1 M ethanol at 25 °C and 10 mV/s scan rate**

At the 5$^{th}$ cycle the oxidation peak almost exactly resembles the oxide formation peaks in the CV without ethanol at the 5$^{th}$ cycle, except with the highest current density reached at the end of the scan, with the ethanol present in solution being magnitudes higher than the

solution without ethanol, which is attributable to the oxidation of ethanol on the oxidised gold surface [114].

On platinum as depicted in Figure 36, the forward scan shows three distinct peaks with 1 M ethanol in solution with gold only exhibiting a single oxidative peak for ethanol oxidation to the contrary of platinum. Literature only explicitly indicated, studied and discussed two peaks in the forward scan [37, 94, 100-102, 106, 107, 110, 111, 116-120]. The *third peak* found might be a finding/discovery that is not covered in literature at all, that needs intensive future investigation, which might be an integral part of understanding the EOR mechanism. The *first peak* starts at ca. 0.4 V *vs.* NHE with a shoulder at 0.68 V reaching a current density maximum peak at ca. 0.8 V of ca. 4.22 mA/cm$^2$. The *second peak* starts just after the minimum reached at ca. 1.0 V *vs.* NHE reaching a maximum at ca. 1.2 V *vs.* NHE of ca. 3.33 mA/cm$^2$. The *third peak* starts right after the minimum reached at ca. 1.4 V *vs.* NHE and reaches its maximum of ca. 2.7 mA/cm$^2$ at ca. 1.64 V *vs.* NHE. With the backward scan a *fourth peak* appears at 0.74 V *vs.* NHE, which is almost the same potential where platinum oxide desorption occurs, and starts to increase into the oxidative current direction and reaches a maximum of ca. 5.1 mA/cm$^2$ at ca. 0.65 V *vs.* NHE.

The consecutive scans on platinum showed interesting phenomena where the *first peak* showed a lower current density for every repeat, the *second peak* almost unchanged, the *third peak* an increase and the fourth peak also an increase. The *first peak*'s decrease is most probably the ethanol concentration decreasing, forming acetaldehyde [101, 111], the *second peak* the acetaldehyde by-product forming acetic acid, and the third most definitely a reaction product produced from the main reagent or intermediate's breakdown, although that is just speculation as there is no literature available that even as much as mentions the third oxidation peak. Extensive studies have been done in literature on the first two peaks in the forward scan and the peak in the backward scan [101, 111]. No third oxidation peak in the forward scan has been covered in literature. The backward scan is one of the least understood and most speculated about peaks, as this occurs after the electrode surface has been reduced [110]. It is speculated in literature, that the backward scan's peak is the oxidation of adsorbed ethanol to form acetaldehyde [101, 110] as the ethanol had ample time to adsorb from the start of the backward scan to where the oxidation peak occurs after electrode surface reduction [110].

There could be a possible relation between the third and the fourth peak as they both increase with every consecutive scan, although the relation of peak three and four is, after all, most likely unrelated as peak three occurs on an oxidised electrode surface and the fourth literally just after the electrode has been reduced [110] in the backward scan. It could

be that a by-product that oxidises on a reduced platinum surface only, is formed during the forward scan.

On gold in Figure 37, at ca. 1.05 V *vs.* NHE the current density starts to increase, with the maximum reaching about 0.086 mA/cm$^2$ at ca. 1.256 V *vs.* NHE, whereas the current density without ethanol in solution starts to increase at about 1.25 V, which is the oxide adsorption peak, reaching a maximum current density at ca. 1.29 V of about 0.027 mA/cm$^2$. According to literature [33, 41, 45, 46] the maximum current, as in the case of Figure 37 in the potential area of 1.2 – 1.4 V *vs.* NHE, shows the voltage area where the surface crystal lattice experiences the adsorption of water, and the turnover process where the gold surface atoms are oxidised to form a monolayer of gold oxide, depicted in reactions (9) – (11). As was previously stated, the interaction of gold with alcohol is weak, and it might account for the decrease in current density with each successive cycle with ethanol in solution, because of intermediate reaction species, such as acetaldehyde, blocking active surface sites [101, 108].

The low activity of gold in acidic medium towards ethanol electro-oxidation, as in comparison of Figure 37 to Figure 48, might also be because of the low presence of $OH^-$ anions as $OH^-$ might play an important role in the oxidation of ethanol in alkaline medium [93, 114].

Regardless of the third, extra oxidation peak detected for platinum, the results produced and depicted in Figure 36 correspond very well with literature findings, as well as the results of gold depicted in Figure 37.

### 4.3.1.2. Effect of Rotation Rate

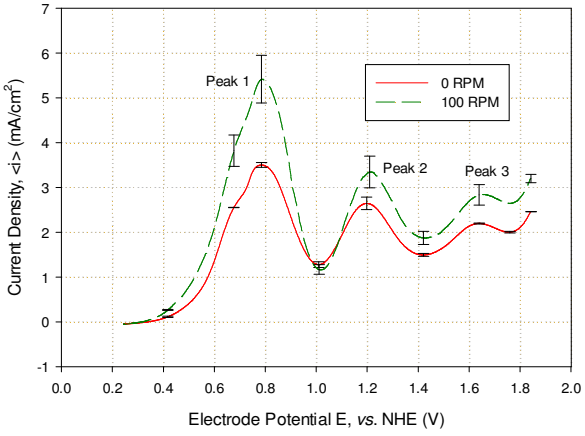


**Figure 38: *LP*s of Pt at different rotation rates at 25 °C with 1 M ethanol in 0.1 M perchloric acid at a scan rate of 10 mV/s**

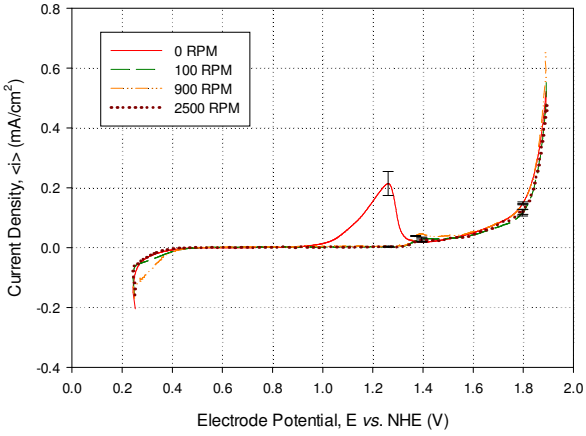


**Figure 39: *LP*s of Au at different rotation rates at 25 °C with 1 M ethanol in 0.1 M perchloric acid at a scan rate of 10 mV/s**

The LP runs for the electro-oxidation of ethanol in 0.1 M perchloric acid on platinum are shown in Figure 38 at 0 and 100 RPM, and gold in Figure 39, at different rotation rates. More rotations weren't produced for platinum as the activity of gold is negligible, with no linear relation of rotation rate to current density as can be seen in Figure 39, which does not justify the production of a full set of platinum results. In literature, platinum is known for the EOR being kinetically, and not mass transfer controlled, and thus there are no extensive studies of polycrystalline platinum at different rotation rates [101, 111].

The different peaks found on platinum in Figure 38 are briefly discussed in section 4.3.1.1. The *first peak* is the initiation of the oxidation of ethanol, forming acetaldehyde [98, 101, 111], where the surface bound hydroxyl ions are formed [98] and the *second peak* appears right after oxide adsorption occurs and is the oxidation of species not completely oxidised at the *first peak* (acetaldehyde or derivative thereof [101]) forming acetic acid, which is oxidised on an oxidised surface that also includes the oxidation of adsorbed CO [92]. The *third peak* might be the further oxidation of by-products produced from the first and second oxidation peaks found in the voltammogram or even the oxidation of ethyl acetate formed by the chemical reaction of ethanol and acetic acid [107] – regardless, there are no literature findings to support this speculation. On gold the current starts to increase from about 1.0 V *vs.* NHE, reaching a maximum current density at ca. 1.26 V of 0.21 mA/cm$^2$ with a standard error of 0.04 mA/cm$^2$, implying relatively low repeatability. It is important to note that only the 0 RPM LP showed activity, whereas the other *RPM*s (> 0 RPM) showed no oxidation peak at ca. 1.26 V *vs.* NHE. On platinum, the observation that the current density becomes less and less repeatable might be due to the poisoning by CO that adsorb on the surface of the electrode. The reaction rate, or current density, on both platinum and gold is thus not mass transport controlled but rather by reaction kinetics [53, 101] or adsorption phenomena [53]. The kinetic inhibition on gold could be due to the less facile surface oxidation of the gold electrode in acidic medium and consequent ineffective adsorption of ethanol molecules to the surface, for oxidation to take place.

The activity of Au with different rotations showed no significant change in the current density between the rotation rates, such that application of Koutecký-Levich or Levich (sections 2.3.2 – 2.3.3) would be rendered useless. Thus, investigating diffusion limitation only was insufficient as to determine reaction characteristics and therefore, as the reactivity is clearly kinetically dependent, the reaction was studied at different temperatures.

#### 4.3.1.3. Effect of Temperature

As gold did not exhibit any significant activity towards the EOR, the reaction was investigated at 10 ℃ and 40 ℃ to determine the effect temperature has on the reaction

kinetics, as depicted in Figure 40 and Figure 41 below. As can be seen in Figure 40 and Figure 41, both platinum and gold do not exhibit a linear increase in current density with temperature increase, thus rendering the application of Arrhenius (equation (20)) not viable.

On platinum (Figure 40), the *third peak* behaves differently form the first and *second peak* with an increase in temperature. Within these specific experimental conditions of Figure 40, it would be expected that the *third peak* should behave similarly to the *first* and *second peaks*. This difference in behaviour is clearly an indication of the complexity of the mechanism of the EOR on platinum in acidic medium at different temperatures and rotation rates. The mechanism was not in the scope of this study, so further investigation was not attempted.

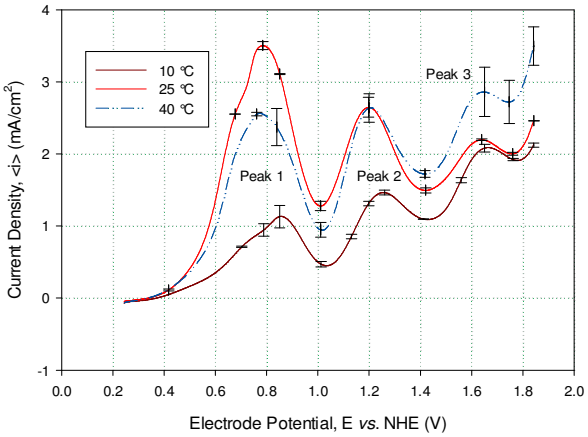


**Figure 40: EtOH oxidation on Pt at 0 RPM in 0.1 M $HClO_4$ and 1 M EtOH at three different temperatures with a scan rate of 10 mV/s**

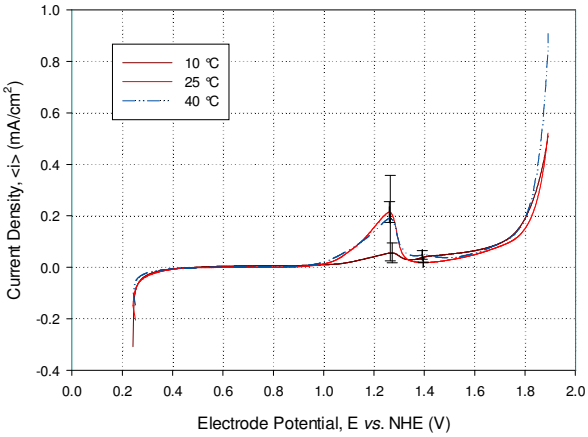


**Figure 41: EtOH oxidation on Au at 0 RPM in 0.1 M $HClO_4$ and 1 M EtOH at three different temperatures with a scan rate of 10 mV/s**

It is clear from Figure 40 and Figure 41 that repeatability for platinum and gold *LP*s are better at lower, rather than higher temperatures. At 10 ℃ the standard error on gold between the experimental runs was 0.04 mA/cm$^2$, which implies poor repeatability, with the 40 ℃ experiments having an increased error of 0.17 mA/cm$^2$. The decrease in repeatability at higher temperatures might have been due to the increased evaporation of ethanol from the electrolyte solution as the temperature was increased [102] or the lack of efficient electrode surface interactions with ethanol [46, 114]. The most appropriate solution for the repeatability issue would be to study the reaction at elevated pressures, in a closed environment, as in literature [102], which was beyond the scope of this project.

The shape of the voltammograms for platinum and gold is the same as their respective voltammograms in Figure 38 and Figure 39. The potential range of the LP runs in Figure 40 and Figure 41 was the same as the different rotation rate *LP*s from Figure 38 and Figure 39,

with the different peaks attributable to the same reaction products and intermediate species as discussed in sections 4.3.1.1 and 4.3.1.2.

An interesting phenomenon on platinum is that the maximum of most 40 ℃ peaks are reached at potentials mainly before the maxima are reached of the different peaks at lower temperatures, as is the case in literature [102]. For the *first peak*, the reaction is not favoured at higher temperatures, although the *second* and *third peaks* show an increase in activity, which ultimately indicates that the different intermediate species have different interactions with the electrode surface that supports the complexity of the mechanism [102] even though the activity and repeatability is not favourable. According to literature, as the temperature increases, the electrode active sites become more readily available, due to easier dissociation of adsorbed reaction intermediates (acetaldehyde and acetic acid) and poisons (CO) for the consequent reaction of the ethanol molecules and intermediate species [102]. Hence the decrease in potential of the peak maxima as the temperature increases.

There is no available literature on polycrystalline gold electrodes for use in EOR at different temperatures. The only available study is for platinum in phosphoric acid by, Camargo *et al.* [102]. It is clear from literature searches, that the effect of temperature on the EOR for different electrode materials lack a tremendous amount of understanding and investigation.

### 4.3.1.4. Tafel Plots

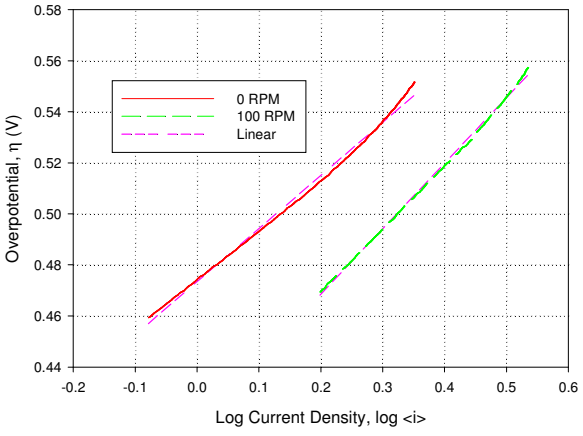


**Figure 42: Tafel plots for Pt in 0.1 M $HClO_4$ and 1 M EtOH at different *RPM*s at 25 ℃**

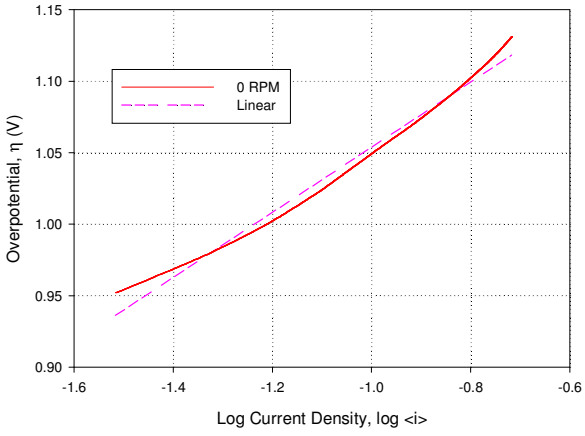


**Figure 43 Tafel plot for Au in 0.1 M $HClO_4$ and 1 M EtOH at 0 RPM at 25 ℃ plotted from the potential range of 1.052 – 1.231 V *vs.* NHE**

The Tafel plots for ethanol oxidation in acidic media are given in Figure 42 above for 0 and 100 RPM at standard temperature of 25 ℃. The Tafel slope for 0 RPM was calculated from the potential range of 0.559 – 0.652 V *vs.* NHE as 209 mV/decade with an $R^2$ of 0.996. For 100 RPM the potential range was taken from 0.569 – 0.659 V *vs.* NHE giving

257 mV/decade with an $R^2$ of 0.998. The 100 RPM Tafel slope is bigger than the 0 RPM, indicating the reaction might be less favourable at higher rotation rates. The calculated Tafel slope for the 0 RPM LP in Figure 39 on gold is 228 mV/decade and the square of correlation ($R^2$) is 0.9862. There are no literature values for the Tafel slope in acidic medium for polycrystalline platinum or gold electrodes that can be used as comparison of the determined values in this study. The EOR is thus less sluggish on platinum than on gold, implying that platinum is the better catalyst for the EOR than gold, in acidic medium.

#### 4.3.1.5. Conclusion

The EOR on platinum in acidic medium showed very good correlation with literature. The Tafel slope for the reaction at 0 RPM was determined as 209 mV/decade on platinum and 228 mV/decade for gold, which indicates the EOR as being more active on platinum than on gold. A third oxidation peak in the forward scan on platinum was discovered, which is not indicated, mentioned, studied or even considered in literature. This third oxidation peak thus needs extensive future studying and breakdown, which might lead to a better understanding of the EOR mechanism on platinum.

Activation parameters (Arrhenius section 2.3.4) and reaction diagnosis techniques (section 2.3.2 – 2.3.3) could not be applied to the produced results as there were no viable linear relationships in the current densities with increased rotation rates or temperatures.

For bulk/polycrystalline/smooth gold electrode surfaces, ethanol oxidation has thus been shown to be electro-catalytically inactive in acidic medium with no literature explicitly focusing on the EOR in acidic medium, to which the produced results could be compared. The lack of surface interactions with alcohols and inertness of gold makes its viability as catalyst for ethanol oxidation in acidic medium extremely low.

The EOR was also shown to be kinetically controlled rather than mass transfer controlled, especially on gold. The reaction products formed on platinum in acidic medium might be acetaldehyde and acetic acid with the possible reaction products on gold, acetaldehyde.

The EOR was investigated in alkaline medium so as to compare the performance to acidic medium.

### 4.3.2. Alkaline

#### 4.3.2.1. Preconditioning Media Concentration Effect

The effect of the concentration of the alkaline medium as preconditioning media with the effect of electrolyte concentration on the preconditioning of the electrode and the consequent effect on the effectiveness of the electrode towards the EOR was investigated.

The preconditioning in 0.1 M KOH is shown in Figure 17 above (section 3.3.2.2) and reproduced in Figure 45 below.

Figure 44 shows the preconditioning voltammogram of gold in 1 M KOH while Figure 45 shows the voltammogram in 0.1 M KOH. For comparison's sake the vertex potentials were set to the maximum of 0.841 V *vs.* NHE and the minimum vertex as -0.78 V *vs.* NHE with the cycling started at -0.78 V *vs.* NHE at 50 mV/s, just as in the 0.1 M KOH experimental settings. The oxide formation and reduction in 1 M KOH commences at potentials slightly lower than in the preconditioning voltammogram of 0.1 M KOH. The oxide adsorption in 1 M KOH occurs at 0.44 V *vs.* NHE compared to 0.5 V for the 0.1 M KOH concentration, with the current density of the peak in the 1 M KOH being higher than the 0.1 M KOH. The oxide reduction peak appeared at a lower potential for the higher concentration KOH (0.27 V *vs.* NHE) than the lower KOH concentration (0.35 V *vs.* NHE).

The reduction current densities were not greatly affected, with the 1 M KOH reduction current density being -0.22 mA/cm$^2$ *vs.* the 0.1 M KOH reduction peak's current density at -0.2 mA/cm$^2$. It can be seen that the surface oxide formation occurs with much more ease in higher concentrations of $OH^-$ as shown by extensive studies of pH effects on electrode reactions found in literature [101, 110] and depicted by reactions (9) to (11) in section 2.1.2.

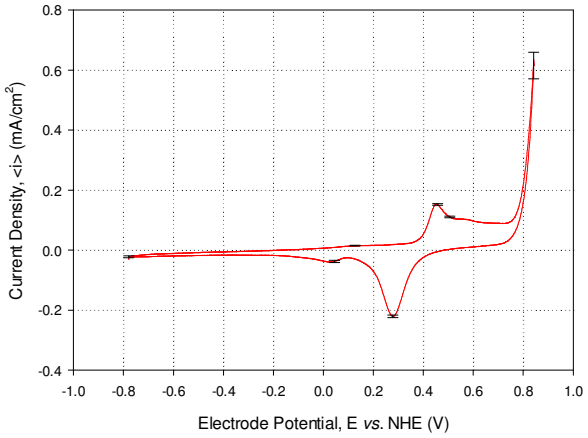


**Figure 44: Preconditioning CV for Au in 1 M KOH at 25 °C and 0 RPM at a scan rate of 50 mV/s**

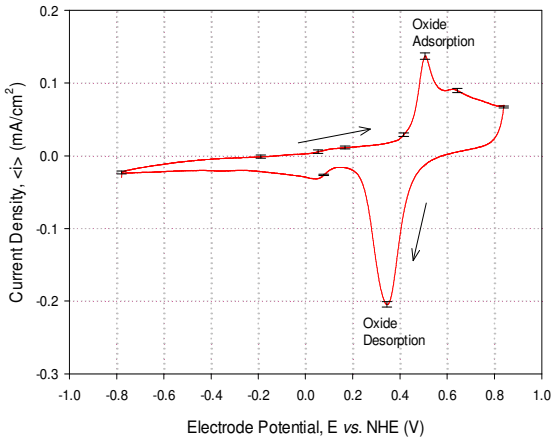


**Figure 45: Preconditioning CV for Au in 0.1 M KOH at 25 °C and 0 RPM at a scan rate of 50 mV/s (Same CV as in Figure 17)**

The performance of *LP*s for each preconditioning medium concentration was compared (Figure 46). The ethanol oxidation *LP*s are shown at 0 RPM in Figure 46 at each different preconditioning KOH concentration with the LP runs done in 1 M KOH with 1 M ethanol in solution. It was found in literature that in alkaline medium, a platinum hydroxyl bond (Pt-OH) is formed [67], with the adsorbed hydroxide (OH) blocking active binding sites [31, 76, 86]. The subsequent active sites are the sites not occupied by adsorbed OH, as to allow, in this

case of literature [31, 76, 86], $O_2$ to bind for reaction. As the concentration of OH increases in the preconditioning electrolyte, the blocking of active sites also increases, thus lowering the effective oxidation of ethanol in solution, as depicted in Figure 46.

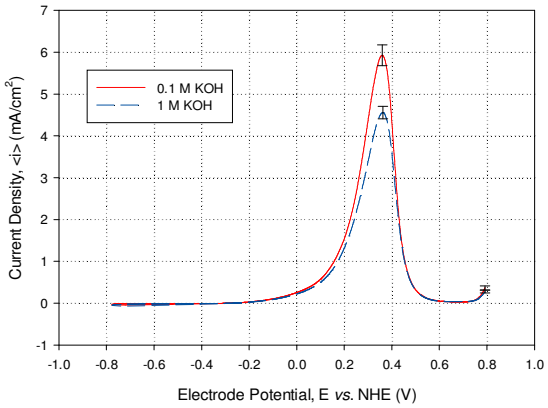


**Figure 46: Au LP comparisons in 1 M KOH with 1 M EtOH at 0 RPM and 25 °C with a scan rate of 10 mV/s after each different KOH concentration preconditioning**

The results from Figure 46 are summarised in the following table:

**Table 7: LP comparison results for the effect of different preconditioning medium concentrations**

| **LP Results for Au in 1 M KOH with 1 M ethanol with different preconditioning concentrations at 0 RPM** | | |
|---|---|---|
| Preconditioning electrolyte concentration (M): | 1 | 0.1 |
| Peak Starting Potential (E *vs.* NHE): | -0.2 | -0.2 |
| Peak Maximum Potential (E *vs.* NHE): | 0.362 | 0.360 |
| Current Density (mA/cm$^2$): | 4.560 | 5.930 |
| Standard Error (mA/cm$^2$): | 0.148 | 0.247 |

The difference between the two preconditioning concentrations on the performance of the electrode can be clearly seen in Figure 46 and Table 7, with the current density of the run after preconditioning in 0.1 M KOH being higher than the current density of the LP run after preconditioning in 1 M KOH. It can therefore be concluded that the performance of the LP runs are better with a higher current density when using 0.1 M KOH to precondition the electrode.

### 4.3.2.2. Effect of Reagent in Solution

After the necessary preconditioning as described in section 3.3.2.2, the following *CV*s in Figure 47 and Figure 48 were generated to act as control to see if the electrodes showed any activity towards the EOR. Electrode cleaning (section 3.2.4.1) and preconditioning was followed as described in section 4.2.1.2 for the control *CV*s. Note the difference in the scale

of the y-axes in Figure 47 and Figure 48 for the *CV*s without ethanol vs. the *CV*s with ethanol. It is set to that scale for legibility purposes.

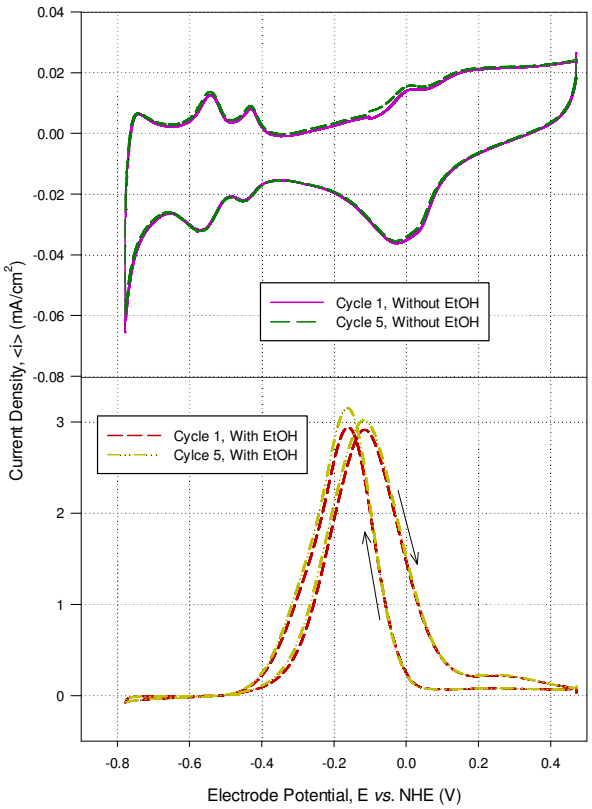


**Figure 47: Control *CV*s for Pt in 1 M KOH with and without 1 M EtOH at 25 ℃ with a scan rate of 10 mV/s**

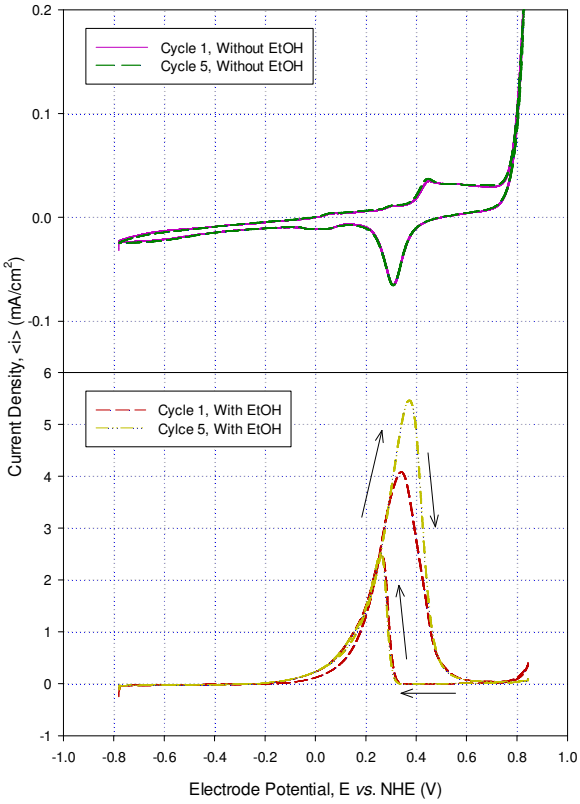


**Figure 48: Control *CV*s for Au in 1 M KOH with and without 1 M EtOH at 25 ℃ with a scan rate of 10 mV/s**

When comparing the two scenarios exhibited in Figure 47, it is clear that the peaks of ethanol oxidation appear in between the oxide adsorption/desorption and hydrogen adsorption/desorption areas of the voltammogram – the double layer region of platinum. It is clear from Figure 48 that the electrochemical oxidation of ethanol on gold is much more effective in alkaline than in acidic medium (compare Figure 37). The current density produced with the ethanol solution in alkaline medium is about a factor of ten higher than the CV of gold without ethanol in 1 M potassium hydroxide.

In the forward scan of the CV for platinum with ethanol, the current density starts to decrease as the area of oxide adsorption is entered (ca. 0.1 V *vs.* NHE), which is also the case for gold at ca. 0.4 V *vs.* NHE. With the backward scan on platinum, the current density starts to increase immediately after the oxide desorption takes place (ca. 0.0 V *vs.* NHE), reaching a low of almost no activity as the potential approaches the hydrogen adsorption region (from ca. -0.4 V *vs.* NHE). After hydrogen desorption takes place the current density starts to increase (from ca. -0.4 V *vs.* NHE) once again for the forward scan.

The oxidation peak in the forward [92] scan on gold at ca. 0.36 V *vs.* NHE with a current density of 4.95 mA/cm$^2$ indicates the oxidation of ethanol species adsorbed on the surface of the electrode [101, 114], right before the surface oxidation of the gold electrode takes place [101]. The product formed is acetic acid, as determined in literature [101, 114] or, in this case, acetate ions, as this product is formed in alkaline medium [34]. On platinum the main oxidation peak (ca. -0.1 V *vs.* NHE) in Figure 47 is the splitting of the C-C bond of ethanol, as has been found by literature [101, 103]. In literature the activity decreased with each successive potential sweep of *CV*s. In the case of Figure 47, the current seems to increase slightly with each successive cycle, which might prove that there are no real poisoning species forming and adsorbing on the electrode surface as is the case with literature [101, 103]. The lack of poisoning might be because of the higher concentration of hydroxyl anions in the solution, assisting the oxidation of adsorbed intermediate species when the potential sweep enters the oxide formation region of the voltammogram, which is quite contrary to literature findings; however the electrolyte from literature is NaOH and not KOH as in this study [103]. It can be deduced that the decrease in current is due to the blocking of the active sites on the electrode surface by oxides adsorbed on the active sites, as it can be seen, when taking the CV in Figure 47 without ethanol in solution into account, that the EOR current declines at the oxide formation region.

On gold, the peak in the reverse scan at 0.23 V *vs.* NHE, with a current density of 1.59 mA/cm$^2$ is the continuation of ethanol oxidation after the electrode surface has been reduced [114]. The coinciding of the backward scan's peak with the forward scan can act as an indication that there are no poisoning species adsorbed on the electrode surface, it also implies that the concentration of ethanol is high enough at the electrode/electrolyte interface that the oxidation reaction of ethanol takes place faster than the reduction of the gold surface molecules [114], hence the increase of current in the oxidative direction. In the backwards scan, the cathodic current density would become smaller as the ethanol concentration increases right before changing to anodic current [114]. In the backward scan on platinum it can also be seen, from the CV in Figure 47 without ethanol, that the hydrogen adsorption region is the region where the EOR peak's current density decreases. The decrease in current density as not to follow diffusion-controlled reaction inhibition behaviour, might be due to competition between oxide, ethanol, or intermediate species for active sites on the platinum surface, or poisoning of the electrode surface by reaction intermediates, or the passivation of active sites by oxide adsorption, and even hydrogen adsorption [101, 107, 110, 115].

The reaction on platinum shows a clear hysteresis that is slightly different from literature's findings where the hysteresis was not so well defined [103]. This difference might be

attributable to the electrolyte used as Lai *et al.* [103] used 0.1 M NaOH, whereas, in the case of Figure 47, 1 M KOH was used. It might also be attributed to the crystal lattices of the polycrystalline platinum, as can be seen in Figure 11 in section 3.3.1. Lai *et al.* [103] found that Pt (111) showed less activity towards ethanol electro-oxidation compared to the (110) lattice, and because the dominant crystal lattice is (111) for the polycrystalline electrode surface.

Lai *et al.* [101] found that the electro-oxidation of ethanol on gold takes place at higher potentials than depicted in Figure 48. They showed the electro-oxidation peak of ethanol in sodium hydroxide starts at ca. 0.4 V *vs.* NHE while Figure 48 shows the electro-oxidation in potassium hydroxide starting at ca. -0.1 V *vs.* NHE. The difference could be ascribed to the molar conductivity of the $K^+$ *vs.* the $Na^+$ cations in solution. The ionic conductivities of potassium and sodium is given as 7.350 $mS.m^2/mol$ and 5.010 $mS.m^2/mol$ respectively [122]. The resistance of the sodium hydroxide is thus higher than the potassium hydroxide electrolyte, implying that higher overpotential is necessary for current to flow in sodium hydroxide solution. Snell *et al.* [110] studied the effect of different anions on the electro-oxidation of ethanol and established that the adsorption of anions on the electrode surface played an intricate role in the activity of the electrode and even overpotential, which can be attributed to isotherms [110] affecting adsorption.

#### 4.3.2.3. Effect of Rotation Rate

After the control *CV*s were done the conventional preconditioning and cleaning procedures were followed (section 3.2.4.1 and 3.3.2.2) prior to conducting the subsequent experiments. The *LP*s for the EOR on platinum and gold are given in Figure 49 and Figure 50 below.

The current density declines as the rotation rate of the electrode increases for both platinum and gold (Figure 49 and Figure 50). In literature it was found that the current density showed little or no increase when electrode rotation was introduced to the experiment.

There are two phenomena that appear in the EOR, as depicted in Figure 49 and Figure 50. The first is that there is no limiting current density as indicated by the decrease in current density from ca. 0.35 V *vs.* NHE to almost 0 $mA/cm^2$ at ca. 0.6 V *vs.* NHE for gold and ca. -0.1 V *vs.* NHE for platinum to close to 0 $mA/cm^2$ at about 0.2 V. The second phenomenon is the current density that decreases as the rotation rate increases for both electrodes.

The first phenomenon is because of the oxidised layer of gold at ca. 0.5 V *vs.* NHE that inhibits the EOR as, according to literature, the EOR prefers an un-oxidised gold electrode surface [47] whereas for platinum, the inhibition might be due to various factors pacifying the electrode active sites as described in section 4.3.2.2 [101, 107, 110, 115].

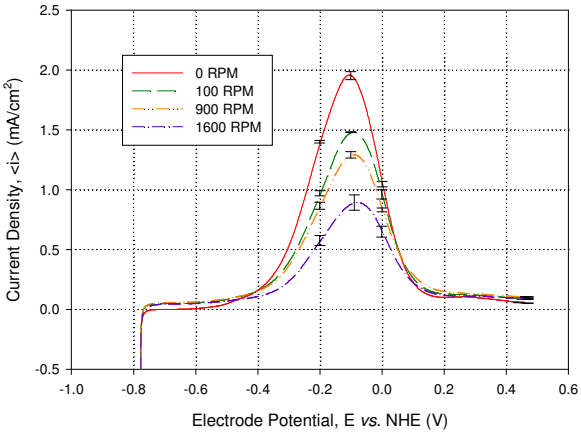


**Figure 49: *LP*s for Pt at different rotation rates in 1 M KOH and 1 M ethanol at 25 °C and 10 mV/s scan rate**

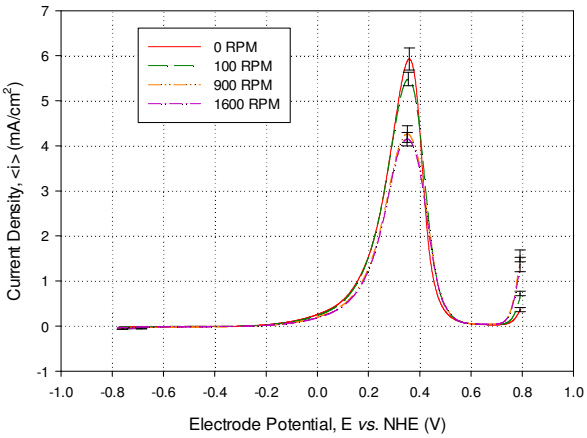


**Figure 50: *LP*s for Au at different rotation rates in 1 M KOH and 1 M ethanol at 25 °C and 10 mV/s scan rate**

There are no established poisoning intermediate species adsorbed on the gold surface, according to literature [114], however, some authors claim it to be the case [108]. Thus the decline of the current density might not be because of poisoning intermediate species adsorbed on the gold electrode surface, as is the case with platinum [114]. The decrease in current density after the main ethanol oxidation peak appearance coincides with the beginning of the oxide adsorption peak on both gold and platinum, as can be seen in Figure 47 and Figure 48 respectively, without ethanol in solution. It thus shows that the ethanol oxidation reaction prefers a reduced surface for proper reaction activity [114].

Regarding the second phenomenon, all the *LP*s depicted in Figure 49 and Figure 50 clearly show that the reaction kinetics of the electro-oxidation of ethanol is not limited by mass transport but rather reaction kinetics on both electrodes [101]. It might be because of a lack of good surface interaction between the gold and platinum catalyst surfaces with the ethanol in solution, as ethanol adsorbs weakly on gold [92, 93, 112] and platinum [101]. As the rotation rate increases the current density falls, which may imply that the species might be forced away from the electrode surface before oxidation as the ethanol evades the active sites on the electrode surface – there are no literature investigations of the EOR on gold or platinum at different rotation rates to support this; regardless, literature indicates the interaction strength of ethanol for both gold [92, 93, 112] and platinum [101] being weak. Because of the kinetic inhibition of the EOR on both electrodes, the following section regarding different temperatures was introduced.

### 4.3.2.4. Effect of Temperature

The different temperatures at which the EOR was studied included 10, 20, 30 and 40 °C at 0 RPM. The electrochemical experimental settings were used as in the LP runs of Figure 49 and Figure 50.

The *LP*s of ethanol oxidation in 1 M KOH and 1 M ethanol at different temperatures is shown in Figure 51 for platinum and Figure 52 for gold. The current density for each temperature's LP maximum peak on platinum increases from 1.219 mA/cm$^2$ at -0.08 V *vs.* NHE for 10 °C to 1.626 mA/cm$^2$ at -0.1 V at 20 °C then to 1.96 mA/cm$^2$ at ca. -0.1 V for 25 °C, which then increases to 2.14 mA/cm$^2$ at -0.12 V for the 30 °C scan and lastly to 2.73 mA/cm$^2$ for the 40 °C scan at ca. -0.146 V *vs.* NHE. The same phenomenon regarding the decrease in onset potential of the EOR peak at increased temperature is visible on the *LP*s for both platinum and gold, as is the case in acidic medium for platinum, as reported in literature [102] with the potential of the maximum peak position also decreasing with increasing temperature.

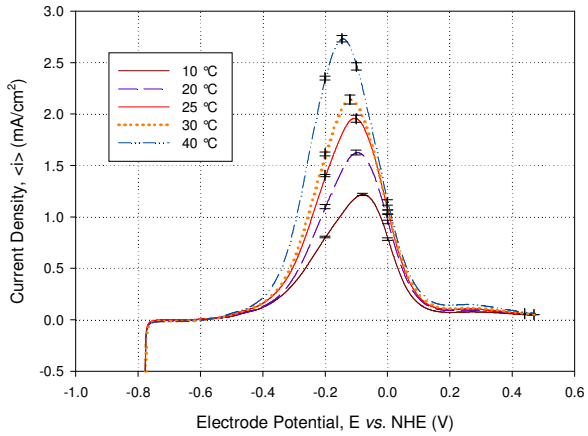


**Figure 51: LP results for ethanol oxidation on platinum in 1 M KOH with 1 M EtOH at different temperatures and 0 RPM and a scan rate of 10 mV/s**

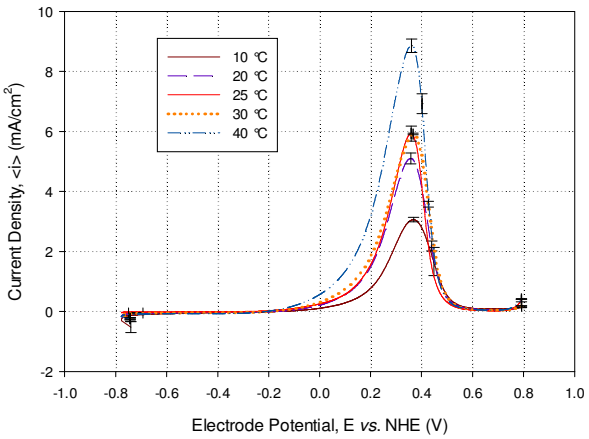


**Figure 52: LP results for ethanol oxidation on gold in 1 M KOH with 1 M EtOH at different temperatures and 0 RPM and a scan rate of 10 mV/s**

This phenomenon is due to the greater ease of dissociation of poisoning species or anions adsorbed on active sites on the electrode surface. For all temperatures on gold the maximum peak current density was reached at ca. 0.35 V *vs.* NHE. The increase in current density was relatively linear with the 10 °C run reaching a maximum current density of 3.063 mA/cm$^2$, 20 °C reaching 5.102 mA/cm$^2$, 25 °C 0.360 mA/cm$^2$, 30 ° about 0.367 mA/cm$^2$ and 40 °C reaching a maximum current density of 8.857 mA/cm$^2$. The phenomenon of the change in peak maxima position with change in temperature is not found on gold as on platinum, supporting literature findings that the EOR on gold is not affected by poisoning intermediate species [114].

By considering Figure 49 and Figure 51 for platinum and Figure 50 and Figure 52 for gold, it is clear that the ethanol oxidation reaction is kinetically inhibited and not by mass transfer, which corresponds with literature findings [101, 103].

The Arrhenius plot of the results from Figure 51 and Figure 52 above is given below. The natural logarithm of the current density is plotted against the inverse of the temperature by using the values of current density for every LP at each temperature at an overpotential of ca. -0.186 V *vs.* NHE for platinum and 0.250 V *vs.* NHE for gold, after which the slope of the linear plot can be used in equation (20) (section 2.3.4) to determine the activation energy. The linear regression values of the plots from Figure 53 and Figure 54 are given in Table 8 below.

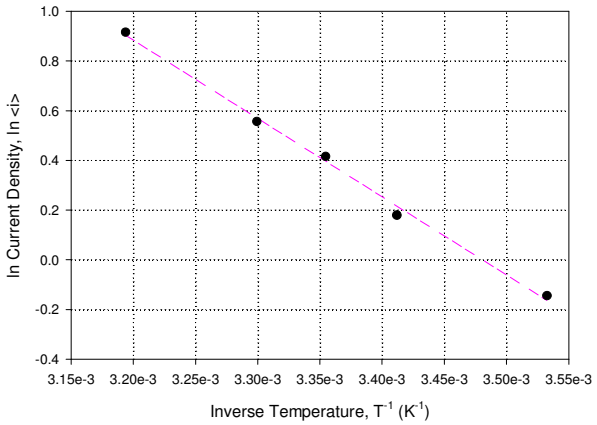


**Figure 53: The Arrhenius plot of the ethanol oxidation reaction on Pt in 1 M KOH and 1 M ethanol at different temperatures taken from the peak potential of ca. -0.186 V *vs.* NHE**

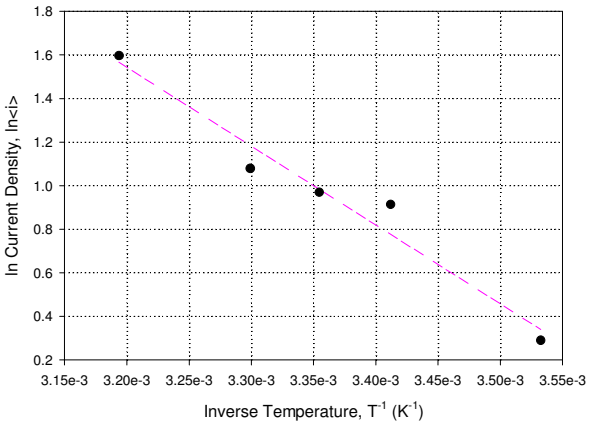


**Figure 54: The Arrhenius plot of the ethanol oxidation reaction on Au in 1 M KOH and 1 M ethanol at different temperatures taken from the peak potential of ca. 0.25 V *vs.* NHE**

**Table 8: The values of the linear plot from Figure 53 and Figure 54**

| Linear Parameters | Platinum | Gold |
|---|---|---|
| Slope: | -3151.251 | -3622.837 |
| Intercept: | 10.967 | 13.136 |
| Correlation square: | 0.9961 | 0.9614 |

The activation energy was calculated using equation (20), the slopes from Table 8 for each respective electrode and the universal gas constant as in Table 24 (Appendix 1 – Data). The calculated activation energy for platinum is $E_a$ = 26.201 kJ/mol and for gold as $E_a$ = 30.121 kJ/mol. There are no literature values to use for comparison purposes as there is no extensive investigation into the temperature effect on ethanol oxidation with polycrystalline platinum or gold electrodes in alkaline medium. The activation energy on platinum for the

EOR (26.201 kJ/mol) is less than the activation energy of the EOR of gold (30.121 kJ/mol) showing that less energy is required on platinum for the EOR.

To further compare the activity of platinum and gold towards the EOR, the Tafel slopes are calculated and compared in the following section.

### 4.3.2.5. Tafel Plots

Figure 55 and Figure 56 below show the Tafel plot for the 0 RPM LP of platinum and gold respectively, in 1 M KOH with 1 M ethanol. The reaction is relatively sluggish on platinum as compared to gold, with a calculated Tafel slope of 249 mV/decade for platinum with an $R^2$ of 0.99 and 227 mV/decade with an $R^2$ of 0.998 for gold. If the magnitudes of the Tafel slope were to be considered, Tafel region used for extrapolation (region of Tafel behaviour - section 2.3.1), as well as uncontrolled variables such as surface lattices and area, and ethanol evaporation, the difference in slope magnitudes could be considered insignificant, with a difference of only 22 units. Thus, platinum and gold's activity could be regarded as similar in this case.

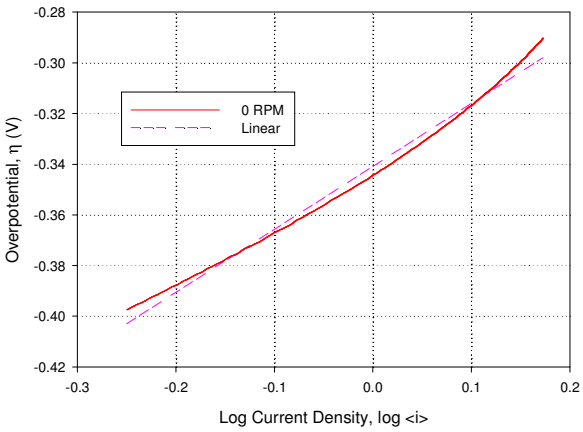


**Figure 55: The Tafel plot for Pt in 1 M KOH and 1 M ethanol at 0 RPM and 25 °C plotted from the potential range of -0.297 – -0.19 V *vs.* NHE**

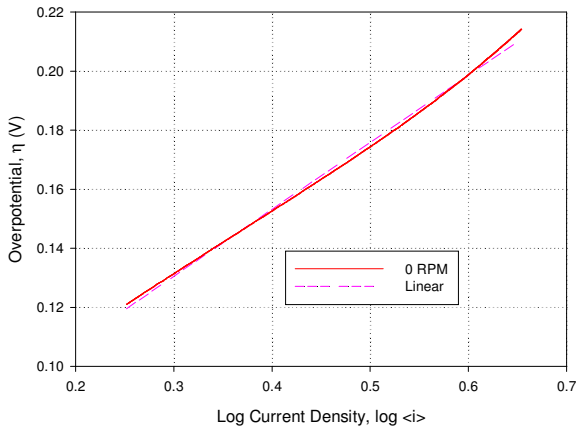


**Figure 56: The Tafel plot for Au in 1 M KOH and 1 M ethanol at 0 RPM and 25 °C plotted from the potential range of 0.221 V – 0.314 V *vs.* NHE**

### 4.3.2.6. Conclusion

The Tafel plot could be established for both electrodes with platinum giving a slope of 249 mV/decade and gold 227 mV/decade, indicating the EOR on platinum as slightly more sluggish compared to gold with the difference of 22 mV/decade to be considered insignificant. The kinetic evaluation, using the Arrhenius equation, was also successfully applied as there was a linear relation of the current density increase with increasing temperature for both platinum and gold, with the activation energy on platinum calculated as

26.201 kJ/mol and on gold as 30.121 kJ/mol. The reaction at different rotation rates also showed no linear increase as to enable the application of the Koutecký-Levich and Levich analyses to determine the number of electrons transferred on each electrode used in this study.

The main products formed on platinum were $CO_2$ and adsorbed species of $CH_x$ and CO, according to literature, and on gold, acetic acid or in the case of alkaline media, acetate.

## 4.4. Conclusion of the Ethanol Oxidation Reaction

In this study, platinum showed superior activity in acidic medium and slightly inferior activity in alkaline medium, compared to gold, when taking the Tafel slopes into account. Regardless, considering all the possible variables that could play a role in the higher Tafel slope value of platinum in alkaline medium, the difference between gold and platinum could be regarded as insignificant. In alkaline medium gold had an apparent increase in activity compared to the acidic medium; nonetheless smooth platinum could be regarded as a more preferred catalyst over a smooth gold electrode. Literature speculation that un-activated gold showed better performance to the ethanol electro-oxidation reaction in alkaline media rather than acid media is supported by the results in Table 9 below [47]. As discussed in section 4.3.2.5, the results from Table 9 support the conclusion that platinum performs better in both alkaline and acidic medium than gold. Gold performs better in alkaline medium as CO poisoning does not occur on the gold surface as with platinum [114], due to the fact that the platinum electrode is prone to CO poisoning [32].

The most accepted electro-oxidation reaction mechanism ($C_2$-pathway) for ethanol on a gold electrode suggests that the reaction takes place without the breaking of the C-C bond, which then forms acetaldehyde and acetic acid [101]. The $C_1$-pathway for the electro-oxidation of ethanol involves the breaking of the C-C bond in ethanol or acetaldehyde, which can produce $CO_2$ or bicarbonate [101]. This pathway is evident on a platinum electrode in the absence of strong adsorbing anions. The C-C bond is broken at low potentials in alkaline medium. The adsorbed species are thus $CH_x$ and CO. The $CH_x$ are firstly oxidised to CO then to $CO_2$ or (bi)carbonate. $CH_x$ intermediate species are found to be more stable in alkaline media, with the dominant poisoning species in alkaline solution being adsorbed CO, implying that $CH_x$ is readily oxidised on a polycrystalline platinum surface in alkaline solution. C-C bond breaking is thus more facile in alkaline medium, which in turn enhances the selectivity of the pathway to the $C_1$-pathway in alkaline medium on a platinum electrode, also evident in the magnitude of the Tafel slope comparison in Table 10 below.

### 4.4.1. Results Comparison

To compare platinum and gold activity the Tafel slopes are given below in Table 9 for alkaline and acid media:

**Table 9: Platinum and gold activity compared in alkaline and acidic media**

| Tafel slopes of platinum and gold in alkaline and acid media at 0 RPM | | | |
|---|---|---|---|
| **Gold Alkaline** | **Gold Acidic** | **Platinum Alkaline** | **Platinum Acidic** |
| 227 | 228 | 249 | 209 |

Using the results from Table 9, the sluggishness of the electrodes can be ordered as $Pt_{alkaline}=Au_{alkaline}>Au_{acid}>Pt_{acid}$. It is clear that the reaction is favoured in both media on platinum.

The following table (Table 10) summarises all the results for the EOR on platinum and gold in both acid and alkaline media.

**Table 10: Comparison table for all the results at 0 RPM for ethanol oxidation in platinum and gold in both acid and alkaline media**

| | | **Peak Potential E *vs.* NHE** | | **Peak Current Density mA/cm$^2$** | | **Tafel Slope mV/decade** | | **Activation Energy kJ/mol** | |
|---|---|---|---|---|---|---|---|---|---|
| **Reaction** | **Medium** | **Au** | **Pt** | **Au** | **Pt** | **Au** | **Pt** | **Au** | **Pt** |
| **Ethanol Oxidation** | **Acid** | 1.26 | 0.8 | 0.21 | 3.5 | 228 | 209 | - | - |
| | **Alkaline** | 0.36 | -0.1 | 5.93 | 1.96 | 227 | 249 | 30.121 | 26.201 |

As stated in literature, a smaller Tafel slope indicates a more favoured reaction whereas a large Tafel slope indicates a more sluggish reaction. It is thus clear from this study and the data shown in Table 10 that the oxidation of ethanol was more favoured on platinum in acid medium than on gold.

If the Tafel slopes were taken into account, platinum would seem to be the lesser active electrode in alkaline medium irrespective of the insignificant difference in slope magnitude (section 4.3.2.5). Therefore all the determined parameters should be taken into consideration when deciding which electrode material is the best. In alkaline medium, the C-C bond is broken and $CO_2$ and adsorbed CO and $CH_x$ is formed with an activation energy requirement less than gold, which only produces acetic acid in alkaline medium. Therefore, platinum is the best catalyst for the electro-oxidation of ethanol in alkaline and acid medium as found in literature [101, 103].

# Chapter 5: Sulphur Dioxide Oxidation Reaction (SDOR)

## 5.1. Literature

$SO_2$ is one of the most dangerous pollutants released into the atmosphere by industries [123-126] and one of the main causes of acid rain [124-127] i.e. the conversion of $SO_2$ and $H_2O$ into $H_2SO_4$. The safety limit of $SO_2$ concentration has been set to 2 ppm as it is an aggressive polluting agent, causing damage to the environment and human health [123, 126]. $SO_2$ is irritating to mucous membranes and the throat, along with the upper respiratory tract [124]. Necessity to reduce concentrations in emissions have arisen, especially at power plants using fossil fuels for driving electricity generation [123, 124, 126]. $SO_2$ is also believed to participate in the reduction of the ozone layer in the stratosphere [125]. Legislation worldwide has thus increased in the last decade leading to development and implementation of cleaner technologies as well as end-of-pipe solutions to decrease $SO_2$ emissions [123, 125].

Electrochemical oxidation of $SO_2$ can thus be used to reduce dissolved $SO_2$ concentrations [125]. Electrochemical oxidation of $SO_2$ in aqueous sulphuric acid produces $H_2SO_4$ at the anode and hydrogen gas at the cathode [125]. Possible adsorbed oxygen species might also be involved in the electrochemical oxidation of $SO_2$. The coverage of $SO_2$ on the electrode surface depends on the potential at which $SO_2$ is adsorbed [18]. Electrode active sites being covered by $SO_2$ cause inhibition of the electrode towards $SO_2$ oxidation.

### 5.1.1. HyS Cycle and Sulphur Depolarised Electrolyser

Refer to section 1.3.1 for more information on the HyS cycle for application in the Sulphur Depolarised Electrolyser (SDE).

The HyS cycle can be applied in the SDE to generate clean energy [23]. The main problems experienced with the SDE are the electrode material being used [23, 25, 26], the electrolyte concentration for most economic application of the system [23, 25], the temperature and pressure that are ideal and lastly how to separate the catholyte from the anolyte so as to prevent $SO_2$ crossover [23, 25] in order to prevent it from reducing at the cathode to form sulphur [25]. The best performance achieved in literature for the electrolysis step thus far was 200 $mA/cm^2$ at a potential of 0.6 V [23]. The slow kinetics of $SO_2$ oxidation at the anode

is the main reduction in performance of the process in equations (4) and (5) in section 1.3.1 above [18, 23].

### 5.1.2. Reaction Kinetics

The kinetics of $SO_2$ oxidation becomes worse as the concentration of sulphuric acid increases [23, 25, 26]. In the literature, the decrease in reactivity has been thought of as being the decrease in activity of the active species with an increase in sulphuric acid concentration [25]. Sulphuric acid plays an important role as too high a concentration reduces the activity of water, which plays an integral part in the electro-oxidation of $SO_2$ [128]. Increased acid concentration also drives the overpotential of the electro-oxidation of $SO_2$ higher, thus requiring more energy to force the reaction to take place, as predicted by thermodynamics. Investigations into less concentrated sulphuric acid solutions have revealed hidden processes occurring in the electro-oxidation of $SO_2$, undetectable in higher sulphuric acid concentrations [23]. The OCP of $SO_2$ containing solutions also increases with increasing sulphuric acid concentrations, indicating an inhibiting effect of high sulphuric acid concentration.

Studies have also been done at elevated temperatures, which were used to determine the activation energy of the electro-oxidation of $SO_2$ by using the Arrhenius equation [18]. Further studies concluded at elevated temperatures are few and thus the effects of increased temperature on the reaction kinetics could not be confirmed [23]. Despite the decreasing solubility of $SO_2$ at elevating temperatures, the kinetics increase when platinum is used as electrode material [23, 25].

### 5.1.3. Reduction of $SO_2$

Cathodic treatment of both gold and platinum electrodes with $SO_2$ containing electrolyte increases the catalytic activity towards the electro-oxidation reaction of $SO_2$ [127]. Adsorbed $SO_2$ is seen to be reduced in the cathodic treating process, which then forms a catalytic sulphur layer [125, 127, 128].

The electroreduction of $SO_2$ to sulphur can be presented as in reaction (47) below [26, 129, 130]:

$$SO_2 + H_2O \longrightarrow H_2SO_3 \quad (46)$$

$$H_2SO_3 + 4H^+ + 4e^- \longrightarrow 3H_2O + S \qquad E^0 = 0.449\ V \quad (47)$$

The best potential for $SO_2$ reduction is 0.15 V *vs.* NHE before oxidation of $SO_2$ on both gold and platinum. Reduced $SO_2$ in the form of sulphur thus increases the $SO_2$ bulk oxidation reaction except if more than a monolayer of sulphur is formed, which consequently inhibits the reaction because of active site passivation [18, 23].

The adsorbed sulphur ad-layer's oxidation can be expressed as reaction (48) below [131]:

$$S + 4H_2O \longrightarrow SO_4^{2-} + 8H^+ + 6e^- \quad (48)$$

### 5.1.4. $SO_2$ Oxidation Reaction Mechanism

The reaction mechanism is quite complicated [125, 127], especially in aqueous sulphate solutions [125], as there are claims in literature [127, 128] that the oxidation and reduction of $SO_2$ takes place at about the same potential region. Literature has speculated that the rest potential in sulphuric acid solution incorporates the simultaneous reduction to sulphur and oxidation to sulphate of $SO_2$ [128] with a sensitivity to pH and significant dependence on the anode material [23, 125]. It has also been speculated in literature that the oxidation of $SO_2$ involves the surface oxide adsorbed on metal surfaces above 1 V *vs.* NHE [127]. Speculation also revolves around the products of oxidation, with dithionate being the product before oxide formation potentials and sulphate the product after oxide formation potentials. Literature also demonstrated that the main soluble product from $SO_2$ oxidation is bisulphate.

O'Brien *et al.* [23] summarised results obtained from literature to conclude the following mechanistic results: i.) higher temperatures might enhance the reaction kinetics ii.) possible kinetic inhibition at higher acid concentrations, iii.) noble metals favour the reaction kinetics rather than carbon materials, iv.) platinum and gold both involve two electron charge transfer with adsorbed reduced $SO_2$ species on the electrode surface, resulting in sulphate production, v.) both gold and platinum have diffusion limited character towards the $SO_2$ oxidation reaction on activated electrode surfaces, vi.) the reaction order is most likely first order or even fractional with respect to the $SO_2$ and dependent on the electrode material used, as well as the $SO_2$ concentration and electrode preconditioning.

From the abovementioned summary, the findings in this investigation can be compared to. The SDOR mechanism is further elaborated in each section for platinum and gold in their respective contexts. Although the mechanism was not of interest in this study, theoretical coverage and investigation was important for the establishment of the reaction activity on each electrode material.

### 5.1.5. Platinum

Platinum has been extensively investigated in the literature for use as a catalyst in the SDOR [26]. The enhancement of $SO_2$ electro-oxidation is largely dependent on the lowest potential the electrode is cycled to [26, 123, 132]. Below 0.2 V *vs.* NHE the electro-oxidation of $SO_2$ is inhibited in both the double layer region and oxide adsorption potential range [128, 132]. Above 0.2 V the oxidation current experienced no increase in activity except for the part of the potential range where oxide adsorption occurs, which remained unchanged [132]. From literature it can be concluded that ~0.2 V *vs.* NHE is the ideal potential for inducing optimum $SO_2$ electro-oxidation catalysis [132] as a catalytic layer of adsorbed sulphur is formed [26, 123, 130, 132]. Adsorption of $SO_2$, known to be very stable on platinum surfaces [23, 123, 130, 132], thus occurs at the OCP (± 0.65 V and dependent on many factors such as electrolyte concentration, etc.) and is reduced [23, 127, 128, 132] at 0.2 V and consequently promotes the electro-oxidation of $SO_2$ even though complete reduction of adsorbed $SO_2$ occurs near 0.05 V – 0.06 V *vs.* NHE.

The reduction of $SO_2$ to sulphur occurs as shown in reaction (47) in section 5.1.3 [26]. Thus, for every decrease in $E_{low}$, the onset potential and peak potential both decrease to more cathodic potentials and consequently, improve the performance of the electrode for $SO_2$ oxidation. In the activation process of platinum the adsorption of hydrogen on the surface also inhibits the electro-oxidation of $SO_2$ [133]. $SO_2$ adsorbates cannot be removed with single cyclic sweeps but require cycling up to at least 1.5 V for five repeats [123].

Kinetic information can thus be acquired from the diffusion limited part of the voltammogram on an activated platinum electrode.

#### 5.1.5.1. Reduced Adsorbed Species and Electrode Activity

For maximum enhanced $SO_2$ oxidation the coverage of the surface with adsorbed reduced $SO_2$ species should not exceed the optimum by too much or too little as the electrode activity drops noticeably [26, 128, 132]. Too much coverage reaches multilayer [23, 123, 132] coverage, which may inhibit [23, 132] the electrode activity for $SO_2$. Lower-than-optimum coverage also decreases the electrode activity but in a lesser degree than over-coverage of sulphur [132]. It can be concluded that the electrode should be completely covered for best activity [26]. Thus poisoning of the electrode occurs if the critical level of adsorbed sulphur coverage is not established [23, 130] as the sulphur physically blocks surface sites [23] from $SO_2$, preventing its adsorption and causing reduction in the electrode activity.

The platinum surface is thus modified by the sulphur, which modifies the binding character of the metal surface through surface electronic interactions [23, 130, 132] – the ligand effect

[132], to substantially promote $SO_2$ oxidation as a result of the deposition of sulphur by $SO_2$ reduction [130, 132]. Because of the sulphur on the electrode surface, the oxidation current increases dramatically and the limiting current has diffusion-limited character [23, 26, 52, 130, 132]. Depletion of the adsorbed species lowers the reactivity of the activated electrode [130, 132]. $SO_2$ is co-adsorbed with elemental sulphur where the latter modifies the surface properties, such as the electronic density at the surface, which in turn changes the way the electrode surface interacts with the dissolved $SO_2$ [127].

In literature it has also been established that the reduction of ad-species at 0.2 V involves mainly adsorbed species and electrode surface reactions, rather than bulk, dissolved sulphur dioxide [132]. At potentials lower than ~0.2 V consumption of bulk $SO_2$ is found and not adsorbed surface species. The $SO_2$ species oxidise at potentials approaching 1.5 V *vs.* NHE. The higher the amount of adsorbed, reduced $SO_2$ or sulphur, the higher the inhibition of $SO_2$ reduction becomes [132]. The oxidation state of the reduced species is still being disputed in literature. It has been determined though that the possible species is composed of sulphur-polysulphide mixtures being either soluble or adsorbed. Regardless, the adsorbed reduced species have a great effect on the oxidative currents of $SO_2$ electro-oxidation [123]. Possible adsorbed reduced species include $SO_3^{2-}$, SO and elemental sulphur [127].

#### 5.1.5.2. SDOR Mechanism

The chemical nature of the oxidised $SO_2$ species had been a cause of dispute and therefore studies had been done to prove that the S(VI) is the only stable reaction product being formed from the electro-oxidation of $SO_2$ that is apparent in the potential range of 0.65 V up to 1.5 V *vs.* NHE [132].

Above all, the mechanism of the electro-oxidation of $SO_2$ is still not fully understood [123, 128]. With the activation of the electrode by pre-treatment in $SO_2$ containing solution (activation), the electro-oxidation subsequently involves two processes where **the first** involves oxide-free platinum surfaces that are greatly enhanced by the activation method [123]. **The second** process involves the oxide-covered platinum electrode surface either at activated or unactivated states [123, 128]. In the end it involves the interaction of surface oxides with $SO_2$, although uncertainty still remains [123]. It was even speculated that oxygen coverage on platinum electrodes involved the coverage of adsorbed S species with oxygen, which inhibits the further electro-oxidation of the adsorbed S species or even $SO_2$ on platinum [23, 123]. It has also been claimed that the adsorption of oxygen on a platinum surface is inhibited by the adsorbed sulphur layer [23, 26].

The adsorption of oxides on the electrode surface also renders the electrode inactive toward the $SO_2$ oxidation reaction [23, 52, 132, 134] as excessive oxides block active sites for the oxidation reaction to take place [23]. On a negative potential sweep the $SO_2$ oxidation current is restored as adsorbed oxygen is removed [132]. The role of platinum oxide in $SO_2$ electro-oxidation remains inconclusive as platinum oxide formation does not render the electrode surface inactive, as the evolution of oxygen still occurs in solutions without $SO_2$ [23]. Inhibition is not absolute thus indicating that $SO_2$ can still be electrochemically oxidised on platinum oxide [23, 52, 123] even though not in dominance [123] (reaction (49) below).

$$Pt{=}O + SO_{2(aq)} + H_2O_{(l)} \longrightarrow H_2SO_4 + Pt \quad [23] \tag{49}$$

The consequent products of $SO_2$ oxidation were determined to be $HSO_4^-$ and $SO_4^{2-}$ mixtures [23, 123, 132]. Even in reverse cycles the oxidation products of $SO_2$ are found to be S(VI) species (see reaction (50) below) [52, 123, 127].

$$SO_{2(aq)} + 2H_2O_{(l)} \rightarrow \begin{cases} HSO_4^-{}_{(aq)} + 3H^+{}_{(aq)} + 2e^- \\ SO_4^{2-}{}_{(aq)} + 4H^+{}_{(aq)} + 2e^- \end{cases} \tag{50}$$

As found in the literature, the electro-oxidation of $SO_2$ depends on the sweep direction, with the oxidative current peaks appearing at two different potentials [52, 123]. In the forward scan the peak appears at ca. 1.25 V and the reverse peak appears at ca. 0.85 V *vs.* NHE [123] with the reverse peak intensity varying with the highest potential cycled to, and with the intensity decreasing as the potential is taken higher [23]. The current density decreases with every cycle on a stationary electrode that can be attributed to the decrease of bulk $SO_2$ concentration at the diffusion layer, which can be overcome by rotation of the electrode as described in section 2.2 [123]. Build-up of reaction products on the platinum surface has been shown not to be the cause of the inhibition of the electro-oxidation reaction of $SO_2$ [26]. The large overpotential found with platinum electrodes can thus be regarded as a result of the strong adsorption of $SO_2$ to the surface, on an un-activated electrode [23].

#### 5.1.5.3. Electrode Preparation

It has been found that the repeatability of results depends greatly on the electrode preconditioning [132-134]. Before any studies are to be done, the electrode should be potentiometrically cycled in the solution containing the test electrolyte until the voltammograms stabilise by steadying out to repeatable and well defined cycles or peaks [123, 128]. In the literature, it is agreed that the electro-oxidation of $SO_2$ can take place on platinum surfaces with or without surface oxides and that the influence of preconditioning of the electrode on the reaction is profoundly affected by electrode pre-treatment in the hydrogen adsorption potential range [123, 133].

### 5.1.6. Gold

The electrochemical oxidation of $SO_2$ has been a neglected subject on gold electrodes as compared to platinum [130]. It has however, been suggested in literature, that gold could be more active for the electro-oxidation of $SO_2$ compared to platinum [23].

The adsorption of $SO_2$ to the gold surface is known to be relatively weak, such that the oxidation thereof takes place on an almost bare Au electrode surface or at the least on a surface with weakly adsorbed $SO_2$ present [23, 130]. Because of this occurrence, the absence of the strongly adsorbed form of $SO_2$ allows for intrinsic electrocatalysis of $SO_2$ on unmodified Au electrodes [130]. The presence of sulphur species adsorbed on the gold surface, which improves the kinetics, may be related to the adatom's capability to modify surface electronic structure [23, 130]. The inherent activity of gold towards the electrochemical oxidation of $SO_2$ can be regarded as the result of weak adsorption of $SO_2$ to the gold surface [23].

It is believed that molecular $SO_2$ adsorb on gold surfaces with two different bonding strengths, which account for two different peaks in the anodic potential region [51, 129]. $SO_2$ and $SO_4^{2-}$ species are adsorbed to a greater degree on gold than on platinum. On gold, weaker adsorbed $SO_2$ might be affected by stronger adsorbed $SO_2$ as can be seen on post experimental voltammograms in electrolyte without $SO_2$ in solution, which, regardless of the high current density with $SO_2$ in solution, did not seem to inhibit the $SO_2$ electro-oxidation [128, 129]. Thus, the rate of oxidation of weak adsorbed $SO_2$ might be influenced by the presence of strongly adsorbed $SO_2$ and other particles [51]. It is thus clear that the electro-oxidation of $SO_2$ is executed through an adsorbed intermediate species, which are being displaced from the electrode surface through the formation of oxides. Hydrogen on the other hand, if adsorbed on the electrode surface, inhibits the $SO_2$ electro-oxidation reaction [133].

### 5.1.6.1. Mechanism of SDOR on Gold

A potential reaction scheme, which can be taken as supplemental to reaction (50), is presented in reaction scheme (51) below [23, 128, 129]:

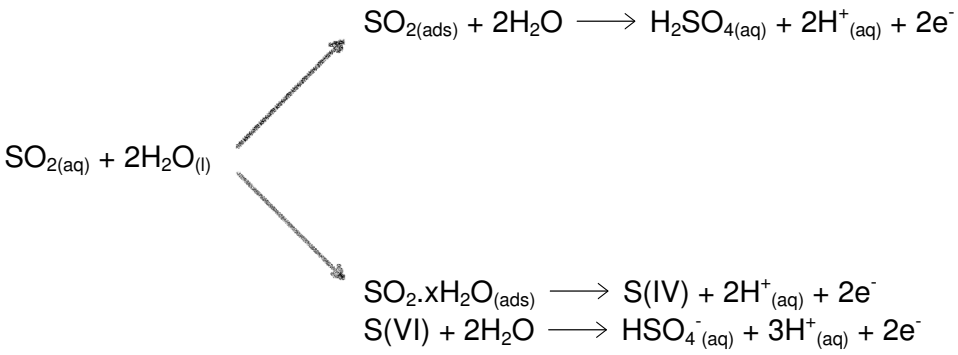


(51)

$SO_2$ adsorption, depicted in reaction scheme (51) above, should be rapid so as to sustain equilibrium when oxidation is complete [129]. These reaction products of reactions (47) and (50), or oxidised reaction species have been found to inhibit the further oxidation of bulk $SO_2$ as they might adsorb strongly on the electrode surface, as found in literature [130].

The possible two-electron [127, 129] mechanism of $SO_2$ electro-oxidation involves the reaction with water to form S(VI) [127, 129] in the form of $HSO_4^-$ or $SO_3^{2-}$ as can be seen in reaction scheme (50) in section 5.1.5.2 and equation (47) in section 5.1.3. The two-electron [23, 52, 129, 130, 133] oxidation of $SO_2$ is followed by a fast, irreversible [129, 133] chemical reaction, which forms inactive $SO_2$ oxidation products such as sulphate [129, 130] or bisulphate [129], which is not necessarily found with gold electrodes. The reaction process for $SO_2$ oxidation on gold can thus be pointed to the bottom part in reaction (51) above [129], with a higher rate of charge transfer than on a clean gold electrode surface, which is much slower [51, 129]. $SO_2$ that had been oxidised was irreversibly oxidised [23, 52, 129].

The oxidation of $SO_2$, as well as the formation of surface oxidation and reduction, occurs at about the same potential region in pure 0.5 M $H_2SO_4$ with oxidation of $SO_2$ occurring simultaneously with the reduction of the surface oxide [127] on a reverse potential sweep. Literature has found that the oxidation current was diffusion controlled in the potential region above 1.0 V *vs.* NHE [26, 129].

Electro-oxidation of $SO_2$ starts at ca. 0.6 V giving rise to a peak between 0.75 and 0.85 V *vs.* NHE [130]. Even on a reverse potential sweep, $SO_2$ is being oxidised at the potential range where electrode surface oxide is being removed, which is typical behaviour of an electrode process being inhibited by surface oxidation. The $SO_2$ oxidation process has an adsorption

character and is diffusion controlled, depending on the state of the electrode surface [23, 26, 129, 130]. Thus at the potential range where inhibition occurs, the $SO_2$ concentration profile at the electrode surface has time to be restored through diffusion, thereby leading to the reverse sweep oxidation of $SO_2$ right after de-inhibition to occur once again [130].

The oxidation process proceeds through an adsorbed particle inherent from reduced $SO_2$ species [23, 52, 129]. A gold surface covered with oxides proved to inhibit the $SO_2$ electro-oxidation reaction [129], even though $SO_2$ enhances oxide formation on gold electrode surfaces [133]. The moment the gold surface is covered by oxides, the current density drops significantly [51, 129, 130] – this occurs at about 1.4 V [130] up to about 1.5 V [51] *vs.* NHE and is clearly seen with rotating disc electrodes. On rotating electrodes the $SO_2$ oxidation beyond the surface oxidation potential is very clearly distinguishable on a voltammogram, as compared to stationary electrodes, as the equilibrium establishment of oxide formation being removed through real-time $SO_2$ oxidation is much more difficult to acquire on a stationary surface [51]. Inhibition was shown to be at a lesser degree, depending on the concentration of $SO_2$, with the lower concentrations of aqueous $SO_2$ experiencing less inhibition [130].

On gold it has also been found that the adsorbed sulphur layer could have inhibiting- instead of reaction-promoting effects [131]. For gold it is speculated that the diffusion of $SO_2$ species is slow, followed by a quick adsorption and charge transfer reaction [23]. Other authors speculate that the straight charge transfer to dissolved $SO_2$ occurs for both platinum and gold.

#### 5.1.6.2. Reduction Products of $SO_2$

When the potential on gold is taken to below 0.4 V *vs.* NHE the electrode surface becomes covered in reduced $SO_2$ species as adsorbed $SO_2$ is being reduced below 0.4 V [129, 130]. The reduced $SO_2$ species coverage on the electrode surface, in the form of sulphur, increases with lowering of $E_{low}$ [130]. As soon as the potential reaches the hydrogen evolution potential region, the reduction of bulk $SO_2$ takes place [51]. In literature it is speculated that the weakly bound reduced species is $H_2S$ [26, 129], which is oxidised prior to surface oxide formation [128, 129] and the stronger adsorbed species oxidise at potentials after the weakly bound species. The more strongly adsorbed reduced $SO_2$ species is most likely sulphur [51, 130]. The adsorbed reduced $SO_2$ species shift the $SO_2$ oxidation peak to between 50 mV and 100 mV more negative than without the reduced ad-species [129, 130]. The optimum coverage determined in literature was between half and full coverage, indicating monolayer coverage of chemisorbed monomeric sulphur [23, 130]. Excessive coverage inhibits the $SO_2$ oxidation reaction and too little coverage also reduces electrode activity [23, 130]. Regardless of the method employed to cover the electrode surface, the

optimum surface coverage for maximum catalytic activity is a monolayer on the surface [23, 128, 130].

It was also found in literature that adsorbed $SO_2$ greatly decreased with the presence of adsorbed reduced $SO_2$ species [51, 129]. It should be noted that the reduced species affect both the strongly and weakly adsorbed $SO_2$ differently [129]. It can also be suggested that the oxidation of bulk $SO_2$ occurs with the molecular $SO_2$ not strongly bound to the electrode surface [130]. The reduction of adsorbed $SO_2$ has two distinct voltammetric peaks, with the first at almost 0.14 V and the second at -0.075 V *vs.* NHE, which respectively indicates the formation of monomeric sulphur and $S^{2-}$ species [130]. Zdeněk and Weber [51] speculated that the $SO_2$ oxidation limiting current has the same values with a clean gold surface as compared to a gold surface covered with reduced $SO_2$ species.

#### 5.1.6.3. Electrode Preparation

The chemical pre-treatment of the gold electrode surface plays an important role in the anodic oxidation rate of $SO_2$ as well as in the clarification of the possible reaction mechanism [129, 133], although the mechanism is not of interest in this investigation, parts of it need to be considered for establishing the reaction activity, using the techniques described in section 2.3. The forming, and then stripping, of oxide films on gold produces an active surface for the electro-oxidation reaction of $SO_2$ [133]. As the oxide layer readily dissolves in acid solutions, the lack of stripping of oxide does not necessarily mean reduced electrode activity.

The electrode should be cleaned thoroughly and polarised cyclically in 0.5 M $H_2SO_4$ between potentials of 0.5 to 1.75 V *vs.* NHE [129]. The anodic oxidation of the surface of gold starts at about 1.3 V *vs.* NHE and decreases right before the molecular evolution of oxygen molecules at about 1.7 V [129]. The oxygen forms a monolayer on the surface and is independent of scan rate and temperature [129, 130].

### 5.1.7. Platinum vs. Gold

Gold is known to be particularly resistant to oxide formation as it occurs at a much higher potential compared to platinum [23]. The onset of oxide formation is about 1.4 V *vs.* NHE. The overlap of the oxide formation with the electro-oxidation of $SO_2$ is thus more easily distinguishable on gold than on platinum. Similar mechanisms for gold and platinum have been proposed that include the straight transfer of charge in the area where the first anodic peak appears with an activated electrode and the chemical oxidation of $SO_2$ at the more positive anodic region where gold oxide formation takes place. Literature has, to the

contrary, shown that the formation of gold oxide completely inhibits the electrochemical oxidation of $SO_2$.

Gold exhibits better catalytic properties towards $SO_2$ oxidation than platinum. $SO_2$ adsorbs much more strongly on platinum than on gold [26, 130], which can be regarded as the steering wheel of the reactiveness and selectivity of the electrodes towards SDOR [130]. Less sulphur is formed on gold than on platinum at the same reduction potentials for each electrode [26]. The catalytic effect of sulphur on the electro-oxidation of $SO_2$ is not as strong on gold as on platinum.

For both gold and platinum the same basic, yet mysterious mechanism is followed on activated electrode surfaces [26, 128, 133]. High overpotentials are still required for the electro-oxidation reaction on both metals even though the reaction is improved with gold as electrode or sulphur modified platinum surfaces [26]. The overall process has been found to involve two electrons, in the rate limiting step, supporting the fact that $SO_2$ is oxidised to sulphate [133].

The oxide formation on gold takes place at a much higher overpotential [128, 133] as the oxide readily dissolves in the aqueous medium, as compared to platinum [128, 133], therefore the voltammograms on gold for SDOR are more distinct than on platinum [133]. When both gold and platinum are in the same active condition, the behaviour of $SO_2$ oxidation is similar. Platinum needs to be oxide free or in a reduced state for improved activity. It is also clear that the presence or absence of surface oxide does not necessarily influence the electro-oxidation of $SO_2$ [128]. Hydrogen adsorbed on both gold and platinum inhibits the electro-oxidation reaction of $SO_2$ [133].

Careful pre-treatment of electrode surfaces indicated that the mechanism involved chemical and electron-transfer processes in concomitance [133]. For both electrodes, the process is thus diffusion controlled and irreversible where $SO_2$ is also consequently oxidised to S(VI), which then reacts with water to form sulphate or bisulphate.

Substrate sensitive oscillations in current density have been found on both gold and platinum electrodes when predetermined starting potentials were held for several minutes [26], due to the active oxidation mechanism of $SO_2$ in the oscillatory potential region.

Platinum has been found to be less inherently active towards $SO_2$ reduction than gold [23].

## 5.2. Experimental Procedure

Sulphur dioxide oxidation was investigated in 0.5 M $H_2SO_4$ only by using (i) high purity $SO_2$ gas (from Afrox) and (ii) sulphite salt (from ACE) for both platinum and gold. All the other reagents used in this investigation are listed in section 3.2.2. For both platinum and gold, preconditioning was done in 0.1 M $HClO_4$ in the fingerprint CV areas of each metal at 50 mV/s scan rate until the voltammograms showed stability and repeatability. For $SO_2$ gas the fresh 0.5 M $H_2SO_4$ solution was vigorously bubbled at least 10 minutes before every LP that was run as, in the literature, the solution was said to be saturated at about 20 minutes [26]. During the experiments, the $SO_2$ gas was set to flow over the electrolyte surface as to ensure the saturated state of the solution.

The $Na_2SO_3$ salt was made up as a stock solution of 1 M concentration from which 10 mL was diluted to 100 mL on demand for every experiment, with inert (bubbled with $N_2$) 0.5 M $H_2SO_4$ to give a final concentration of 0.1 M $Na_2SO_3$ in 0.5 M $H_2SO_4$.

### 5.2.1. Platinum

#### 5.2.1.1. Preconditioning

The preconditioning of platinum was performed after polishing and sonication by doing *CV*s in 0.1 M $HClO_4$, made inert by bubbling $N_2$ gas into solution for a minimum of 10 minutes, from -0.831 V up to 1.5 V *vs.* SCE at a scan rate of 50 mV/s for at least 10 cycles or until the voltammograms showed repeatability of subsequent *CV*s.

#### 5.2.1.2. Gaseous $SO_2$

Different starting potentials for *CV*s were run at 10 mV/s scan rate and at 0 RPM rotation rate in $SO_2$ saturated 0.5 M $H_2SO_4$ by using -0.241, -0.141, -0.041, 0.059 and 0.159 V *vs.* SCE as starting potentials and ending the CV scan at 1.5 V *vs.* SCE. For platinum the best activity was found to occur when the starting potential of the scan was taken as -0.141 V *vs.* SCE, which is equivalent to 0.1 V *vs.* NHE. *LP*s were subsequently started from -0.141 V *vs.* SCE and ended at 2.159 V *vs.* SCE at a scan rate of 10 mV/s and rotations of 0, 100, 400, 1600 and 2500 RPM in $SO_2$ saturated 0.5 M $H_2SO_4$ solution.

#### 5.2.1.3. $Na_2SO_3$ Salt

0.1 M $Na_2SO_3$ in 0.5 M $H_2SO_4$ was used for all experiments. The platinum experiments for the $Na_2SO_3$ salt were done exactly as the gaseous experiments above were, with the only difference being the salt in solution instead of the saturated gas in solution, by investigating

the activity at different starting potentials for *CV*s and at different rotation rates for *LP*s starting at the potential that showed the best activity i.e. 0.1 V *vs.* NHE.

### 5.2.2. Gold

#### 5.2.2.1. Preconditioning

The preconditioning of gold was performed after proper polishing and sonication as described in section 3.2.4.1. After each experiment with $SO_2$ gas, an adsorbed reaction product contaminated (poisoned) the electrode surface, which required a CA to be run at the potential where the adsorbate was detected. The potential was ca. 0.425 V *vs.* SCE at which the CA was held for at least 5 minutes or until the current density stabilised at a low value. Depending on the severity of the contamination, the preconditioning *CV*s had to be repeated up to 40 times in some instances before the voltammograms showed stable repeatability. To summarise: After polishing and sonication a CA was run in inert 0.1 M $HClO_4$ at 0.425 V *vs.* SCE for at least 5 minutes after which a CV was run at a scan rate of 50 mV/s for a minimum 20 cycles starting from the OCP up to 1.6 V *vs.* SCE and back again to 0.1 V *vs.* SCE and ending at 0.1 V.

#### 5.2.2.2. Gaseous $SO_2$

After preconditioning as described in section 5.2.2.1, the effect of starting potential was investigated in $SO_2$ saturated 0.5 M $H_2SO_4$ by doing *CV*s starting at 0.0, 0.1, 0.2, 0.3 and 0.4 V *vs.* NHE (-0.241, -0.141, -0.041, 0.059 and 0.159V *vs.* SCE respectively) with each CV ending at 1.5 V *vs.* SCE for 1 cycle at each starting potential scanning at a rate of 10 mV/s at 0 RPM for every run. The best starting potential was -0.141 V *vs.* SCE (0.1 V *vs.* NHE, which is different to the literature's 0.2 V *vs.* NHE [23]) to be used for all further experiments. As a control, a CV was run from -0.241 V – 1.5 V *vs.* SCE in 0.5 M $H_2SO_4$ as to compare what a CV would resemble without $SO_2$ in solution. *LP*s were run at 0, 100, 400, 900, 1600 and 2500 *RPM*s starting at -0.141 V *vs.* SCE and ending at 2.4, 2.4, 2.5, 2.6, 2.8 and 2.9 V *vs.* SCE for each respective rotation rate with a scan rate of 10 mV/s. The 2500 RPM runs were unsuccessful as the current density reached a high of over 2 $A/cm^2$, which is out of the detection range of the potentiostat.

#### 5.2.2.3. $Na_2SO_3$ Salt

0.1 M $Na_2SO_3$ in 0.5 M $H_2SO_4$ was used for all experiments. The same investigation of starting potentials on the performance of the electrode was investigated starting at -0.241, -0.141, -0.041, 0.059 and 0.159 V *vs.* SCE. It was determined that -0.141 V *vs.* SCE was the best potential to start at. The same control *CV*s for the $SO_2$ gas experiments were used to

compare the activity of the electrode with and without $Na_2SO_3$ in 0.5 M $H_2SO_4$. All subsequent *LP*s were run in 0.1 M $Na_2SO_3$ and 0.5 M $H_2SO_4$ at 10 mV/s scan rate, starting from -0.141 V *vs.* SCE and ending at 2.0 V *vs.* SCE for all *RPM*s, which consisted of 0, 100, 400, 1600 and 2500 RPM.

## 5.3. Results and Discussion

The literature covered SDOR using a certain known concentration of $SO_2$ in solution using a salt [26], or saturated $SO_2$ in solution using gas [18]. This led to the study of gaseous $SO_2$ (direct) and $SO_2$ administered in the form of $Na_2SO_3$ (indirect) for the experiments. The first part covers the electrode behaviour in 0.5 M $H_2SO_4$ using a direct administration of gas and the second part, the indirect administration of gas using a salt.

### 5.3.1. Gaseous $SO_2$

#### 5.3.1.1. Effect of Starting Potentials

Before every experiment, the electrode preparation and preconditioning was done as described in section 5.2.1, with the preconditioning CV for platinum resembling the typical voltammogram depicted in Figure 13 on page 30, and for gold resembling that of Figure 14 on page 30, with the only deviation being the lowest potential the electrode was cycled to.

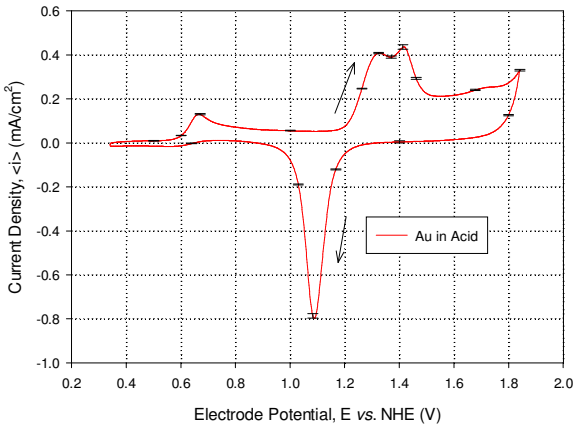


**Figure 57: Preconditioning CV of gold in 0.1 M $HClO_4$ as it appeared after studying $SO_2$ oxidation using gaseous $SO_2$. Scan rate = 50 mV/s at 0 RPM rotation rate without $SO_2$ gas in solution**

In the voltammogram shown in Figure 57 for gold, a strongly adsorbed chemical species was observed in the double layer voltage zone at ca. 0.666 V *vs.* NHE. The peak might be attributable to the very strong adsorption of $SO_2$ [128, 129], which, according to literature, would not negatively influence the reactivity of gold towards the SDOR. Regardless of literature stating no negative influence of strongly adsorbed sulphur dioxide chemical

species on electrode activity, *CA*s were run before subsequent preconditioning *CV*s at 0.666 V *vs.* NHE for as long as necessary to let the current density reach a limiting current flow right before the CV was performed, in an attempt to rid the electrode surface of the adsorbed species, so as to ensure proper electrode cleanliness.

According to literature, adsorbed reduced $SO_2$ catalysed the oxidation of bulk $SO_2$ [129, 130], with the reduced $SO_2$ species being generated at ca. 0.14 V *vs.* NHE [130]. The activity of the electrode in this study was to be determined at different starting potentials for voltage scan initiation. The scans were set to start at different potentials and not held at the starting potential before executing the voltage scan, as too little or too much electrode coverage of the adsorbed reduced $SO_2$ species might also render the electrode surface inactive towards $SO_2$ oxidation in the oxidative potential scan range [23, 128, 130].

Before the *CV*s in Figure 58 and Figure 59 were carried out, the 0.5 M $H_2SO_4$ solution was bubbled with $SO_2$ gas for at least 10 minutes, as, according to literature [26], 30 minutes should produce a saturated solution, whereas in this study, repeated CV runs in $H_2SO_4$ solution with 10 minute bubbling produced the same voltammetric repeatability as 30 minutes bubbling, thus 10 minute bubbling produced solution saturation with $SO_2$.

In Figure 58 and Figure 59 the effect of different starting potentials are compared to the voltammograms without saturated $SO_2$ gas in solution for both platinum and gold respectively. The CV scans for platinum and gold were started from 0.0, 0.1, 0.2, 0.3 and 0.4 V *vs.* NHE and ended at ca. 1.7 V *vs.* NHE for all *CV*s on platinum and ca. 1.74 V *vs.* NHE for gold. It can be seen in Figure 58 for platinum that the current density for each voltammogram starts to increase at different potentials and reaches different maximum current densities depending on the starting potential. When compared, the starting potential of investigative scans that would provide more catalytic activity was determined to be 0.1 V *vs.* NHE. The *CV*s for gold in Figure 59 below clearly shows that the starting potential of 0.1 V *vs.* NHE produced the lowest SDOR onset potential versus the highest limiting current density ratio, which is in accordance with the literature findings of around 0.1 V *vs.* NHE being the potential of the reduction of $SO_2$ species that ultimately catalyses the oxidation of $SO_2$ [130]. Both platinum and gold, in this case, showed the best starting potential to be 0.1 V *vs.* NHE. Literature investigations on platinum found that at 0.14 V *vs.* NHE adsorbed $SO_2$ is reduced and subsequently catalyses the SDOR [130]. For the 0.1 V starting potential on platinum, the current density starts to increase from ca. 0.55 V *vs.* NHE, reaching a high of about 380 mA/cm$^2$ at 1.35 V *vs.* NHE with a rapid decline in current density from ca. 1.45 V *vs.* NHE.

Literature states that the reduction of adsorbed $SO_2$ species occurs in the potential range from ca. 0.1 V – 0.4 V *vs.* NHE [129, 130], which might account for the very slight difference in the onset potential for the different starting potential scans depicted in Figure 59 for gold.

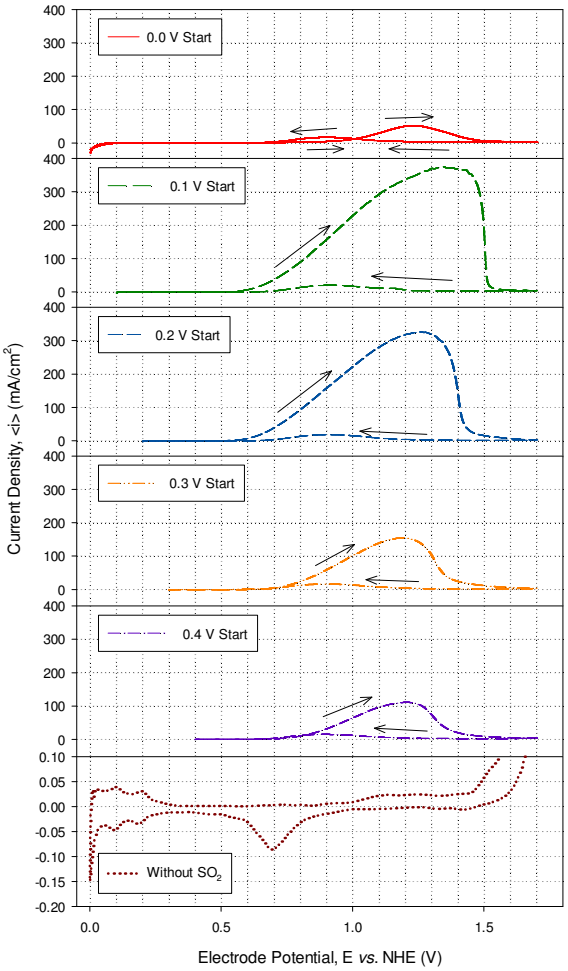


**Figure 58: Control *CV*s for the SDOR on Pt in 0.5 M $H_2SO_4$ at different starting potentials using a $SO_2$ saturated solution with a scan rate of 10 mV/s and no electrode rotation**

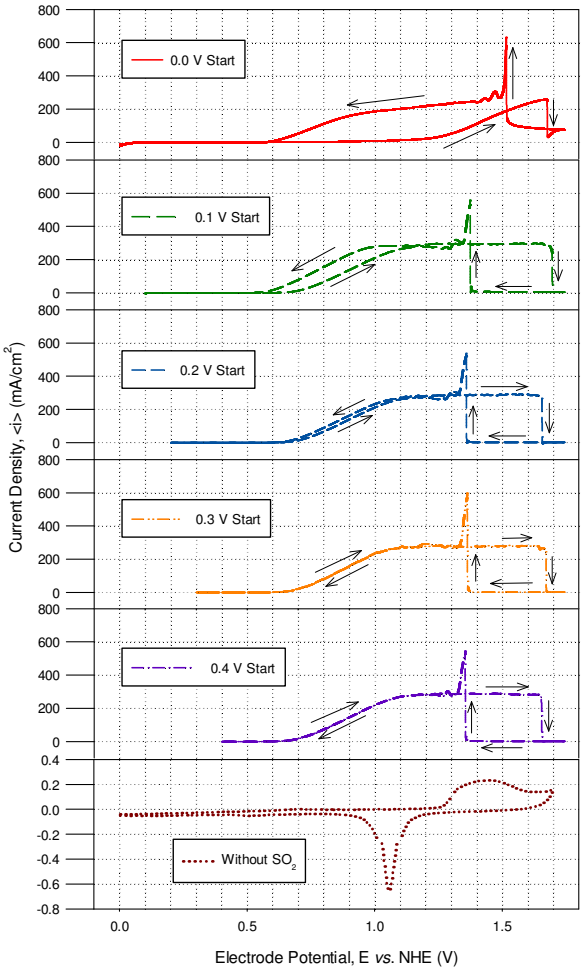


**Figure 59: Control *CV*s for the SDOR on Au in 0.5 M $H_2SO_4$ at different starting potentials using a $SO_2$ saturated solution with a scan rate of 10 mV/s and no electrode rotation**

According to literature, oxide adsorption might inhibit the electrode activity towards $SO_2$ oxidation once the surface has been covered in oxides [23, 52, 132, 134] due to the blocking of the active surface sites by adsorbed oxygen [23] or by depletion of the catalytically active reduced $SO_2$ species. The backward scan on platinum showed a peak appearing at ca. 0.9 V *vs.* NHE for all the different starting potential scans. The peak increases, along with the decrease in reductive current for the electrode oxide desorption current. The adsorbed oxygen is removed from the electrode surface's active sites thus activating the electrode by restoration of the $SO_2$ oxidation current in the backward scan [132]. This is in accordance with literature and, consequently, supports literature findings [23, 52, 132, 134] for both

platinum and gold as depicted in Figure 58 and Figure 59. All the following voltammetric investigation scans regarding $SO_2$ electro-oxidation were started from 0.1 V *vs.* NHE.

### 5.3.1.2. Effect of Rotation Rate

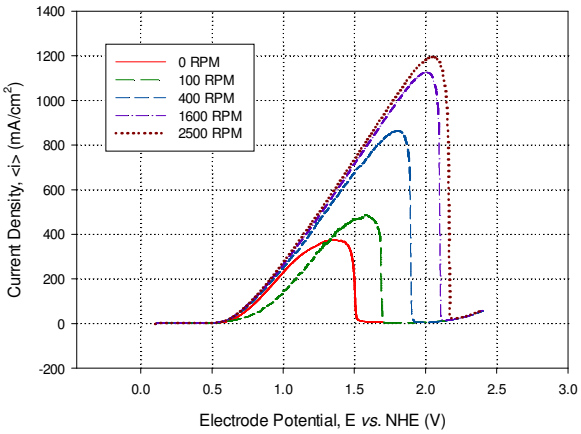


**Figure 60: *LP*s of Pt in 0.5 M $H_2SO_4$ saturated with $SO_2$ gas at different rotation rates with a scan rate of 10 mV/s ($E_{low}$ = 0.1 V)**

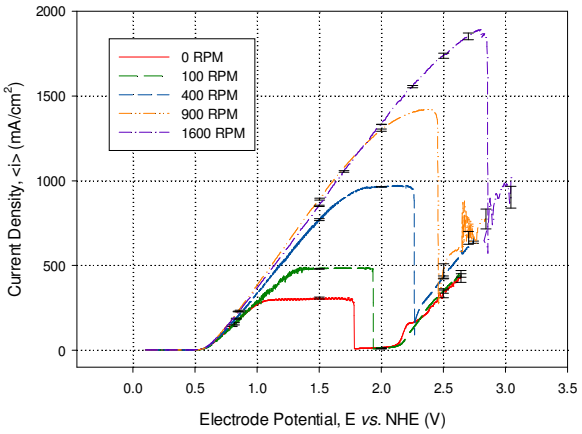


**Figure 61: *LP*s of Au in 0.5 M $H_2SO_4$ saturated with $SO_2$ gas at different rotation rates with a scan rate of 10 mV/s ($E_{low}$ = 0.1 V)**

In Figure 60 and Figure 61 above, *LP*s for the SDOR at different rotation rates are shown. The starting potential for all the runs was 0.1 V *vs.* NHE. In Figure 60 for platinum, the current density starts to increase just after 0.5 V *vs.* NHE with the maximum current density reached for the 2500 RPM scan about 1200 mA/cm$^2$ past 2.0 V *vs.* NHE. The maximum current density at 0 RPM is ca. 400 mA/cm$^2$. The current density on gold in Figure 61 starts to increase from ca. 0.52 V *vs.* NHE and reaches an amazing high of almost 2000 mA/cm$^2$ or 2 A/cm$^2$ for the 1600 RPM run, almost out of range of the current density the potentiostat is able to detect. The current density reached too high a level for a 2500 RPM run to be executed on gold, with the diffusion limited maximum current density reached for 0 RPM being ca. 300 mA/cm$^2$.

The sudden drop in current density, which can be seen for all rotations in Figure 60 and Figure 61 from about 1.6 V *vs.* NHE for platinum and from ca. 1.75 V for gold, is attributable to oxide adsorption on the surface of the electrode, inhibiting the activity of the electro-oxidation reaction of $SO_2$ [23, 51, 52, 129, 130, 132, 134]. As the rotation rate increases, the sudden current density decrease increases in overpotential. It is clear that the faster the electrode rotates, the more delayed the inhibition effect of oxide adsorption is. The delayed inhibition might be attributable to the competition for available active sites on the platinum between $SO_2$ and $O_2$ [123], or the establishment of oxide formation equilibrium being more difficult to acquire due to its removal by real-time $SO_2$ oxidation [51] and thus the subsequent

delay in inhibition of the electrode activity by oxide formation [51, 129, 130]; therefore, as the rotation rate increases with both electrodes, so too does the constant fresh supply of $SO_2$ to active sites increase, consequently retarding the inhibition effect of oxygen adsorption on the electrode activity. Displacement of the catalytic sulphur layer by the formation of oxides might also contribute to the sudden fall in oxidation current [51].

As $SO_2$ can still be oxidised on platinum oxide (reaction (49)) as according to literature [23, 52, 123], it might be possible that oxides still adsorb on the platinum surface, with the constant fresh supply of $SO_2$ to the electrode surface at higher rotation rates maintaining the SDOR activity. It might be possible that the catalytic sulphur layer might be displaced by the formation of electrode surface oxides that could also contribute to the sudden fall in oxidation current [51].

Oscillations in current density on gold, characteristic of the mechanistic oxidation of $SO_2$ had been found in the results depicted in Figure 59 and Figure 61, which corresponds well with literature findings [26].

The results in Figure 60 and Figure 61 show a definite mass transfer inhibition, as is found in literature [23] for both electrodes. The reaction is clearly mass transfer inhibited as indicated by the increase of the current density as the rotation rate increases. This is in accordance with literature findings for the SDOR, especially at lower rotation rates, from about 1.0 V *vs.* NHE for gold, which is in accordance with literature findings [26, 129].

### 5.3.1.3. Tafel Plots

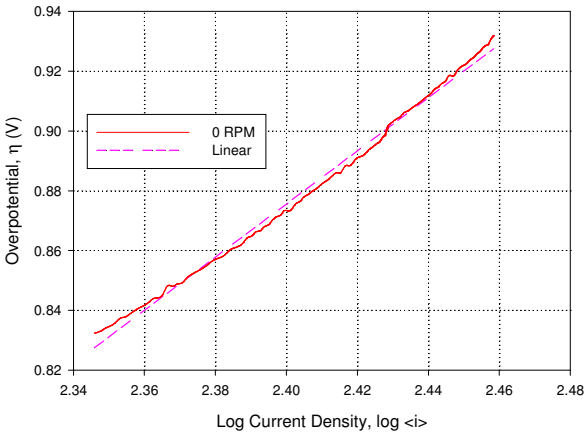


**Figure 62: Tafel plot for the electro-oxidation of $SO_2$ in 0.5 M $H_2SO_4$ using a gaseous $SO_2$ feed at 0 RPM on Pt plotted from the potential range 0.990 – 1.09 V *vs.* NHE from the results in Figure 60**

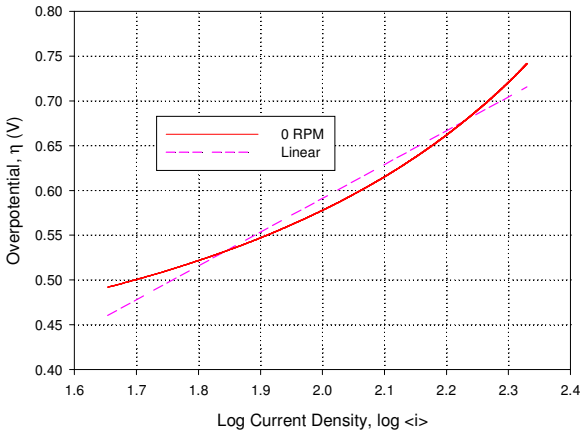


**Figure 63: Tafel plot for the electro-oxidation of $SO_2$ in 0.5 M $H_2SO_4$ using a gaseous $SO_2$ feed at 0 RPM on Au plotted from the potential range 0.650 V – 0.900 V *vs.* NHE from the results in Figure 61**

The Tafel slope for platinum and gold has been calculated from the plots in Figure 62 and Figure 63 above as 891 mV/decade for platinum and 378 mV/decade, which is high for both electrodes and subsequently indicative of a sluggish reaction. The literature values for the Tafel slope is mainly for $Na_2SO_3$ and not for $SO_2$ gas and ranges from ca. 30 – 140 mV for platinum and 50 – 60 mV for gold [23]. It can be concluded that the SDOR is more active on gold than on platinum in 0.5 M $H_2SO_4$ using a direct administration of $SO_2$ gas and taking the magnitude of the slopes into consideration. To further investigate the reaction activity, Koutecký-Levich and Levich analyses were executed on the data produced in Figure 60 and Figure 61 for platinum and gold respectively.

### 5.3.1.4. Koutecký-Levich Plots

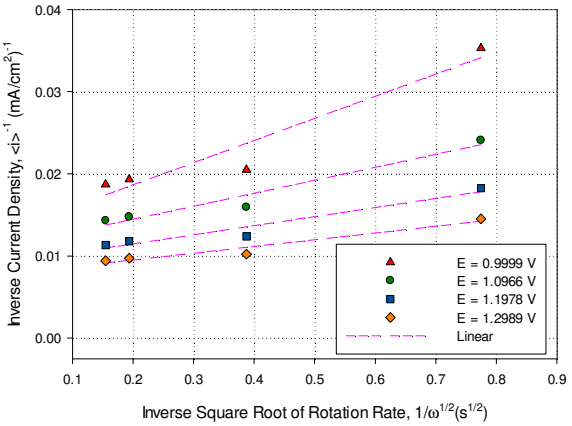


Figure 64: Koutecký-Levich plots for Pt in 0.5 M $H_2SO_4$ and $SO_2$ gas, based on the results in Figure 60

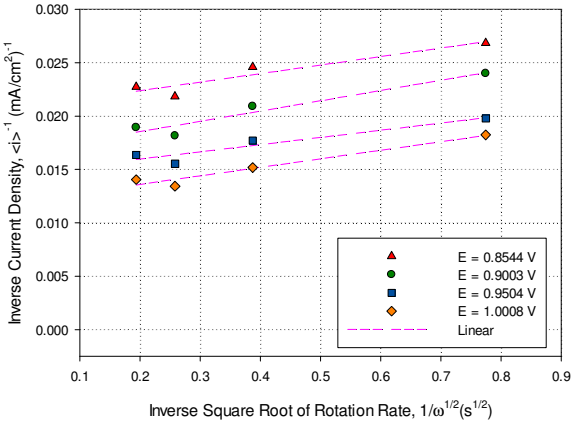


Figure 65: Koutecký-Levich plots for Au in 0.5 M $H_2SO_4$ and $SO_2$ gas, based on the results in Figure 61

Table 11: Koutecký-Levich plot results for Pt and Au in 0.5 M $H_2SO_4$ saturated with $SO_2$ gas

| Catalyst | Potential used (E *vs.* | Corresponding Slope | Number of |
|---|---|---|---|
| Pt | 0.9999 | 0.027 | 0.4 |
| | 1.0966 | 0.016 | 0.7 |
| | 1.1978 | 0.011 | 1.0 |
| | 1.2989 | 0.008 | 1.3 |
| | | Average Electrons: | 0.9 |
| | | | |
| Au | 0.8544 | 0.008 | 1.4 |
| | 0.9003 | 0.010 | 1.1 |
| | 0.9504 | 0.007 | 1.6 |
| | 1.0008 | 0.008 | 1.4 |
| | | Average Electrons: | 1.4 |

From the *LP*s depicted in Figure 60 and Figure 61 for platinum and gold, the Koutecký-Levich plots were produced as in Figure 64 for platinum and Figure 65 for gold. Table 11 summarises the results. The values for the variables used from Table 20, Table 22 and Table 24 (in Appendix 1 – Data) for the calculation of the Koutecký-Levich results, is summarised in the following table:

**Table 12: Values used in the Koutecký-Levich equation for Au in 0.5 M $H_2SO_4$ saturated with $SO_2$ gas**

| | |
|---|---|
| **Kinematic Viscosity ($cm^2/s$)** | $1.068\times10^{-03}$ [60] |
| **Diffusivity ($cm^2/s$)** | $1.830\times10^{-05}$ [60] |
| **Radius (cm)** | $2.50\times10^{-01}$ |
| **Faraday Constant (mA.s/mol)** | $9.65\times10^{7}$ |
| **Concentration Sat. $SO_2$ ($mol/cm^3$)** | $1.4\times10^{-03}$ [60] |

The kinematic viscosity of the solution was calculated by using the values in Table 25 (Appendix 1 – Data), with the range of values used from Table 25 summarised in Table 26 (Appendix 2 – Sample Calculations).

The Koutecký-Levich analysis brought forth a value of 0.9 electrons that can be rounded to 1 and 1.4 for gold, which can also be rounded to 1 electron transferred in the SDOR using $SO_2$ gas for platinum and gold.

For platinum and gold, there is no literature that supports the finding of a 1 electron transfer. Regardless, the slopes of the plots in Figure 64 show a very clear lack of parallelism on platinum. This implies a mechanism that changes [53, 81, 85] during the mixed control region's step of the SDOR on platinum. The lack of strict linearity of the plots in Figure 64 and Figure 65 for both platinum and gold can also indicate a change in the mechanism [63]. To support these conclusions, the Levich plots were constructed and presented in the following section.

#### 5.3.1.5. Levich Plots

For both platinum and gold, the maximum peak current densities from Figure 60 and Figure 61 above were used to calculate the number of electrons transferred using the Levich equation (15) from section 2.3.2. The values of the variables used in equation (15) are listed in Table 12 above.

The plots for platinum in Figure 66 do not show strict linearity, as do gold's to a lesser degree in Figure 67; regardless, the plots lie more linearly positioned than platinum. The number of electrons calculated for platinum using Levich was 1 and for gold 2.

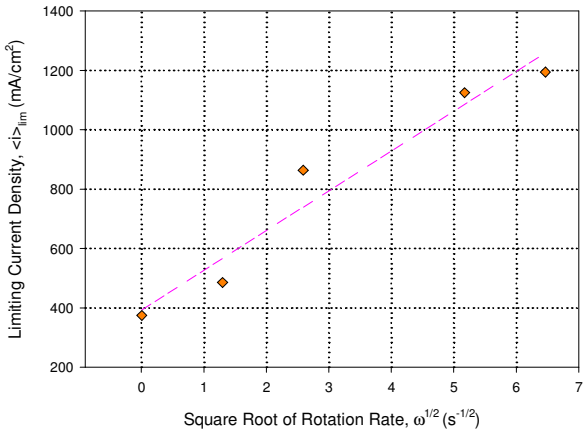


**Figure 66: Levich plot for the SDOR on platinum in 0.5 M $H_2SO_4$ using direct administration of $SO_2$ gas**

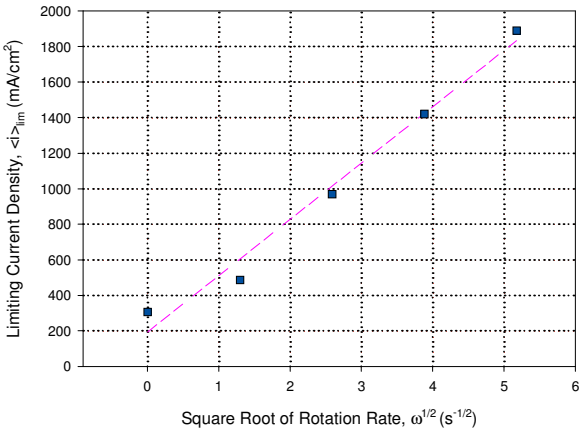


**Figure 67: Levich plot for the SDOR on gold in 0.5 M $H_2SO_4$ using direct administration of $SO_2$ gas**

For a two electron process, as for gold, the SDOR follows the same reaction path as depicted in reaction (51) above to produce $H_2SO_4$, demonstrated below in reaction (52) [23, 128, 129]:

$$SO_2 + 2H_2O \longrightarrow H_2SO_4 + 2H^+ + 2e^- \quad (52)$$

This finding for gold is in correspondence with literature [23, 128, 129].

The lack of linearity, as with platinum, is indicative of a mechanism that involves more than one step [53]. The slopes of the linear plots in the Koutecký-Levich plot showed a lack of parallelism, which indicates a change in the reaction mechanism in the mixed control region of the *LP*s. Therefore on platinum, the mechanism followed in the mixed control region might differ from the mechanism followed in the diffusion controlled region. The Levich plot determined the 2 electron oxidation reaction of $SO_2$ on gold, using direct administration of $SO_2$ gas while Kouteký-Levich established 1, ultimately indicating a different mechanism in the diffusion- and mixed control- regions. On platinum, Levich analysis confirmed the 1 electron transfer with a lack of linearity in the plots, indicating a complex mechanism. As the mechanism was not in the scope of this study, further investigation was not attempted in that context.

### 5.3.1.6. Conclusion

The voltammetric scans showed the best activity for a starting potential of 0.1 V *vs.* NHE as was determined in section 5.3.1.1. This starting point of voltammetric scans showed the

lowest SDOR onset potential with the highest maximum current density as depicted in Figure 58 and Figure 59 for platinum and gold respectively. The literature value for the reduction of adsorbed $SO_2$ was determined as 0.14 V *vs.* NHE [130]. The improved catalytic activity towards the SDOR, as described by literature [129, 130] in section 5.1.3, is due to a catalytic layer of adsorbed reduced $SO_2$ forming, that subsequently acts as a donor ligand for the electrode surface [127], as adsorbed $SO_2$ could potentially act as an electrode active site inhibiter [18], which was also found in this study to be the case for both platinum and gold. It was also speculated in this study that there are very strong adsorbed $SO_2$ on the gold electrode surface (section 5.3.1.1) that is clear on preconditioning *CV*s although it does not affect the electrode activity in a negative manner.

The number of electrons could be determined using Koutecký-Levich and Levich analyses for both platinum and gold. There was a lack of a linear increase in current density as the electrode rotation rate increased for platinum. Regardless, the use of Koutecký-Levich and Levich analysis was still applied to the results, giving a result of 1 electron in both analyses' approaches for platinum, which is a value not found in literature as most literature investigations focused on indirect administration of $SO_2$ gas by means of $Na_2SO_3$. The platinum electrode is active towards the SDOR nonetheless.

The number of electrons transferred on gold was calculated as 1 using Koutecký-Levich and 2 using Levich analyses, which is indicative of the oxidation of $SO_2$ to form $H_2SO_4$ in the diffusion limited region, as is indicated in literature [129, 130] with the overall reaction depicted in reaction (53), based on reaction scheme (51) [52, 123, 127] in section 5.1.5.2:

$$SO_2 + 2H_2O \longrightarrow H_2SO_4 + 2H^+ + 2e^- \quad (53)$$

The Tafel slope for the SDOR, using a direct administration for $SO_2$ gas on platinum in 0.5 M $H_2SO_4$ was determined as 891 mV/decade and as 378 mV/decade on gold, which is several magnitudes higher than literature values found for the $Na_2SO_3$ salt [23] as there are no literature values for the gaseous form of $SO_2$ to be compared to. The magnitudes of the Tafel slopes imply a sluggish reaction on both platinum and gold. When taking the Tafel slopes into account, the SDOR is more favoured on gold than on platinum.

The SDOR onset potential was determined as ca. 0.52 V *vs.* NHE for both electrodes with the maximum current density reached for the 1600 RPM scan on platinum about 1100 $mA/cm^2$ at ca. 2.0 V *vs.* NHE and on gold 2000 $mA/cm^2$ for the 1600 RPM rotation scan. The maximum current density at 0 RPM is ca. 400 $mA/cm^2$ for platinum and 300 $mA.cm^2$ for gold.

Regardless of the lack of confirmation of the 2 electron transfer reaction, the platinum electrode showed activity towards the SDOR with a good correspondence to literature [52, 123, 127], except that literature used $Na_2SO_3$ to produce dissolved $SO_2$ gas. The behaviour of platinum and gold in aqueous sulphuric acid is thus in accordance with literature findings [129, 130].

### 5.3.2. Sulphite Salt

The reaction of $Na_2SO_3$ as substrate to the $SO_2$ electro-oxidation is investigated on platinum and gold in this section using 0.1 M $Na_2SO_3$ dissolved in 0.5 M $H_2SO_4$.

$$Na_2SO_3 + H_2SO_4 \longrightarrow Na_2SO_4 + H_2O + SO_2 \quad (54)$$

The preconditioning and electrode preparation was done as described in section 5.2.1 and 5.2.2 for both electrodes. On gold the preconditioning CV typically resembled the voltammogram of Figure 13 on page 30. No strongly adsorbed chemical species on the gold surface was found, as with the gaseous study of $SO_2$ oxidation (Figure 57) that showed an oxidation peak at ca. 0.666 V *vs.* NHE in the preconditioning voltammogram. The difference of this adsorption phenomenon, when using $Na_2SO_3$ to administer $SO_2$ with the direct administration of $SO_2$ gas, might be attributable to the $Na_2SO_3$ in the solution that may influence the adsorption of $SO_2$ to the gold active sites, as according to literature the $SO_2$ oxidation rate or activity might be influenced by chemical species in solution adsorbing on the electrode surface [51].

#### 5.3.2.1. Effect of Starting Potential

Refer to section 5.3.1.1 for the reason behind the investigation into the different starting potentials' effect on the SDOR.

The voltammograms in Figure 68 and Figure 69 show the activity of the SDOR on platinum and gold in 0.5 M $H_2SO_4$ compared to a CV without $Na_2SO_3$ in solution, so as to control if the electrode is active or not. The scans on each electrode were started from 0.0, 0.1, 0.2, 0.3, and 0.4 V with each and every scan ending at 2.34 V *vs.* NHE for gold and 1.75 V for platinum. From the plots for platinum and gold, it can be seen that the starting potential of 0.1 V *vs.* NHE showed the lowest SDOR onset potential (0.5 V *vs.* NHE on platinum) compared to 0.0 V, 0.2 V, 0.3 V and 0.4 V with their respective onset potentials on platinum as 0.6 V, 0.55 V, 0.7 V and 0.75 V *vs.* NHE. The onset potential on gold for the 0.1 V *vs.* NHE starting potential is ca. 0.55 V *vs.* NHE compared to ca. 0.6 V *vs.* NHE for the starting

potentials 0.2, 0.3 and 0.4 V *vs.* NHE and an increase in current density at ca. 1.0 V *vs.* NHE for the 0.0 V starting potential.

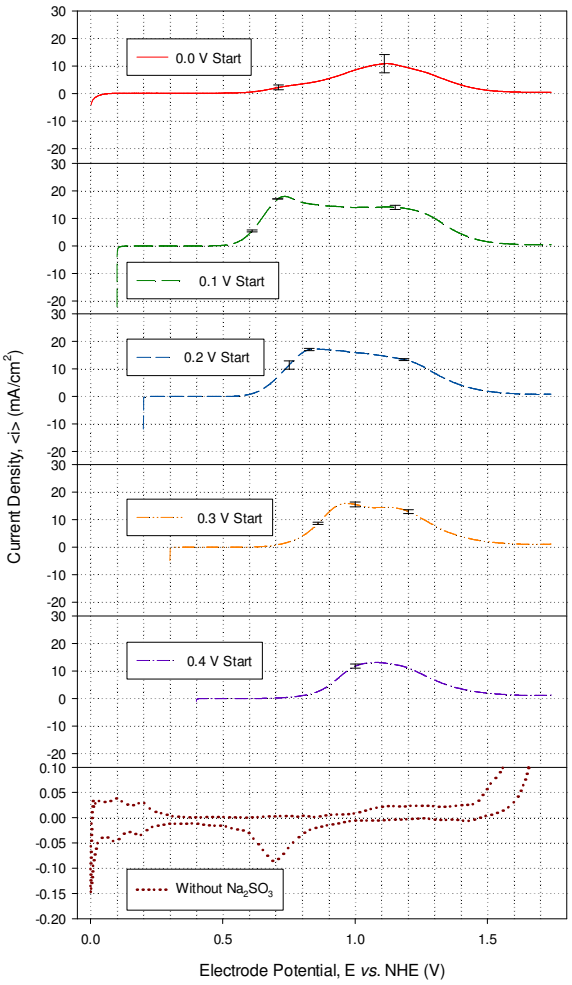


**Figure 68: *CV*s of $SO_2$ oxidation using 0.1 M $Na_2SO_3$ in 0.5 M $H_2SO_4$ at different starting potentials on platinum at a scan rate of 10 mV/s and 0 RPM electrode rotation rate**

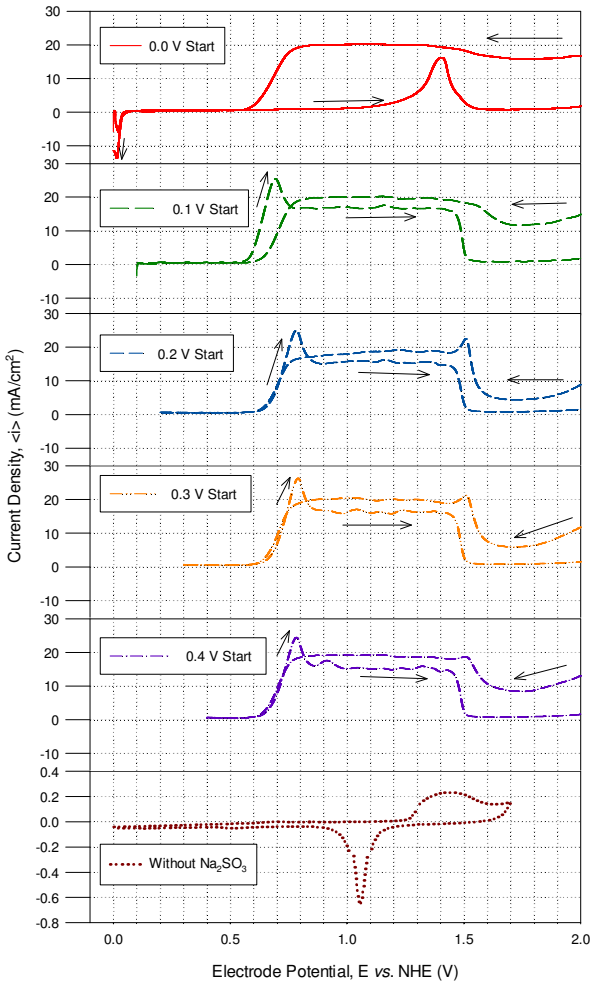


**Figure 69: *CV*s of $SO_2$ oxidation using 0.1 M $Na_2SO_3$ in 0.5 M $H_2SO_4$ at different starting potentials on gold at a scan rate of 10 mV/s and 0 RPM electrode rotation rate**

The scan for the starting potential of 0.1 V *vs.* NHE showed an increase in current density from ca. 0.5 V *vs.* NHE, reaching a maximum peak at ca. 0.72 V *vs.* NHE with a maximum current density of about 18 mA/cm$^2$. For the 0.1 V starting potential scan on gold, the current density reaches a well-defined peak at about 0.69 V *vs.* NHE with a current density of ca. 25 mA/cm$^2$, decreasing slightly to a diffusion limited current density of ca. 18 mA/cm$^2$. The diffusion limited current carries on until the electrode surface oxide forms, as according to literature the oxide inhibits the electrode activity towards SDOR [130].

According to literature the adsorption of $SO_2$ to the electrode surface might inhibit the activity of the electrode surface towards the oxidation of $SO_2$ [18]. Adsorbed $SO_2$ is reduced at potentials below ca. 0.65 V *vs.* NHE with the best potential for $SO_2$ reduction at ca. 0.15 V

*vs.* NHE [18, 23]. Some authors state that the ideal potential for $SO_2$ reduction is 0.2 V *vs.* NHE [132]. It was found by many authors that a layer of reduced $SO_2$ in the form of sulphur formed a catalytic layer [26, 123, 130, 132]. More than a single layer of sulphur might also inhibit the electrode activity due to active site passivation [18, 23]; for that reason the scans were only initiated at the different starting potentials, so as to ensure result repeatability.

$$H_2SO_3 + 4H^+ + 4e^- \longrightarrow 3H_2O + S \qquad E^0 = 0.449 \text{ V [26, 129, 130]} \qquad (55)$$

As can be seen in Figure 68 and Figure 69 the electrodes showed activity for the $SO_2$ electro-oxidation reaction in 0.5 M $H_2SO_4$ using an indirect administration of $SO_2$ gas. All the following voltammetric experiments were thus started from 0.1 V *vs.* NHE.

### 5.3.2.2. Effect of Rotation Rate

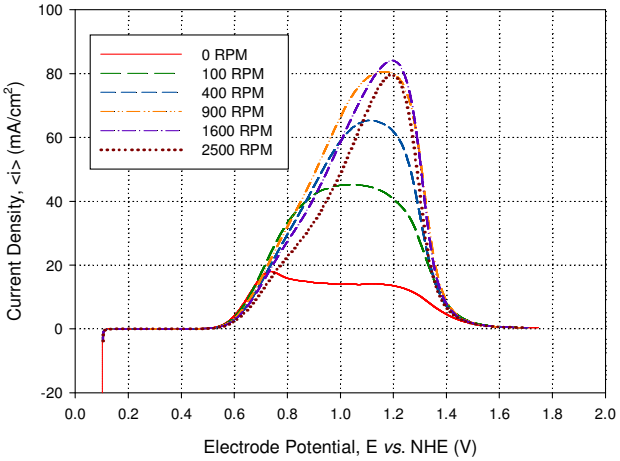


**Figure 70: *LP*s of Pt for SDOR using 0.1 M $Na_2SO_3$ salt in 0.5 M $H_2SO_4$ at different rotation rates at a scan rate of 10 mV/s ($E_{low}$ = 0.1 V)**

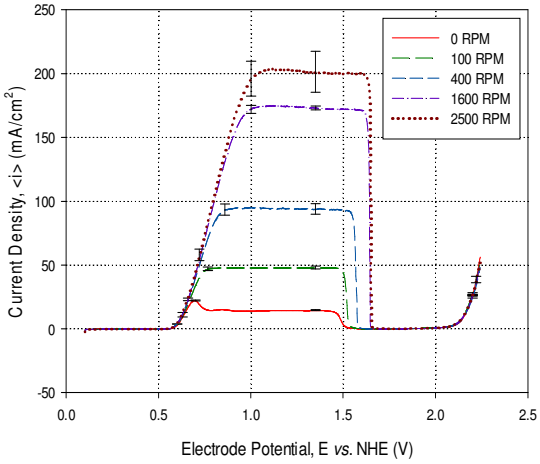


**Figure 71: *LP*s of Au for SDOR using 0.1 M $Na_2SO_3$ salt in 0.5 M $H_2SO_4$ at different rotation rates at a scan rate of 10 mV/s ($E_{low}$ = 0.1 V)**

The *LP*s in Figure 70 for platinum showed a current density increase for SDOR from the onset potential of about 0.5 V, reaching a maximum peak at about 1.2 V *vs.* NHE with a current density of ca. 83.7 mA/cm$^2$ for the 1600 RPM LP scan. For the 0 RPM scan, the maximum current density reached was determined as 18 mA/cm$^2$ at ca. 0.72 V *vs.* NHE. The current density on gold starts to increase from about 0.54 V *vs.* NHE, reaching a maximum current density of about 204 mA/cm$^2$ for the 2500 RPM scan. Depending on the electrode rotation rate, the current density showed a sudden drop from about 1.5 V *vs.* NHE. The sudden drop was also found in literature due to the coverage of the electrode surface by oxides during the oxide adsorption process, ultimately inhibiting the SDOR [51, 129, 130].

The findings thus correspond with literature. Gold showed a sudden drop in current density while platinum showed a steady decrease in current density after the peak maxima was reached.

The current density increase for the peak maxima on platinum is not linear with rotation rate increase with the order of current density increase maxima 0, 100, 400, 2500, 900 and 1600 RPM. To the contrary, the *LP*s displayed in Figure 71 for gold showed a steady increase in current density, with increase of electrode rotation rate compared to platinum. The lack of linear increase with rotation rate increase on platinum, might be due to the strong or weakly adsorbed species on the electrode surface pacifying the electrode active sites towards the SDOR [23, 26, 127] by intermediate or reaction species. As the scans are only initiated and not held for a defined amount of time at 0.1 V *vs.* NHE, it is possible that the reduced catalytic sulphur layer coverage might not be constant between each LP run, as too little reduced $SO_2$ (increased adsorbed $SO_2$ amount) might inhibit the electrode activity [18] or too much reduced $SO_2$ coverage that might also inhibit the SDOR [18, 23] as according to literature the ideal coverage of reduced $SO_2$ is a monolayer [26, 123, 130, 132].

The sudden drop in current density on gold occurs slightly later in the run for every increase in rotation rate, as was the case with gaseous (direct) administration of $SO_2$ (section 5.3.1.2), which might be the establishment of oxide formation equilibrium being more difficult to acquire, due to its removal by real-time $SO_2$ oxidation [51] and thus the delay in inhibition of the electrode activity [51, 129, 130]. The displacement of the catalytic sulphur layer by formation of the surface oxides may also contribute to the sudden fall in oxidation current [51]. From Figure 71 it is clear that the reaction is mass transfer inhibited as the current density increases with an increase in electrode rotation rate [23]. The results in Figure 71 correspond with literature findings [51, 129, 130].

To further investigate the reaction activity on the platinum and gold electrodes, the Tafel slope was determined as in the following section.

#### 5.3.2.3. Tafel Plots

The Tafel plot for platinum is based on the results in Figure 70 and is depicted in Figure 72 and for gold on Figure 71 and depicted in Figure 73. The slope of the plot for platinum was calculated as 172 mV/decade, which is slightly high compared to literature values that range from as low as ca. 30 – 145 mV with gold's Tafel slope calculated as 59 mV/decade where the values published in literature range from 50 – 70 mV [23].

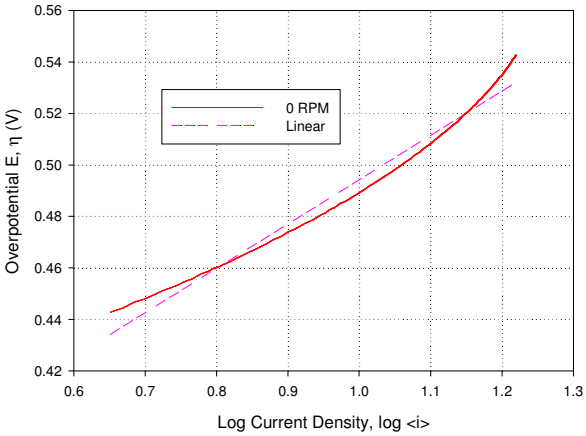


**Figure 72: Tafel plot of Pt for indirect administration of $SO_2$ in 0.5 M $H_2SO_4$ plotted from the potential range 0.601 – 0.701 V *vs.* NHE for the 0 RPM scan in Figure 70 with an $R^2$ of 0.977**

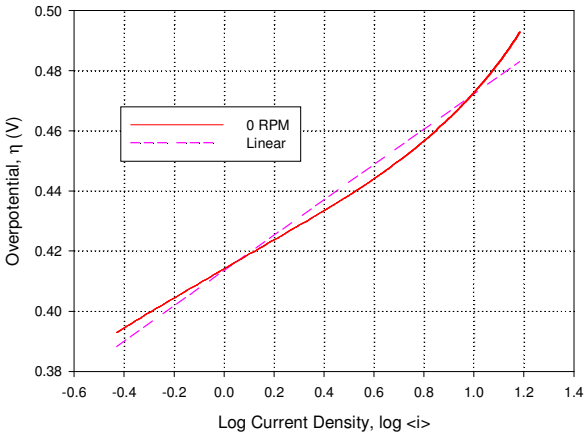


**Figure 73: Tafel plot of Au for indirect administration of $SO_2$ in 0.5 M $H_2SO_4$ plotted from the potential range 0.551 – 0.651 V *vs.* NHE for the 0 RPM scan in Figure 71 with an $R^2$ of 0.983**

The SDOR is thus slightly more sluggish on platinum than found in literature. The calculated Tafel slope is therefore in correspondence with literature findings. The reaction activity was thus further investigated with the use of Koutecký-Levich and Levich analyses.

### 5.3.2.4. Koutecký-Levich Plots

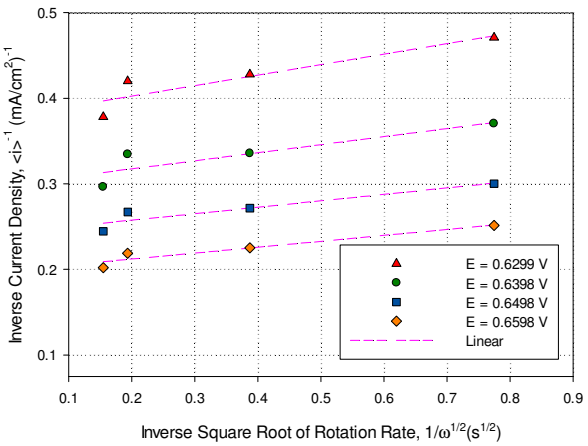


**Figure 74: The Koutecký-Levich plots of Au for $SO_2$ oxidation in 0.5 M $H_2SO_4$ using 0.1 M $Na_2SO_3$**

The Koutecký-Levich plot shown in Figure 74 is plotted from the *LP*s in Figure 71. The *LP*s in Figure 70 for platinum do not show a linear current density increase in the mixed control regions, which makes the application of the Koutecký-Levich analyses not viable.

The results for the Koutecký-Levich plot are given in Table 13 below, with the values used in the calculations given in Table 14 below.

**Table 13: Results for Au Koutecký-Levich plot in 0.5 M $H_2SO_4$ with 0.1 M $Na_2SO_3$**

| Potential used (E *vs.* NHE) | Corresponding Slope (1/mA.s$^{-1/2}$) | Number of electrons |
|---|---|---|
| 0.6299 | 0.1226 | 1.3 |
| 0.6398 | 0.0942 | 1.6 |
| 0.6498 | 0.0756 | 2.0 |
| 0.6598 | 0.0692 | 2.2 |
| | Average Electrons: | 1.8 |

The values used from Table 20, Table 22 and Table 24 (in Appendix 1 – Data) for the calculation of the Koutecký-Levich results, is summarised in the following table:

**Table 14: Values used for the variables of the Koutecký-Levich plots for $Na_2SO_3$ as reagent in 0.5 M $H_2SO_4$**

| | |
|---|---|
| **Kinematic Viscosity (cm$^2$/s)** | $1.068\times10^{-03}$ [60] |
| **Diffusivity ($SO_2$ gas) (cm$^2$/s)** | $1.830\times10^{-05}$ [60] |
| **Radius (cm)** | $2.50\times10^{-01}$ |
| **Faraday Constant (mA.s/mol)** | $9.65\times10^{7}$ |
| **Concentration $Na_2SO_3$ (mol/cm$^3$)** | $1.0\times10^{-04}$ |

The kinematic viscosity of the solution was calculated by using the values in Table 25 (Appendix 1 – Data) with the range of values used from Table 25 summarised in Table 26 (Appendix 2 – Sample Calculations). The diffusion constant or diffusivity of $Na_2SO_3$ was used as the diffusivity of $SO_2$ gas as $Na_2SO_3$ produces $SO_2$ gas in $H_2SO_4$ (reaction (54)).

The slopes of the linear plots of the Koutecký-Levich plot are not parallel for gold. The number of electrons lost in the SDOR was determined as 2 on gold. For a two electron process, the SDOR follows the same reaction path as depicted in reaction scheme (51) above to produce $H_2SO_4$, demonstrated in reaction (56) below [23, 128, 129]:

$$SO_2 + 2H_2O \longrightarrow H_2SO_4 + 2H^+ + 2e^- \quad (56)$$

This finding is in correspondence with literature [23, 128, 129] and with the finding in section 5.3.1.4 when using direct administration of $SO_2$ gas.

For platinum the number of electrons could not be determined using Koutecký-Levich, because the *LP*s in Figure 70 for platinum do not show a linear current density increase in the mixed control regions.

The lack of parallelism in Figure 74 implies a mechanism that changes [53, 81, 85] during the mixed control step of the SDOR electro-oxidation process on gold. The lack of strict linearity of the plots in Figure 74 can also indicate a change in the mechanism [63].

Further investigation was done using the Levich equation to either support or contradict the results from the Koutecký-Levich analysis and to make useful conclusions on the reaction mechanism.

### 5.3.2.5. Levich Plots

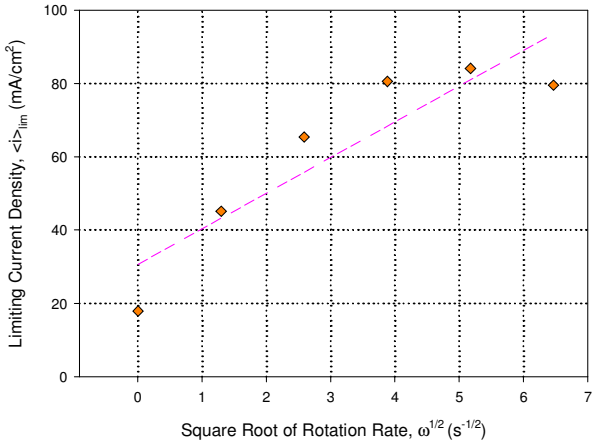


**Figure 75: Levich plot for the SDOR on platinum in 0.5 M $H_2SO_4$ using indirect administration of $SO_2$ gas using $Na_2SO_3$**

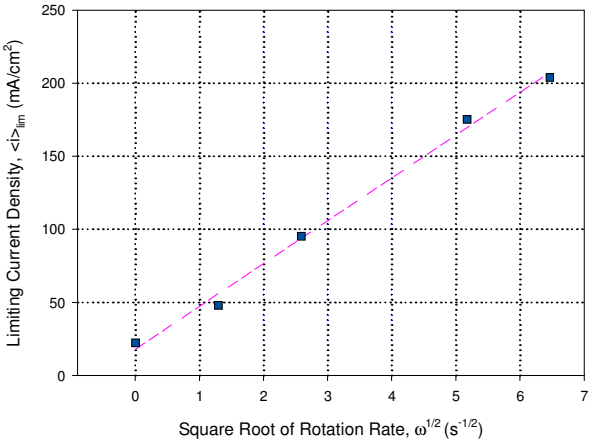


**Figure 76: Levich plot for the SDOR on gold in 0.5 M $H_2SO_4$ using indirect administration of $SO_2$ gas using $Na_2SO_3$**

The plots for platinum in Figure 75 do not show strict linearity, whereas the gold plots (Figure 76) are linearly positioned. The number of electrons calculated for platinum using Levich was 0.5 and for gold 2. The lack of linearity, as with platinum, indicates a mechanism that involves more than one step [53].

The Levich plots confirmed the 2 electron oxidation reaction of $SO_2$ on gold, using indirect administration of $SO_2$ using $Na_2SO_3$ salt. On platinum, Levich analysis showed a 1 electron (rounded from 0.5) transfer with a lack of linearity in the plots, indicating a complex mechanism. Further investigation was not attempted in that context as the mechanism was not in the scope of this study.

### 5.3.2.6. Conclusion

The starting potential of 0.1 V *vs.* NHE was determined to be the best scan starting potential showing the lowest onset potential for the SDOR on both the platinum and gold electrodes, using indirect ($Na_2SO_3$ salt) administration of the $SO_2$ gas. The potential for the reduction of adsorbed $SO_2$ was determined as 0.14 V *vs.* NHE in literature [130]. The improved catalytic

activity towards the SDOR, according to literature, is due to a catalytic layer of adsorbed reduced $SO_2$ forming [129, 130], subsequently acting as a donor ligand for the electrode surface [127], as electrode activity might be inhibited by adsorbed $SO_2$ [18].

Both electrodes are active towards the SDOR with gold exhibiting a transfer of 2 electrons and platinum 0.5, which can be rounded to 1. The possible reaction on gold could be as depicted in reaction (57), which is based on reaction scheme (50) and (51) [52, 123, 127] in sections 5.1.5.2 and 5.1.6.1 whereas there is no literature covering a 1 electron oxidation process:

$$SO_2 + 2H_2O \longrightarrow H_2SO_4 + 2H^+ + 2e^- \quad (57)$$

The Tafel slope for $Na_2SO_3$ generated $SO_2$ was calculated as 172 mV/decade, which is slightly higher than the published literature values found for the SDOR using $Na_2SO_3$ salt as $SO_2$ administration [23] on platinum, with gold as 59 mV/decade, which is within the range of the stated literature values [23].

The SDOR onset potential on platinum was determined as ca. 0.5 V *vs.* NHE with a maximum current density of about 83.7 mA/cm$^2$ for the LP scan at 1600 RPM rotation rate and for the 0 RPM scan ca. 18 mA/cm$^2$ for the peak at ca. 0.72 V *vs.* NHE. The onset potential on gold was determined as ca. 0.54 V *vs.* NHE with a maximum current density of about 175 mA/cm$^2$ for the 1600 RPM rotation rate LP scan and at 0 RPM ca. 18 mA/cm$^2$. The difference in current density for the rotation rates thus indicates that, if diffusion control had not inhibited the reaction activity, the best suited catalyst would have been gold, as it exhibited the higher current density that translates to reaction rate [135].

When considering the indirect means of $SO_2$ administration ($Na_2SO_3$), the behaviour of platinum in aqueous sulphuric acid is thus in accordance with literature findings [23, 26], except that the linear increase in current density with the increase in rotation rate was not found, with the possible lack of linearity due to the lack of constant catalytic layer coverage of reduced $SO_2$ on the electrode surface (section 5.3.2.2). Platinum also showed less correspondence to literature findings with the number of electrons transferred determined to be less than 2. The behaviour of gold in aqueous sulphuric acid is thus in accordance with literature findings when considering $Na_2SO_3$ as means of $SO_2$ administration [129, 130].

## 5.4. Conclusion of the Sulphur Dioxide Oxidation Reaction

### 5.4.1. Platinum vs. Gold (Gaseous $SO_2$)

The whole investigation should be taken into account when establishing the best catalyst for the SDOR; thus, when considering the maximum current density reached at higher rotation rates, gold shows the better performance compared to platinum (almost 2000 mA/cm$^2$ at 1600 RPM and 1100 mA/cm$^2$ at 1600 RPM respectively). Gold shows almost double the current density at high rotation than platinum, which indicates a much higher reaction rate [135] on gold than on platinum. Both catalysts showed mass transfer inhibition due to the increase in current density with rotation rate, in correspondence to literature findings [23].

In conclusion, gold is the better catalyst for the electro-oxidation of $SO_2$ gas in 0.5 M $H_2SO_4$ compared to platinum. Using gold as a catalyst for the SDE (section 1.3.1) could really be considered, as the onset potential is low with a maximum current density reached for the SDOR considerably high indicating a very fast reaction rate as the current density is a direct indication of the reaction rate [135].

### 5.4.2. Platinum vs. Gold ($Na_2SO_3$ Generated $SO_2$)

When taking the maximum current density as well as the Tafel slopes into consideration, the SDOR using indirect $SO_2$ administration is more facile on gold in 0.5 M $H_2SO_4$ than on platinum. The maximum current density acquired on platinum is lower than the maximum current density found on gold. The SDE can be regarded as a stationary electrode (section 5.1.1), therefore the maximum current density at 0 RPM is considered. The SDOR onset potential should also be considered, with gold at a slightly higher onset potential than platinum.

The study of the reaction activity should be regarded as a whole in the establishment of the best catalyst for SDOR. Therefore, when considering the maximum current density reached at higher rotation rates, gold shows the better performance as compared to platinum (about 170 mA/cm$^2$ at 1600 RPM and 83.7 mA/cm$^2$ at 1600 RPM respectively). Gold shows slightly more than double the current density at high rotation than platinum, indicating a much higher reaction rate [135] on gold than on platinum. Both catalysts showed mass transfer inhibition due to the increase in current density with rotation rate, in correspondence with literature findings [23] except for platinum, which did not show a steady or linear increase in current density with electrode rotation rate, which was speculated to be due to the possible lack of constant coverage of reduced $SO_2$ on the electrode surface (section 5.3.2.2).

In conclusion, gold is the better catalyst for the electro-oxidation of $SO_2$ using indirect administration in 0.5 M $H_2SO_4$ as compared to platinum. As is the case with the direct administration of $SO_2$ gas, using gold as a catalyst for the SDE (section 1.3.1).

To conclude, gold is a better catalyst for the electro-oxidation of $SO_2$ than platinum by using 0.1 M $Na_2SO_3$ salt to indirectly produce $SO_2$ in 0.5 M $H_2SO_4$.

### 5.4.3. Platinum *vs.* Gold for SDOR

Consider the following summary of results for the SDOR using direct ($SO_2$ gas) and indirect ($Na_2SO_3$ salt) administration of $SO_2$ gas to the electrolyte solution.

**Table 15: Comparison of SDOR results for gold and platinum using direct and indirect $SO_2$ administration in 0.5 M $H_2SO_4$**

| | | SDOR Onset Potential (E *vs.* NHE) | | Maximum Current Density at 0 RPM ($mA/cm^2$) | | Tafel Slope (mV/decade) | | $e^-$ Number | |
|---|---|---|---|---|---|---|---|---|---|
| **Reaction** | **Medium** | **Au** | **Pt** | **Au** | **Pt** | **Au** | **Pt** | **Au** | **Pt** |
| **SDOR ($SO_2$)** | **Acid** | 0.52 V | 0.52 V | 300 | 400 | 378 | 891 | 2 | 1 |
| **SDOR ($Na_2SO_3$)** | **Acid** | 0.54 V | 0.5 V | 25 | 18 | 59 | 172 | 2 | 1 |

The Tafel slope is a good measure of electrode activity, with the results in Table 15 showing that gold is more facile towards the SDOR for both direct and indirect administration of $SO_2$, with gold exhibiting the lower slope for both types of administration, as compared to platinum. The big difference in the Tafel slope magnitudes as well as the maximum current densities for the different forms of administration might be due to the difference in dissolved $SO_2$ concentration – increased $SO_2$ concentration leads to an increase in current density [23]. The increase in Tafel slope magnitude with increase of $SO_2$ concentration might be due to $SO_2$ adsorption saturating the electrode surface [23]. The saturated concentration of $SO_2$ (direct administration) was ca. 1.4 M (Table 12) whereas the salt concentration (indirect administration) was 0.1 M, with the saturated concentration more than ten (10) times more concentrated than the indirect form.

The onset potential for SDOR on gold using direct $SO_2$ administration was lower than the onset potential on platinum except with the indirect administration of $SO_2$ where platinum exhibited a lower onset potential than gold. The maximum current density reached at 0 RPM electrode rotation rate for gold with direct administration of $SO_2$ is lower than platinum, whereas the indirect administration of $SO_2$ gas showed a higher current density than

platinum. When taking the maximum current density reached at high electrode rotation rate into account, gold performed better than platinum with both direct and indirect $SO_2$ gas administration. The number of electrons involved in the SDOR was calculated as 1 for platinum with both $SO_2$ administration methods, which is not found in literature. Using Levich and Koutecký-Levich methods, it could be seen that the reaction mechanism is very complex on platinum and that might lead to determination of 1 electron. The reaction mechanism was not within the scope of this study and thus further investigation into it was not attempted. Regardless, the electrode showed activity. For gold the number of electrons calculated was 2 for both direct and indirect $SO_2$ administration.

The oxidation of $SO_2$ can be depicted in the following reaction for gold, using direct and indirect administration of $SO_2$ [23, 52, 123, 127-129]:

$$SO_2 + 2H_2O \longrightarrow H_2SO_4 + 2H^+ + 2e^- \quad (58)$$

Gold showed an interesting phenomenon with a strong adsorbed chemical species appearing on preconditioning *CV*s when investigating direct administration of $SO_2$ gas, which is $SO_2$, according to literature, that would not affect catalytic effectiveness [128, 129] as was found in this study, whereas there was no such species in the indirect administration of $SO_2$ gas.

Both platinum and gold exhibited reliance on the catalytic layer of reduced $SO_2$ to improve activity of the electrode towards bulk $SO_2$ oxidation [26, 129, 130]. The inhibition of the electrode activity, once oxide adsorption occurs, is apparent on both gold and platinum [23, 52, 132, 134]. It might be due to the displacement of the catalytic sulphur layer by the formation of oxides that could contribute to the sudden fall in oxidation current [51]. The sudden decrease in current density was not found on platinum, with the indirect administration of $SO_2$ gas using $Na_2SO_3$. Taking into account the onset potential, the maximum current density on a stationary electrode and on a rotating electrode as well as the Tafel slope, it can be concluded that gold is ultimately the superior catalyst for the SDOR, as compared to platinum. Literature also speculates that gold might be a superior catalyst to platinum for the SDOR [23]. As literature states, gold exhibits better catalytic properties towards SDOR than platinum as $SO_2$ adsorbs much more strongly on platinum than on gold [26, 130], which can be regarded as the main drive behind the reactiveness and selectivity of the electrodes towards the SDOR [130].

# Chapter 6: Conclusion

For each respective reaction studied in this investigation the best catalyst material was determined. In fuel cell applications, the best cathode or anode material was determined for the ORR and EOR. The catalyst material for use in the SDE was also investigated for the $SO_2$ oxidation reaction.

## 6.1. Oxygen Reduction Reaction (ORR)

Gold is known to bind oxygen strongly enough so as not to inhibit its reactivity or so weakly that the electrode would be inactive towards ORR [49], while platinum is known to bind oxygen to a degree of strength that might inhibit its activity towards the ORR [31, 74]. It is speculated that platinum's activity could be hampered by the adsorption of $O_2$ [31, 74], OH [31, 76], H [83] or anions such as $ClO_4^-$ or $HSO_4^-$ that provide steric hindrance towards oxygen adsorption [83]. As gold is also softer than platinum, and that increased hardness is related to less activity [28], it can be concluded that the softness of gold can also contribute to the higher efficiency of reaction towards ORR.

The ORR is known to be structure sensitive on platinum [74, 76, 79, 83] and gold [40, 49, 59] in both acidic and alkaline medium. Pt(111) showed higher activity towards ORR in perchloric acid [76, 79] than Pt(100) with the (111) lattice exhibiting a greater ease of interaction with OH in alkaline medium [76]. Gold on the other hand had been established to rely significantly on the plane of orientation of crystal lattices for the reduction of oxygen or peroxide with Au(111) having a weak effect on the transformation of peroxide to water [82]. The results for platinum and gold are thus summarised in the table below:

**Table 16: Results summary for ORR in alkaline and acid medium for Au and Pt**

| | Onset Potential E *vs.* NHE | | Tafel Slope (mV/decade) | | $e^-$ Number | |
|---|---|---|---|---|---|---|
| **Medium** | **Au** | **Pt** | **Au** | **Pt** | **Au** | **Pt** |
| **Acid** | 0.4 | 0.8 | -129 | -205 | - | 4 |
| **Alkaline** | 0.1 | 0.14 | -80 | -72 | 2 | 4 |

It can be concluded that gold is a good competing electrode material and worthy alternative material to platinum for the ORR in alkaline media, should the price of gold per fine ounce decrease to much lower levels compared to platinum. Gold showed crossover of *LP*s in the mixed control region with no diffusion limited character in acidic medium; therefore the number of electrons could not be determined using either Levich or Koutecký-Levich analyses. Onset potential and number of electrons play an extremely important role along

with the Tafel slope to determine the best performing electrode, as platinum had the lowest Tafel slope in alkaline medium, and almost equal to gold, and the highest in acidic medium, with a higher onset potential than gold in both media. Therefore, platinum is overall an effective ORR electrode with gold a good alternative to platinum in alkaline medium.

Ultimately, platinum showed the most effective reduction for the ORR with a total reduction of oxygen to water in both media, which is suitable for use in fuel cell technology, as there is no corrosive peroxide forming that can potentially damage or decrease the lifespan of a fuel cell [73]. More power can also be drawn from a four electron process [73]. Gold was also established to be a good competitive catalyst material as an alternative to platinum towards the ORR in alkaline media, should the price of gold per fine ounce become cheaper than platinum.

Platinum can therefore be considered as the ideal catalyst material for the cathode in an acidic fuel cell so as to reduce oxygen to water and to increase the lifetime of the fuel cell. Gold and platinum could be regarded as equally competitive catalysts for the ORR in alkaline medium.

$$O_2 + 4e^- + 4H^+ \longrightarrow 2H_2O \quad \text{(Acidic)} \tag{59}$$

$$O_2 + 4e^- + 2H_2O \longrightarrow 4OH^- \quad \text{(Alkaline)} \tag{60}$$

In this study platinum was concluded to be the more effective catalyst towards the ORR in both media, which is the same conclusion, reached in literature [40, 79] with gold an equally competitive catalyst to platinum in alkaline medium and worthy alternative to platinum should the price per fine ounce decrease below that of platinum.

## 6.2. Ethanol Oxidation Reaction (EOR)

In this study, platinum showed superior activity in both acidic and alkaline medium.

In alkaline medium, gold had an apparent increase in activity compared to the acidic medium; nonetheless smooth platinum could be regarded as a preferred catalyst rather than a smooth gold electrode. Literature speculation that un-activated gold showed better performance to the ethanol electro-oxidation reaction in alkaline media rather than acid media is supported by the results in Table 17 [47]. Gold seems to perform better in alkaline medium as CO poisoning does not occur on the gold surface, unlike platinum [114].

**Table 17: Comparison table for all the results at 0 RPM for ethanol oxidation in platinum and gold in both acid and alkaline media**

| | | Peak Potential E *vs.* NHE | | Peak Current Density mA/cm$^2$ | | Tafel Slope mV/decade | | Activation Energy kJ/mol | |
|---|---|---|---|---|---|---|---|---|---|
| **Reaction** | **Medium** | **Au** | **Pt** | **Au** | **Pt** | **Au** | **Pt** | **Au** | **Pt** |
| **Ethanol Oxidation** | **Acid** | 1.26 | 0.8 | 0.21 | 3.5 | 228 | 209 | - | - |
| | **Alkaline** | 0.36 | -0.1 | 5.93 | 1.96 | 227 | 249 | 30.121 | 26.201 |

The most accepted electro-oxidation reaction mechanism ($C_2$-pathway) for ethanol on a gold electrode suggests that the reaction takes place without the breaking of the C-C bond, which then forms acetaldehyde and acetic acid [101], as the platinum electrode is prone to CO poisoning [32].

On platinum the C-C bond is broken at low potentials in alkaline medium. Adsorbed species are thus $CH_x$ and CO. The $CH_x$ are firstly oxidised to CO then to $CO_2$ or (bi)carbonate. $CH_x$ intermediate species are found to be more stable in alkaline media, with the dominant poisoning species in alkaline solution being adsorbed CO, implying that $CH_x$ is readily oxidised on polycrystalline platinum surface in alkaline solution. C-C bond breaking is thus more facile in alkaline medium, which in turn enhances the selectivity of the pathway to the $C_1$-pathway in alkaline medium on a platinum electrode, also evident in the magnitude of the Tafel slope comparison in Table 17.

With platinum in alkaline medium, the C-C bond is broken and $CO_2$ and adsorbed CO and $CH_x$ is formed with an activation energy requirement less than gold, which only produces acetic acid in alkaline medium.

Thus, platinum is the best catalyst for the electro-oxidation of ethanol in alkaline and acid medium.

In a fuel cell application with ethanol, platinum would be the best suited electrode material in both acidic and alkaline medium, especially at elevated temperatures in alkaline fuel cells. At this stage, as literature indicated, there are many issues that need to be resolved before alkaline fuel cells can be used; at elevated temperatures especially.

## 6.3. Sulphur Dioxide Oxidation Reaction (SDOR)

The Tafel slope is a good measure of electrode activity, with the results in Table 18 showing that gold is more facile towards the SDOR for both direct and indirect administration of $SO_2$, with gold exhibiting the lower slope for both types of administration compared to platinum. The maximum current density reached at 0 RPM electrode rotation rate for gold with direct

administration of $SO_2$ is lower than platinum, whereas the indirect administration of $SO_2$ gas showed a higher current density than platinum. When taking the maximum current density reached at high electrode rotation rates into account, gold performed better than platinum with both direct and indirect $SO_2$ gas administration (Table 18).

**Table 18: Comparison of SDOR results for gold and platinum using direct and indirect $SO_2$ administration in 0.5 M $H_2SO_4$**

| | | SDOR Onset | | Maximum | | Tafel Slope | | $e^-$ | |
|---|---|---|---|---|---|---|---|---|---|
| **Reaction** | **Medium** | **Au** | **Pt** | **Au** | **Pt** | **Au** | **Pt** | **Au** | **Pt** |
| SDOR | Acid | 0.52 V | 0.52 V | 300 | 400 | 378 | 891 | 2 | 1 |
| SDOR | Acid | 0.54 V | 0.5 V | 25 | 18 | 59 | 172 | 2 | 1 |

The number of electrons involved in the SDOR was calculated as 1 for platinum with both $SO_2$ administration methods, which is not found in literature. Using Levich and Koutecký-Levich methods, it could be seen that the reaction mechanism is very complex on platinum and that might lead to determination of 1 electron. The reaction mechanism was not within the scope of this study and thus further investigation into it was not attempted. For gold the number of electrons calculated was 2 for both direct and indirect $SO_2$ administration.

The oxidation of $SO_2$ can be depicted in the following reaction for gold electrodes using direct and indirect administration of $SO_2$ [23, 52, 123, 127-129]:

$$SO_2 + 2H_2O \longrightarrow H_2SO_4 + 2H^+ + 2e^- \quad (61)$$

Gold showed an interesting phenomenon with a strong adsorbed chemical species appearing on preconditioning *CV*s, which is $SO_2$, according to literature, that would not affect catalytic effectiveness [128, 129] as was found in this study, whereas there was no such species in the indirect administration of $SO_2$ gas. This adsorbed specie might contribute to the magnitude of the Tafel slope in the direct administration of $SO_2$ with both platinum and gold. Both platinum and gold exhibited reliance on the catalytic layer of reduced $SO_2$ to improve activity of the electrode towards bulk $SO_2$ oxidation [26, 129, 130]. The inhibition of the electrode activity, once oxide adsorption occurs, is apparent on both gold and platinum [23, 52, 132, 134]. It might be due to the displacement of the catalytic sulphur layer by the formation of oxides that could contribute to the sudden decrease in oxidation current [51]. The sudden decrease in current density was not found on platinum with the indirect administration of $SO_2$ gas using $Na_2SO_3$. Taking into account the onset potential, the maximum current density on a stationary electrode as well as the Tafel slope, it can be

concluded that gold is ultimately the superior catalyst for the SDOR, as compared to platinum. Literature also speculated that gold might be a superior catalyst to platinum for the SDOR [23]. As literature states, gold exhibits better catalytic properties towards SDOR than platinum as $SO_2$ adsorbs much stronger on platinum than on gold [26, 130], which can be regarded as the main drive behind the reactiveness and selectivity of the electrodes towards the SDOR [130].

### 6.3.1. Sulphur Depolarised Electrolyser (SDE) Applications

As gold had been established, in this study, to be the superior catalyst for the SDOR, the anode in a fuel cell for use in the oxidation of $SO_2$ within the HyS cycle (section 1.3.1) so as to generate hydrogen gas and sulphuric acid in the SDE (reaction (3)), can be made of gold, as its activity towards the SDOR is superior to platinum.

$$SO_2 + 2H_2O \longrightarrow H_2SO_4 + H_2 \quad (62)$$

## 6.4. Summary

The results in Table 19 indicate which electrode material had the better activity towards every investigated reaction in each electrolyte medium. Platinum was the dominant material, with better activity in four of the six studied reactions. Gold would therefore be the best electrode to use with the SDOR.

**Table 19: The electrode with the better activity towards each reaction in all electrolyte media**

| Best electrode for each reaction in every electrolyte medium | | | | | |
|---|---|---|---|---|---|
| **EOR Acid** | **EOR Alkaline** | **ORR Acid** | **ORR Alkaline** | **SDOR ($Na_2SO_3$)** | **SDOR ($SO_{2(g)}$)** |
| Pt | Pt | Pt | Pt = Au | Au | Au |

Extensive mechanistic studies will have to be done to get a more in-depth understanding of each reaction so as to develop the ultimate performing catalyst material.

Based on this study for each reaction, the best catalyst setup would be as follows: ORR – Platinum or gold for the cathode and anode in alkaline and platinum in acidic media for fuel cells. EOR: - Platinum for both the cathode and anode in alkaline and acidic medium fuel cells. SDOR - Gold for the anode and platinum for the cathode.

### 6.4.1. Further Work

During the course of this investigation, there were a few concepts that came to light that could enjoy some further future investigation. A concise list follows:

- The lack of linearity in the increase of current density with increasing rotation rate with gold in acidic medium in the ORR (Figure 21). This behaviour might be due to different mechanistic pathways, electrode preparation techniques, or even surface structure anomalies.
- Gold as electrode material for the ORR in alkaline media for use in fuel cell technology. As gold performed very competitively against platinum towards the ORR in alkaline medium, implementing it as an alternative catalyst to platinum for the ORR in alkaline medium can be seriously considered or further investigated.
- The third peak of the EOR on platinum in acidic medium (Figure 36 & Figure 38). As there was no literature that even mentioned the third oxidation peak of the EOR on platinum in acidic medium, its peculiar behaviour with temperature changes, and the possible by-products could be identified and investigated in-depth, which might contribute to solving the mysteries behind the EOR mechanism.
- The strongly adsorbed specie on gold in the SDOR in acidic medium using $SO_2$ gas as administration form (Figure 57). The $SO_2$ electro-oxidation mechanism is very complex and the adsorbed specie that does not negatively affect the electrode activity, supports that conclusion. There is also no literature found that discusses the peak found in Figure 57. Investigation into this peak might help solving the mystery.
- Alloying of platinum and gold could also be investigated for the different reactions as well as alloying of the two catalysts with different *PGM*s or noble metals. There is a wide variety of literature coverage of alloying, although many different aspects thereof have not been considered yet.
- Extensive mechanistic studies on each reaction on different catalyst materials in different electrolyte media, as most of the electrochemical reactions in this study's mechanisms are still very mysterious with many varying pathways found in literature.

# Bibliography


1. Penner, S.S., *Steps toward the hydrogen economy.* Energy, 2006. **31**(1): p. 33-43.
2. Conte, M., *ENERGY | Hydrogen Economy*, in *Encyclopedia of Electrochemical Power Sources*, J. Garche, Editor. 2009, Elsevier: Amsterdam. p. 232-254.
3. Miller, C.A., *3.02 - Energy Resources and Policy: Vulnerability of Energy Resources and Resource Availability – Fossil Fuels (Oil, Coal, Natural Gas, Oil Shale)*, in *Climate Vulnerability*, R.A. Pielke, Editor. 2013, Academic Press: Oxford. p. 37-51.
4. Fujita, R., et al., *Revisiting ocean thermal energy conversion.* Marine Policy, 2012. **36**(2): p. 463-465.
5. Crabtree, G.W., M.S. Dresselhaus, and M.V. Buchanan, *The hydrogen economy.* Physics Today, 2004. **57**(12): p. 39-44.
6. Balat, M., *Potential importance of hydrogen as a future solution to environmental and transportation problems.* International Journal of Hydrogen Energy, 2008. **33**(15): p. 4013-4029.
7. Balat, H. and E. Kırtay, *Hydrogen from biomass – Present scenario and future prospects.* International Journal of Hydrogen Energy, 2010. **35**(14): p. 7416-7426.
8. Yilmaz, C. and M. Kanoglu, *Thermodynamic evaluation of geothermal energy powered hydrogen production by PEM water electrolysis.* Energy, 2014. **69**(0): p. 592-602.
9. van der Zwaan, B., *The role of nuclear power in mitigating emissions from electricity generation.* Energy Strategy Reviews, 2013. **1**(4): p. 296-301.
10. Raja Singh, R., T. Raj Chelliah, and P. Agarwal, *Power electronics in hydro electric energy systems – A review.* Renewable and Sustainable Energy Reviews, 2014. **32**(0): p. 944-959.
11. De Ladurantaye, D., M. Gendreau, and J.-Y. Potvin, *Optimizing profits from hydroelectricity production.* Computers & Operations Research, 2009. **36**(2): p. 499-529.
12. Heller, A., *Conversion of sunlight into electrical power and photoassisted electrolysis of water in photoelectrochemical cells.* Accounts of Chemical Research, 1981. **14**(5): p. 154-162.
13. Guha, S. and J. Yang, *Progress in amorphous and nanocrystalline silicon solar cells.* Journal of Non-Crystalline Solids, 2006. **352**(9–20): p. 1917-1921.
14. Darwish, M.A., F.M. Al Awadhi, and A.O. Bin Amer, *Combining the nuclear power plant steam cycle with gas turbines.* Energy, 2010. **35**(12): p. 4562-4571.
15. Zarrouk, S.J. and H. Moon, *Efficiency of geothermal power plants: A worldwide review.* Geothermics, 2014. **51**: p. 142-153.

16. Mohiuddin, A.K.M., M.F.B. Chemani, and M.B.B. Zakaria, *Design and investigation of a fuel cell car prototype.* International Journal of Vehicle Systems Modelling and Testing, 2014. **9**(3-4): p. 321-333.
17. Katikaneni, S.P., F. Jahnke, and P.S. Patel. *Onsite hydrogen production and electricity generation using high temperature fuel cells: An overview*. in *ACS National Meeting Book of Abstracts*. 2006.
18. Colón-Mercado, H.R. and D.T. Hobbs, *Catalyst evaluation for a sulfur dioxide-depolarized electrolyzer.* Electrochemistry Communications, 2007. **9**: p. 2649-2653.
19. Teo, J.S.K., et al., *Monolithic gold catalysts: Preparation and their catalytic performances in water gas shift and CO oxidation reactions.* International Journal of Hydrogen Energy, 2011.
20. Kotz, J.C., P.M. Treichel, and P.A. Harman, *Chemistry & Chemical Reactivity*. 2003, Thomson Brooks/Cole: London. p. 239, Table 6.4.
21. Lamy, C., et al., *Clean hydrogen generation through the electrocatalytic oxidation of formic acid in a Proton Exchange Membrane Electrolysis Cell (PEMEC).* Electrochimica Acta, 2012. **60**(0): p. 112-120.
22. Gorensek, M.B. and W.A. Summers, *Hybrid sulfur flowsheets using PEM electrolysis and a bayonet decomposition reactor.* International Journal of Hydrogen Energy, 2009. **34**(9): p. 4097-4114.
23. O'Brien, J.A., et al., *The electrochemical oxidation of aqueous sulfur dioxide: A critical review of work with respect to the hybrid sulfur cycle.* Electrochimica Acta, 2010. **55**(3): p. 573-591.
24. Summers, W., et al., *Hybrid Sulfur Thermochemical Process Development*. 2007, FY 2007 Publications/Presentations. p. 212-215.
25. Struck, B.D., et al., *The anodic oxidation of sulfur dioxide in the sulfuric acid hybrid cycle.* International Journal of Hydrogen Energy, 1980. **5**(5): p. 487-497.
26. O'Brien, J.A., J.T. Hinkley, and S.W. Donne, *Electrochemical Oxidation of Aqueous Sulfur Dioxide II. Comparative Studies on Platinum and Gold Electrodes.* Journal of The Electrochemical Society, 2012. **159**(9): p. F585-F593.
27. Steimke, J., *Design and Performance Objectives of the Single Cell Test System for SO2 Depolarized Electrolyzer Development*. 2007: Westinghouse Savannah River Company. p. 1-7.
28. Shi, Z., et al., *Current status of ab initio quantum chemistry study for oxygen electroreduction on fuel cell catalysts.* Electrochimica Acta, 2006. **51**(10): p. 1905-1916.
29. Chen, W., D. Ny, and S. Chen, *SnO2–Au hybrid nanoparticles as effective catalysts for oxygen electroreduction in alkaline media.* Journal of Power Sources, 2010. **195**(2): p. 412-418.
30. Quaino, P., et al., *Why is gold such a good catalyst for oxygen reduction in alkaline media?* Angewandte Chemie - International Edition, 2012. **51**(52): p. 12997-13000.

31. Sarapuu, A., et al., *Electroreduction of oxygen on gold-supported thin Pt films in acid solutions.* Journal of Electroanalytical Chemistry, 2008. **624**(1–2): p. 144-150.
32. Dimos, M.M. and G.J. Blanchard, *Evaluating the Role of Pt and Pd Catalyst Morphology on Electrocatalytic Methanol and Ethanol Oxidation.* The Journal of Physical Chemistry C, 2010. **114**(13): p. 6019-6026.
33. Martins, M.E., R.O. Córdova, and A.J. Arvía, *The potentiodynamic electroformation and electroreduction of the O-containing layer on gold in alkaline solutions.* Electrochimica Acta, 1981. **26**(11): p. 1547-1554.
34. Beyhan, S., et al., *Electrochemical and in situ FTIR studies of ethanol adsorption and oxidation on gold single crystal electrodes in alkaline media.* Journal of Electroanalytical Chemistry, 2013. **707**(0): p. 89-94.
35. Hamelin, A., *Cyclic voltammetry at gold single-crystal surfaces. Part 1. Behaviour at low-index faces.* Journal of Electroanalytical Chemistry, 1996. **407**(1–2): p. 1-11.
36. Hamelin, A. and A.M. Martins, *Cyclic voltammetry at gold single-crystal surfaces. Part 2. Behaviour of high-index faces.* Journal of Electroanalytical Chemistry, 1996. **407**(1–2): p. 13-21.
37. Sen Gupta, S. and J. Datta, *A comparative study on ethanol oxidation behavior at Pt and PtRh electrodeposits.* Journal of Electroanalytical Chemistry, 2006. **594**(1): p. 65-72.
38. Solla-Gullón, J., et al., *A combination of SERS and electrochemistry in Pt nanoparticle electrocatalysis: Promotion of formic acid oxidation by ethylidyne.* Electrochemistry Communications, 2008. **10**(2): p. 319-322.
39. Wang, Y., et al., *Electrocatalysis of gold nanoparticles/layered double hydroxides nanocomposites toward methanol electro-oxidation in alkaline medium.* Electrochimica Acta, 2010. **55**: p. 4045-4049.
40. Solla-Gullón, J., F.J. Vidal-Iglesias, and J.M. Feliu, *Shape dependent electrocatalysis.* Annu. Rep. Prog. Chem., Sect. C: Phys. Chem., 2011. **107**(Copyright (C) 2012 American Chemical Society (ACS). All Rights Reserved.): p. 263-297.
41. Bruckenstein, S. and M. Shay, *An in situ weighing study of the mechanism for the formation of the adsorbed oxygen monolayer at a gold electrode.* Journal of Electroanalytical Chemistry and Interfacial Electrochemistry, 1985. **188**(1–2): p. 131-136.
42. Angerstein-Kozlowska, H., et al., *Elementary steps of electrochemical oxidation of single-crystal planes of gold. Part II. Chemical and structural basis of oxidation of the (111) plane.* J. Electroanal. Chem. Interfacial Electrochem., 1987. **228**(Copyright (C) 2012 American Chemical Society (ACS). All Rights Reserved.): p. 429-53.
43. Jalili, S., A. Zeini Isfahani, and R. Habibpour, *Atomic oxygen adsorption on Au (100) and bimetallic Au/M (M=Pt and Cu) surfaces.* Computational and Theoretical Chemistry, 2012(0).

44. Raj, C.R., A.I. Abdelrahman, and T. Ohsaka, *Gold nanoparticle-assisted electroreduction of oxygen.* Electrochemistry Communications, 2005. **7**(9): p. 888-893.
45. O'Mullane, A.P., et al., *Premonolayer Oxidation of Nanostructured Gold: An Important Factor influencing Electrocatalytic Activity.* Langmuir, 2009. **25**(6): p. 3845-3852.
46. Pineda, T., et al., *Electrooxidation of pyridoxal (PL) on a polycrystalline gold electrode in alkaline solutions.* Journal of Electroanalytical Chemistry, 2000. **492**(1): p. 38-45.
47. Cherevko, S., N. Kulyk, and C.-H. Chung, *Utilization of surface active sites on gold in preparation of highly reactive interfaces for alcohols electrooxidation in alkaline media.* Electrochimica Acta, 2012. **69**(0): p. 190-196.
48. Xu, J.B., et al., *Synthesis and characterization of the Au-modified Pd cathode catalyst for alkaline direct ethanol fuel cells.* International Journal of Hydrogen Energy, 2010. **35**(18): p. 9693-9700.
49. Sarapuu, A., et al., *Electroreduction of oxygen on gold-supported nanostructured palladium films in acid solutions.* Electrochimica Acta, 2010. **55**(22): p. 6768-6774.
50. Xu, J.B., et al., *Stabilization of the palladium electrocatalyst with alloyed gold for ethanol oxidation.* International Journal of Hydrogen Energy, 2010. **35**(13): p. 6490-6500.
51. Zdeněk, S. and J. Weber, *Study of the oxidation of SO2 dissolved in 0.5 M H2SO4 on a gold electrode—II. A rotating disc electrode.* Electrochimica Acta, 1975. **20**: p. 413-419.
52. Appleby, A.J. and B. Pichon, *The mechanism of the electrochemical oxidation of sulfur dioxide in sulfuric acid solutions.* Journal of Electroanalytical Chemistry and Interfacial Electrochemistry, 1979. **95**(1): p. 59-71.
53. Treimer, S., A. Tang, and D.C. Johnson, *A Consideration of the Application of Koutecký-Levich Plots in the Diagnoses of Charge-Transfer Mechanisms at Rotated Disk Electrodes.* Electroanalysis, 2002. **14**(3): p. 165-171.
54. Pletcher, D., *A First Course in Electrode Processes*. 2009, The Royal Society of Chemistry Publishing: Cambridge. p. 187.
55. Pletcher, D., *A First Course in Electrode Processes*. 2009, The Royal Society of Chemistry Publishing: Cambridge. p. 27-28.
56. Pletcher, D., *A First Course in Electrode Processes*. 2009, The Royal Society of Chemistry Publishing: Cambridge. p. 17.
57. Pletcher, D., *A First Course in Electrode Processes*. 2009, The Royal Society of Chemistry Publishing: Cambridge. p. 31 & 164.
58. Jeon, M.K. and P.J. McGinn, *Carbon supported Pt-Y electrocatalysts for the oxygen reduction reaction.* Journal of Power Sources, 2011. **196**: p. 1127-1131.
59. Erikson, H., et al., *Electroreduction of oxygen on carbon-supported gold catalysts.* Electrochimica Acta, 2009. **54**(28): p. 7483-7489.

60. Haynes, W.M. and D.R. Lide, *CRC handbook of chemistry and physics: a ready-reference book of chemical and physical data*. CRC handbook of chemistry and physics, ed. W.M. Haynes and D.R. Lide. Vol. 92. 2011, Boca Raton, Florida.: CRC Press.
61. Atkins, P. and J.d. Paula, *Atkins' Physical Chemistry*. 2006, Oxford University Press: Oxford. p. 808.
62. Kotz, J.C., P.M. Treichel, and P.A. Harman, *Chemistry & Chemical Reactivity*. 2003, Thomson Brooks/Cole: London. p. 626.
63. Paliteiro, C., *(100)-Type behaviour of polycrystalline gold towards O2 reduction.* Electrochimica Acta, 1994. **39**(11–12): p. 1633-1639.
64. Caselli, M., G. Scarano, and A. Traini, *Catalytic electroreduction of oxygen at a dropping mercury electrode in the presence of colloidal gold.* Journal of Electroanalytical Chemistry and Interfacial Electrochemistry, 1973. **44**(1): p. 91-106.
65. Bron, M., *Carbon black supported gold nanoparticles for oxygen electroreduction in acidic electrolyte solution.* Journal of Electroanalytical Chemistry, 2008. **624**(1–2): p. 64-68.
66. Kumar, S. and S. Zou, *Electroreduction of O2 on uniform arrays of Pt and PtCo nanoparticles.* Electrochemistry Communications, 2006. **8**(7): p. 1151-1157.
67. Van Brussel, M., et al., *Oxygen reduction at platinum modified gold electrodes.* Electrochimica Acta, 2003. **48**(25–26): p. 3909-3919.
68. Alexeyeva, N. and K. Tammeveski, *Electroreduction of oxygen on gold nanoparticle/PDDA-MWCNT nanocomposites in acid solution.* Analytica Chimica Acta, 2008. **618**(2): p. 140-146.
69. Wang, F., et al., *Electroreduction of dioxygen on Aunano–DNA film electrode in acidic electrolyte.* Bioelectrochemistry, 2006. **69**(2): p. 148-157.
70. Chakraborty, S. and C. Retna Raj, *Electrocatalytic performance of carbon nanotube-supported palladium particles in the oxidation of formic acid and the reduction of oxygen.* Carbon, 2010. **48**(11): p. 3242-3249.
71. Bakır, Ç.C., et al., *Electrocatalytic reduction of oxygen on bimetallic copper–gold nanoparticles–multiwalled carbon nanotube modified glassy carbon electrode in alkaline solution.* Journal of Electroanalytical Chemistry, 2011. **662**(2): p. 275-280.
72. Shao, M.H. and R.R. Adzic, *Spectroscopic identification of the reaction intermediates in oxygen reduction on gold in alkaline solutions.* Journal of Physical Chemistry B, 2005. **109**(35): p. 16563-16566.
73. Zhang, T. and A.B. Anderson, *Oxygen reduction on platinum electrodes in base: Theoretical study.* Electrochimica Acta, 2007. **53**(2): p. 982-989.
74. Kuzume, A., E. Herrero, and J.M. Feliu, *Oxygen reduction on stepped platinum surfaces in acidic media.* Journal of Electroanalytical Chemistry, 2007. **599**(2): p. 333-343.

75. Cameron, D.S., *RECYCLING | Noble Metal Recycling*, in *Encyclopedia of Electrochemical Power Sources*, J. Garche, Editor. 2009, Elsevier: Amsterdam. p. 209-214.
76. Rizo, R., E. Herrero, and J.M. Feliu, *Oxygen reduction reaction on stepped platinum surfaces in alkaline media.* Physical Chemistry Chemical Physics, 2013. **15**(37): p. 15416-15425.
77. Valdes, J.L. and H.Y. Cheh, *A SYSTEMATIC APPROACH TO THE DETERMINATION OF POSSIBLE REACTION MECHANISMS OF OXYGEN REDUCTION ON PLATINUM IN ALKALINE MEDIUM.* Journal of The Electrochemical Society, 1985. **132**(11): p. 2635-2640.
78. Kullapere, M., et al., *Oxygen electroreduction on chemically modified glassy carbon electrodes in alkaline solution.* Journal of Electroanalytical Chemistry, 2007. **599**(2): p. 183-193.
79. Maciá, M.D., et al., *On the kinetics of oxygen reduction on platinum stepped surfaces in acidic media.* Journal of Electroanalytical Chemistry, 2004. **564**(0): p. 141-150.
80. Vilambi, N.R.K. and E.J. Taylor, *Quantitative detection of peroxide formation during oxygen reduction on platinum in alkaline media.* Electrochimica Acta, 1989. **34**(10): p. 1449-1454.
81. Paliteiro, C. and N. Martins, *Electroreduction of oxygen on a (100)-like polycrystalline gold surface in an alkaline solution containing Pb(II).* Electrochimica Acta, 1998. **44**(8–9): p. 1359-1368.
82. Andoralov, V.M., M.R. Tarasevich, and O.V. Tripachev, *Oxygen reduction reaction on polycrystalline gold. Pathways of hydrogen peroxide transformation in the acidic medium.* Russian Journal of Electrochemistry, 2011. **47**(12): p. 1327-1336.
83. Devivaraprasad, R., et al., *Oxygen Reduction Reaction and Peroxide Generation on Shape-Controlled and Polycrystalline Platinum Nanoparticles in Acidic and Alkaline Electrolytes.* Langmuir, 2014. **30**(29): p. 8995-9006.
84. Ramaswamy, N. and S. Mukerjee, *Fundamental mechanistic understanding of electrocatalysis of oxygen reduction on Pt and non-Pt surfaces: Acid versus alkaline media.* Advances in Physical Chemistry, 2012. **2012**.
85. Lima, F.H.B., et al., *Catalytic Activity–d-Band Center Correlation for the O2 Reduction Reaction on Platinum in Alkaline Solutions.* The Journal of Physical Chemistry C, 2006. **111**(1): p. 404-410.
86. Luk'yanycheva, V.I., et al., *MOLECULAR OXYGEN REDUCTION KINETICS AT PREOXIDIZED PLATINUM ELECTRODES IN ALKALINE SOLUTIONS.* Sov Electrochem, 1977. **13**(4): p. 432-437.
87. Paliteiro, C., A. Hamnett, and J.B. Goodenough, *The electroreduction of dioxygen on thin films of gold in alkaline solution.* Journal of Electroanalytical Chemistry and Interfacial Electrochemistry, 1987. **234**(1–2): p. 193-211.
88. Amadelli, R., A. De Battisti, and O. Enea, *Gas-phase electroreduction of O2 on gold—Nafion and (underpotential deposition, gold)—Nafion®*

*electrodes.* Journal of Electroanalytical Chemistry, 1992. **339**(1–2): p. 85-100.
89. Toimil-Molares, M.E., *Characterization and properties of micro- and nanowires of controlled size, composition, and geometry fabricated by electrodeposition and ion-track technology.* Beilstein Journal of Nanotechnology, 2012. **3**: p. 860-883.
90. Anandhakumar, S., J. Mathiyarasu, and K.L.N. Phani, *Anodic stripping voltammetric detection of mercury(II) using Au-PEDOT modified carbon paste electrode.* Analytical Methods, 2012. **4**(8): p. 2486-2489.
91. Chen, W., et al., *Study of carbon-supported Au catalyst as the cathodic catalyst in a direct formic acid fuel cell prepared using a polyvinyl alcohol protection method.* Journal of Power Sources, 2007. **167**(2): p. 315-318.
92. Cheng, F., et al., *Synergistic effect of Pd–Au bimetallic surfaces in Au-covered Pd nanowires studied for ethanol oxidation.* Electrochimica Acta, 2010. **55**(7): p. 2295-2298.
93. Cherevko, S., X. Xing, and C.-H. Chung, *Pt and Pd decorated Au nanowires: Extremely high activity of ethanol oxidation in alkaline media.* Electrochimica Acta, 2011. **56**(16): p. 5771-5775.
94. González Pereira, M., et al., *Study of the electrooxidation of ethanol on hydrophobic electrodes by DEMS and HPLC.* Electrochimica Acta, 2004. **49**(22–23): p. 3917-3925.
95. Ma, J., et al., *Ethanol electrooxidation on carbon-supported Pt nanoparticles catalyst prepared using complexing self-reduction method.* International Journal of Hydrogen Energy, 2011. **36**(12): p. 7265-7274.
96. Xu, Z., J. Yu, and G. Liu, *Enhancement of ethanol electrooxidation on plasmonic Au/TiO2 nanotube arrays.* Electrochemistry Communications, 2011. **13**(11): p. 1260-1263.
97. Barczuk, P.J., et al., *Enhancement of catalytic activity of platinum-based nanoparticles towards electrooxidation of ethanol through interfacial modification with heteropolymolybdates.* Journal of Power Sources, 2010. **195**(9): p. 2507-2513.
98. Simões, F.C., et al., *Electroactivity of tin modified platinum electrodes for ethanol electrooxidation.* Journal of Power Sources, 2007. **167**(1): p. 1-10.
99. Zhu, L.D., et al., *Preparation and characterization of carbon-supported sub-monolayer palladium decorated gold nanoparticles for the electro-oxidation of ethanol in alkaline media.* Journal of Power Sources, 2009. **187**: p. 80-84.
100. Hazzazi, O.A., et al., *Electrochemical characterisation of gold on Pt{h k l } for ethanol electrocatalysis.* Journal of Electroanalytical Chemistry, 2009. **625**(2): p. 123-130.
101. Lai, S.C.S., et al., *Effects of electrolyte pH and composition on the ethanol electro-oxidation reaction.* Catalysis Today, 2010. **154**: p. 92-104.

102. Camargo, A.P.M., et al., *Effect of temperature on the electro-oxidation of ethanol on platinum.* Quimica Nova, 2010. **33**(10): p. 2143-2147.
103. Lai, S.C.S. and M.T.M. Koper, *Ethanol electro-oxidation on platinum in alkaline media.* Physical Chemistry Chemical Physics, 2009. **11**(44): p. 10446-10456.
104. Metikoš-Hukovic, M., R. Babic, and Y. Piljac, *Kinetics and Electrocatalysis of Methanol Oxidation on Electrodeposited Pt and Pt70Ru30 Catalysts.* Journal of New Materials for Electrochemical Systems, 2003. **7**(3): p. 179-190.
105. Tanaka, S., et al., *Preparation and evaluation of a multi-component catalyst by using a co-sputtering system for anodic oxidation of ethanol.* Journal of Power Sources, 2005. **152**(0): p. 34-39.
106. Shao, M.H. and R.R. Adzic, *Electrooxidation of ethanol on a Pt electrode in acid solutions: In situ ATR-SEIRAS study.* Electrochimica Acta, 2005. **50**(12): p. 2415-2422.
107. Iwasita, T., et al., *A sniftirs study of ethanol oxidation on platinum.* Electrochimica Acta, 1989. **34**(8): p. 1073-1079.
108. Strbac, S. and M. Ivic Avramov, *Oxidation of formaldehyde and ethanol on Au(111) and Au(111) modified by spontaneously deposited Ru in sulfuric acid solution.* Electrochimica Acta, 2009. **54**: p. 5408-5412.
109. Souza, J.P.I., et al., *Performance of a co-electrodeposited Pt-Ru electrode for the electro-oxidation of ethanol studied by in situ FTIR spectroscopy.* Journal of Electroanalytical Chemistry, 1997. **420**: p. 17-20.
110. Snell, K.D. and A.G. Keenan, *Effect of anions and pH on the ethanol electro-oxidation at a platinum electrode.* Electrochimica Acta, 1982. **27**(12): p. 1683-1696.
111. Hitmi, H., et al., *A kinetic analysis of the electro-oxidation of ethanol at a platinum electrode in acid medium.* Electrochimica Acta, 1994. **39**(3): p. 407-415.
112. Casella, I.G., *Electrooxidation of aliphatic alcohols on palladium oxide catalyst prepared by pulsed electrodeposition technique.* Electrochimica Acta, 2009. **54**(15): p. 3866-3871.
113. Xu, C., et al., *Ni hollow spheres as catalysts for methanol and ethanol electrooxidation.* Electrochemistry Communications, 2007. **9**(8): p. 2009-2012.
114. Tremiliosi-Filho, G., et al., *Electro-oxidation of ethanol on gold: analysis of the reaction products and mechanism.* Journal of Electroanalytical Chemistry, 1998. **444**: p. 31-39.
115. Yáñez, C., C. Gutiérrez, and M.S. Ureta-Zañartu, *Electrooxidation of primary alcohols on smooth and electrodeposited platinum in acidic solution.* Journal of Electroanalytical Chemistry, 2003. **541**(0): p. 39-49.
116. Abd-El-Latif, A.A., et al., *Electrooxidation of ethanol at polycrystalline and platinum stepped single crystals: A study by differential electrochemical mass spectrometry.* Electrochimica Acta, 2010. **55**(27): p. 7951-7960.

117. Bianchini, C., et al., *Selective oxidation of ethanol to acetic acid in highly efficient polymer electrolyte membrane-direct ethanol fuel cells.* Electrochemistry Communications, 2009. **11**(5): p. 1077-1080.
118. Iwasita, T. and E. Pastor, *A dems and FTir spectroscopic investigation of adsorbed ethanol on polycrystalline platinum.* Electrochimica Acta, 1994. **39**(4): p. 531-537.
119. Oliveira, R.T.S., et al., *Ethanol oxidation using a metallic bilayer Rh/Pt deposited over Pt as electrocatalyst.* Journal of Power Sources, 2006. **157**(1): p. 212-216.
120. Razmi, H., E. Habibi, and H. Heidari, *Electrocatalytic oxidation of methanol and ethanol at carbon ceramic electrode modified with platinum nanoparticles.* Electrochimica Acta, 2008. **53**(28): p. 8178-8185.
121. Ye, J., et al., *Electrooxidation of 2-propanol on Pt, Pd and Au in alkaline medium.* Electrochemistry Communications, 2007. **9**(12): p. 2760-2763.
122. Atkins, P. and J.d. Paula, *Atkins' Physical Chemistry*. 2006, Oxford University Press: Oxford. p. 763, Table 21.5.
123. Quijada, C., et al., *Electrochemical behaviour of aqueous SO2 at Pt electrodes in acidic medium. A voltammetric and in situ Fourier transform IR study Part I. Oxidation of SO2 on Pt electrodes with sulphur-oxygen adsorbed species.* Journal of Electroanalytical Chemistry, 1995. **394**(1–2): p. 217-227.
124. Marzouk, S.A.M., M.H. Al-Marzouqi, and S.M.S.M. Baomran, *Simple analyzer for continuous monitoring of sulfur dioxide in gas streams.* Microchemical Journal, 2010. **95**(2): p. 207-212.
125. Ün, Ü.T., A.S. Koparal, and Ü.B. Öğütveren, *Sulfur dioxide removal from flue gases by electrochemical absorption.* Separation and Purification Technology, 2007. **53**(1): p. 57-63.
126. West, P.W. and G.C. Gaeke, *Fixation of Sulfur Dioxide as Disulfitomercurate(II) and Subsequent Colorimetric Estimation.* Analytical Chemistry, 1956. **28**(12): p. 1816-1819.
127. Moraes, I.R., M. Weber, and F.C. Nart, *On the structure of adsorbed sulfur dioxide at the platinum electrode.* Electrochimica Acta, 1997. **42**(4): p. 617-625.
128. Spotniz, R.M., J.A. Colucci, and S.H. Langer, *The activated electro-oxidation of sulphur dioxide on smooth platinum.* Electrochimica Acta, 1983. **28**(8): p. 1053-1062.
129. Zdeněk, S. and J. Weber, *Study of the oxidation of SO2 dissolved in 0.5 M H2SO4 on a gold electrode—I Stationary electrode.* Electrochimica Acta, 1975. **20**: p. 403-412.
130. Quijada, C., et al., *Electrochemical behaviour of aqueous SO2 at polycrystalline gold electrodes in acidic media. A voltammetric and in-situ vibrational study. Part II. Oxidation of SO2 on bare and sulphur-modified electrodes.* Electrochimica Acta, 2000. **46**(5): p. 651-659.

131. Miah, M.R., M.T. Alam, and T. Ohsaka, *Sulfur-adlayer-coated gold electrode for the in vitro electrochemical detection of uric acid in urine.* Analytica Chimica Acta, 2010. **669**(1–2): p. 75-80.
132. Quijada, C., et al., *Electrochemical behaviour of aqueous sulphur dioxide at polycrystalline Pt electrodes in acidic medium. A voltammetric and in-situ FT-IR study Part II. Promoted oxidation of sulphur dioxide. Reduction of sulphur dioxide.* Journal of Electroanalytical Chemistry, 1995. **398**(1–2): p. 105-115.
133. Seo, E.T. and D.T. Sawyer, *Electrochemical oxidation of dissolved sulphur dioxide at platinum and gold electrodes.* Electrochimica Acta, 1965. **10**(3): p. 239-252.
134. Seo, E.T. and D.T. Sawyer, *Determination of sulfur dioxide in solution by anodic voltammetry and by u.v. spectrophotometry.* Journal of Electroanalytical Chemistry (1959), 1964. **7**(3): p. 184-189.
135. Pletcher, D., *A First Course in Electrode Processes*. 2009, The Royal Society of Chemistry Publishing: Cambridge. p. 7.
136. *CRC Handbook of Chemistry and Physics, Internet Version 2007*, D.R. Lide, Editor. 2007, Taylor and Francis: Boca Raton, Florida.

# Appendix 1 – Data

This appendix lists the data used for all formulas in this dissertation to calculate values of certain wanted variables or constants.

The diffusion coefficient for gases and liquids in water is given in Table 20 below [60]:

**Table 20: Diffusion coefficients for different gases and liquids in water**

| Diffusion Coefficients (D) of Gases in $H_2O$ at 25 °C | |
|---|---|
| $O_2$ | 2.42 x$10^{-5}$ $cm^2/s$ |
| $SO_2$ | 1.83 x$10^{-5}$ $cm^2/s$ |
| EtOH | 1.24 x$10^{-5}$ $cm^2/s$ |

The following table (Table 21) gives the values for different compounds' viscosity at different concentrations at standard temperature [60]:

**Table 21: Viscosity of different compounds at different concentrations at 25 °C**

| | c (mol/L) | $\rho$ (g/cm$^3$) | $\mu$ (mPa.s) |
|---|---|---|---|
| **EtOH** | 1.008 | 1.0764 | 1.625 |
| | 0.311 | 0.9964 | 1.040 |
| | 0.621 | 0.9947 | 1.070 |
| | 0.930 | 0.9930 | 1.100 |
| | 1.238 | 0.9913 | 1.131 |
| | 1.544 | 0.9896 | 1.163 |
| | 1.850 | 0.9880 | 1.196 |
| **KOH** | **c (mol/L)** | **$\rho$ (g/cm$^3$)** | **$\mu$ (mPa.s)** |
| | 0.089 | 1.0025 | 1.010 |
| | 0.179 | 1.0068 | 1.019 |
| | 0.362 | 1.0155 | 1.038 |
| | 0.548 | 1.0242 | 1.058 |
| | 0.736 | 1.0330 | 1.079 |
| | 0.929 | 1.0419 | 1.102 |
| | 1.124 | 1.0509 | 1.126 |
| | 1.322 | 1.0599 | 1.151 |
| | 1.524 | 1.0690 | 1.177 |
| | 1.729 | 1.0781 | 1.205 |

The solubility of oxygen and sulphur dioxide is given below in Table 22 [60]:

**Table 22: Mole fraction solubility of different gases**

| | T (K) | Solubility $X_1$ | Equation Constants |
|---|---|---|---|
| $O_2$ | 288.15 | $2.756 \times 10^{-5}$ | A = -66.7354 |
| | 293.15 | $2.501 \times 10^{-5}$ | B = 87.4755 |
| | 298.15 | $2.293 \times 10^{-5}$ | C = 24.4526 |
| | 303.15 | $2.122 \times 10^{-5}$ | Std. dev. = ±0.36% |
| | 308.15 | $1.982 \times 10^{-5}$ | Temp. Range 273.15 - 348.15K |
| $SO_2$ | 288.15 | $3.45 \times 10^{-2}$ | A = -25.2629 |
| | 293.15 | $2.90 \times 10^{-2}$ | B = 45.7552 |
| | 298.15 | $2.46 \times 10^{-2}$ | C = 5.6855 |
| | 303.15 | $2.10 \times 10^{-2}$ | Std. dev. = ±1.8% |
| | 308.15 | $1.80 \times 10^{-2}$ | Temp. Range 278.15 - 328.15K |

The equation used for the solubility is given as:

$$\ln X_1 = A + \frac{B}{T^*} + C \ln T^* \qquad T^* = \frac{T}{100K} \tag{63}$$

In equation (63), $X_1$ is the mole fraction solubility, A, B & C the constants, as listed in Table 22 for each gas, and T the temperature in Kelvin. All these values are valid for a partial pressure of 1 atmosphere.

Summarised in Table 23 below are variables used by some authors in the literature, for use in the Koutecký-Levich equation (16) & (18) to determine the number of electrons involved in the electrochemical reaction under investigation:

**Table 23: Values of the Koutecký-Levich variables for the calculation of the number of electrons**

| Source | Electrolyte | Kinematic | Diffusivity of $O_2$ | Oxygen |
|---|---|---|---|---|
| Kullapere *et al.* [78] | 0.1 M KOH | 0.01 $cm^2/s$ | $1.9X10^{-5}$ $cm^2/s$ | $1.2X10^{-6}$ $mol/cm^3$ |
| Jeon *et al.* [58] | 0.5 M $H_2SO_4$ | 0.010 $cm^2/s$ | $1.8x10^{-5}$ $cm^2/s$ | $1.136x10^{-6}$ $mol/cm^3$ |
| Sarapuu *et al.* [31, 49] | $H_2SO_4$ & $HClO_4$ | 0.01 $cm^2/s$ | $1.93x10^{-5}$ $cm^2/s$ | $1.22x10^{-6}$ $mol/cm^3$ |
| Paliteiro *et al.* [63, 81, 87] | 1 M NaOH | $1.062x10^{-2}$ $cm^2/s$ | $1.65x10^{-5}$ $cm^2/s$ | $8.4x10^{-7}$ $mol/cm^3$ |
| Bron [65] | $H_2SO_4$ | $1.078x10^{-5}$ $cm^2/s$ | $1.8x10^{-5}$ $cm^2/s$ | $1.13x10^{-6}$ $mol/cm^3$ |
| Erikson *et al.* [59] | 0.5 M $H_2SO_4$ | 0.01 $cm^2/s$ | $1.8x10^{-5}$ $cm^2/s$ | $1.13x10^{-6}$ $mol/cm^3$ |
| Erikson *et al.* [59] | 0.1 M KOH | 0.01 $cm^2/s$ | $1.9x10^{-5}$ $cm^2/s$ | $1.2x10^{-6}$ $mol/cm^3$ |
| Van Brussel *et al.* [67] | $HClO_4$ | $8.93x10^{-3}$ $cm^2/s$ | $1.93x10^{-5}$ $cm^2/s$ | $1.22x10^{-6}$ $mol/cm^3$ |
| Alexeyeva *et al.* [68] | $H_2SO_4$ | 0.01 $cm^2/s$ | $1.8x10^{-5}$ $cm^2/s$ | $1.13x10^{-6}$ $mol/cm^3$ |
| Chen *et al.* [29] | NaOH | $9.97x10^{-5}$ $cm^2/s$ | $1.9x10^{-5}$ $cm^2/s$ | $2.5x10^{-6}$ $mol/cm^3$ |
| Zdeněk *et al.* [129] | $H_2SO_4$ | - | $1.8x10^{-5}$ $cm^2/s$ | - |
| Zdeněk *et al.* [129] | $H_2SO_4$ | - | $2.0x10^{-5}$ $cm^2/s$ | - |
| Zdeněk *et al.* [129] | 0.5 M $H_2SO_4$ | $0.98x10^{-2}$ $cm^2/s$ | - | - |

| | | | | |
|---|---|---|---|---|
| O' Brien *et al.* [26] | 0.1-0.5 M $H_2SO_4$ | - | $2.0x10^{-5}$ $cm^2/s$ | - |
| O' Brien *et al.* [26] | 1 M $H_2SO_4$ | - | $1.03x10^{-5}$ $cm^2/s$ | - |
| Seo and Sawyer [133, 134] | 0.1 M $H_2SO_4$ | - | $2.0x10^{-5}$ $cm^2/s$ | - |

**Table 24: Universal gas constant R for use in the Arrhenius equation**

| | |
|---|---|
| Universal Gas Constant, R | 8.31447 $J/K.mol^{-1}$ |

**Table 25: Data from Lide *et al.* to calculate the kinematic viscosity of 0.5 M $H_2SO_4$ for use in the Koutecký-Levich analysis [136]**

| Mass % | m/mol $kg^{-1}$ | c/mol $L^{-1}$ | ρ/g $cm^{-3}$ | n | Δ/℃ | η/mPa s |
|---|---|---|---|---|---|---|
| 0.5000 | 0.0510 | 0.0510 | 1.0016 | 1.3336 | 0.2100 | 1.0100 |
| 1.0000 | 0.1030 | 0.1020 | 1.0049 | 1.3342 | 0.4200 | 1.0190 |
| 2.0000 | 0.2080 | 0.2060 | 1.0116 | 1.3355 | 0.8000 | 1.0360 |
| 3.0000 | 0.3150 | 0.3110 | 1.0183 | 1.3367 | 1.1700 | 1.0590 |
| 4.0000 | 0.4250 | 0.4180 | 1.0250 | 1.3379 | 1.6000 | 1.0850 |
| 5.0000 | 0.5370 | 0.5260 | 1.0318 | 1.3391 | 2.0500 | 1.1120 |
| 6.0000 | 0.6510 | 0.6350 | 1.0385 | 1.3403 | 2.5000 | 1.1360 |
| 7.0000 | 0.7670 | 0.7460 | 1.0453 | 1.3415 | 2.9500 | 1.1590 |
| 8.0000 | 0.8870 | 0.8580 | 1.0522 | 1.3427 | 3.4900 | 1.1820 |
| 9.0000 | 1.0080 | 0.9720 | 1.0591 | 1.3439 | 4.0800 | 1.2060 |
| 10.0000 | 1.1330 | 1.0870 | 1.0661 | 1.3451 | 4.6400 | 1.2300 |
| 12.0000 | 1.3900 | 1.3220 | 1.0802 | 1.3475 | 5.9300 | 1.2820 |
| 14.0000 | 1.6600 | 1.5630 | 1.0947 | 1.3500 | 7.4900 | 1.3370 |
| 16.0000 | 1.9420 | 1.8100 | 1.1094 | 1.3525 | 9.2600 | 1.3990 |
| 18.0000 | 2.2380 | 2.0640 | 1.1245 | 1.3551 | 11.2900 | 1.4700 |
| 20.0000 | 2.5490 | 2.3240 | 1.1398 | 1.3576 | 13.6400 | 1.5460 |
| 22.0000 | 2.8760 | 2.5920 | 1.1554 | 1.3602 | 16.4800 | 1.6240 |
| 24.0000 | 3.2200 | 2.8660 | 1.1714 | 1.3628 | 19.8500 | 1.7060 |
| 26.0000 | 3.5820 | 3.1470 | 1.1872 | 1.3653 | 24.2900 | 1.7970 |
| 28.0000 | 3.9650 | 3.4350 | 1.2031 | 1.3677 | 29.6500 | 1.8940 |
| 30.0000 | 4.3700 | 3.7290 | 1.2191 | 1.3701 | 36.2100 | 2.0010 |
| 32.0000 | 4.7980 | 4.0300 | 1.2353 | 1.3725 | 44.7600 | 2.1220 |
| 34.0000 | 5.2520 | 4.3390 | 1.2518 | 1.3749 | 55.2800 | 2.2550 |
| 36.0000 | 5.7350 | 4.6560 | 1.2685 | 1.3773 | | 2.3920 |
| 38.0000 | 6.2490 | 4.9810 | 1.2855 | 1.3797 | | 2.5330 |
| 40.0000 | 6.7970 | 5.3130 | 1.3028 | 1.3821 | | 2.6900 |
| 42.0000 | 7.3830 | 5.6550 | 1.3205 | 1.3846 | | 2.8720 |
| 44.0000 | 8.0110 | 6.0050 | 1.3386 | 1.3870 | | 3.0730 |
| 46.0000 | 8.6850 | 6.3640 | 1.3570 | 1.3895 | | 3.2990 |
| 48.0000 | 9.4110 | 6.7340 | 1.3759 | 1.3920 | | 3.5460 |
| 50.0000 | 10.1960 | 7.1130 | 1.3952 | 1.3945 | | 3.8260 |
| 52.0000 | 11.0450 | 7.5020 | 1.4149 | 1.3971 | | 4.1420 |
| 54.0000 | 11.9690 | 7.9010 | 1.4351 | 1.3997 | | 4.4990 |
| 56.0000 | 12.9760 | 8.3120 | 1.4558 | 1.4024 | | 4.9060 |

| | | | | | | |
|---|---|---|---|---|---|---|
| 58.0000 | 14.0800 | 8.7340 | 1.4770 | 1.4050 | | 5.3540 |
| 60.0000 | 15.2940 | 9.1680 | 1.4987 | 1.4077 | | 5.9170 |
| 70.0000 | 23.7900 | 11.4940 | 1.6105 | | | |
| 80.0000 | 40.7830 | 14.0880 | 1.7272 | | | |
| 90.0000 | 91.7620 | 16.6490 | 1.8144 | | | |
| 92.0000 | 117.2510 | 17.1090 | 1.8240 | | | |
| 94.0000 | 159.7340 | 17.5500 | 1.8312 | | | |
| 96.0000 | 244.6980 | 17.9660 | 1.8355 | | | |
| 98.0000 | 499.5920 | 18.3460 | 1.8361 | | | |
| 100.0000 | | 18.6630 | 1.8305 | | | |

The columns in Table 25 each represent the following: Mass percent; m = molality (moles of solute per kilogram of water); c = molarity (moles of solute per litre of solution); ρ = the density of the solution in g/cm$^3$; n = refractive index relative to air; Δ = the freezing point depression relative to water in ℃; η = absolute dynamic viscosity in mPa.s equivalent to centipoise cP.

# Appendix 2 – Sample Calculations

This chapter shows examples of how calculations were done to determine certain important values for certain concepts or methods.

**Tafel Slope:**

Let's consider ethanol oxidation in acidic medium for gold. The range of current densities was used to extrapolate the slope, which was used to determine the Tafel slope.

$$m = 0.228 V/decade$$

To determine the actual Tafel slope, the slope had to be multiplied by 1000 to get into the mV unit of measurement:

$$\begin{aligned}\text{Tafel Slope} &= 0.228 V/decade \times 1000 \\ &= 228 mV/decade\end{aligned}$$

**Arrhenius Plots:**

Consider the electro-oxidation reaction of ethanol in alkaline medium and the Arrhenius equation (20):

$$\ln k = \ln A - \frac{E_a}{RT}$$

The linear plot of the inverted temperatures and the logarithmic of the current density at a given potential was used to calculate the activation energy by using values such as the slope of the linear plot and the universal gas constant from Table 54:

$$Slope = -\frac{E_a}{R}$$
$$\therefore E_a = -Slope \times R$$
$$E_a = -\left(-3622.8369 K^{-1}\right) \times 8.31447 J/K.mol^{-1})$$
$$E_a = 30121.96898 J/mol$$
$$E_a = 30.121 kJ/mol$$

**Koutecký-Levich:**

The Koutecký-Levich plots consisted of the different plots of the inverse of the current density, plotted against the inverse of the rotation rate, for a series of results for a given potential across the different rotation rates. Consider oxygen reduction in acidic medium. Let's use the range of values for the 0.3100 V plot. The current densities at those potentials

was used over the range of different rotation rates and plotted. The slope of the linear plot was used to calculate the number of electrons for each rotation rate and the average was taken thereof. The final average of electron number was taken across all the potentials for which a plot was created. Thus the calculation using the Koutecký-Levich equation was done as follows, starting by using the formula in equation (18):

$$Slope = \frac{1}{0.62nF\pi r^2 D_A^{2/3} \nu^{-1/6} \omega^{1/2} C_A^b}$$

$$n = \frac{1}{0.62(slope)F\pi r^2 D_A^{2/3} \nu^{-1/6} \omega^{1/2} C_A^b}$$

$$n = \frac{1}{0.62 \cdot (-2.48) \cdot (9.65\times10^7\ mA.s/mol) \cdot (3.14) \cdot (0.62cm^2) \cdot (8.37\times10^{-4} cm^2/s) \cdot (2.2.cm^2/s) \cdot (1.291s^{-1}) \cdot (1.27\times10^{-6})}$$

$$n = -11.4$$

The same calculation was done using all the rotation rates and taking the average thereof to determine the number of electrons involved in the reaction at that potential:

$$\bar{n}_{0.3110V} = -5.8$$

**Levich:**

The Levich equation (15) was used to determine the number of electrons as follows:

$$Slope = \frac{0.62nF\pi r^2 D_A^{2/3} \omega^{1/2} C_A^b}{\nu^{1/6}}$$

$$n = \frac{\nu^{1/6} \cdot slope}{0.62F\pi r^2 D_A^{2/3} \omega^{1/2} C_A^b}$$

$$= \frac{\left(0.001^{1/6} cm^2/s\right) \cdot (-0.48)}{0.62 \cdot \left(9.65\times10^7\ mA.s/mol\right) \cdot \left(2.42\times10^{-5} cm^2/s\right)^{2/3} \cdot \left(1.269\times10^{-5}\right)}$$

$$= 2.39$$

The kinematic viscosity of 0.5 M $H_2SO_4$ was calculated using the values from Table 25 to produce the following results depicted in Table 26.

**Table 26: The values used for extrapolation of the kinematic viscosity of 0.5 M $H_2SO_4$**

| **Values and equation constants used to calculate the Kinematic Viscosity of $H_2SO_4$** | | | | |
|---|---|---|---|---|
| Concentration ranges from Table 25 used for extrapolation: | | | | 0.051 - 4.03 |
| **Equation Constants:** | **$Ax^2$** | **Bx** | **C** | **Correlation$^2$** |
| **ρ vs. [ ]:** | - | 0.05906409 | 1.000882911 | 0.999584664 |
| **η vs. [ ]:** | 0.024680388 | 0.174747211 | 1.006895346 | 0.999740159 |
| | | | **Known Concentration:** | 0.5 |
| | | | **Corresponding calculated ρ:** | 1.030414956 |
| | | | **Corresponding calculated η:** | 1.100439048 |
| | | | **Calculated Kinematic Viscosity:** | 0.001067957 |

# Acknowledgements

First of all I would like to thank my Saviour the Holy Trinity, Father, Son and Holy Spirit for guiding me, supporting me and helping me through all the obstacles I encountered in finishing my studies. Thank you Jesus.

I would like to thank my dearest husband Wimpi Visser-Steyn for all his support and patience in the time I completed my degree, as he kept the household going when I was studying.

My parents I would like to thank for their moral and financial support and for the academic registration paid by my mother, Ansa for my final year 2014 and my father, Martin, for paying the language care of my dissertation. Thank you Aunt Melanie for doing the language care.

I want to thank my friends for their support while I completed my studies: Johnny and Alizéa Steyn for supporting me morally and enabling me to set up my computer when ESKOM would implement loadshedding; Charmé Coetzee, Minzelle and Johan van der Schyff for giving me a roof over my head when I had to go do experiments at the university campus; Mr André and Mrs. Hannelie Coetzee for always opening their home for me when I needed a place to stay, and Marthinus Janse van Rensburg and Gert Maritz, who also gave me a place to stay when I had to go to campus for academic work.

Mrs. Hestelle Stoppel I would like to thank for always kindly assisting me with administrative issues regarding my degree, and for her motivation and kindness. I would also like to thank Miss Anriëtte Pretorius for helping me with literature, and guidance in terms of literature searches and also for her motivation and moral support.

My sincere appreciation for my supervisor Dr. Kriek for all his feedback and advice. Also my co-supervisor Prof. Vijay Ramani – Thank you.

One of the most important acknowledgements is of two co-students who helped me with the platinum results – Adri Young and Marcelle Potgieter. Without your help, I would still be studying. Thank you. May God bless you always.

Last but not least – NWU, HySA and CRB. Thank you for the financial support during the first half of my degree before I started working and finishing my degree on a part time basis, and for giving me the opportunity to do my MSc degree.

Additionally I would like to thank my bosses at Mirren (Pty) Ltd for kindly giving me study-leave when I needed it – Thomas Macinnes and Justine Daniels; also Charlene Stoltz for assisting me with study-leave issues and all my colleagues for all their moral support.